Université de Montréal

The Effects of Lactate Receptor G Protein-Coupled Receptor 81 (GPR81) on the Integrity of the Choroidal Vasculature

by

Xiaojuan Yang

School of Optometry

This thesis is presented to the Faculty of Graduate Studies

in order to obtain the degree of Doctor of Philosophy (Ph.D) in

Vision Science, option NEUROSC.VISION/PSYCHOPHYS.

February 21, 2019

Résumé

Plutôt qu'un simple déchet corporel, le lactate participe à plusieurs fonctions biologiques via son récepteur, GPR81, tel que l'angiogenèse, l'inhibition de l'inflammation et de la lipolyse. Plusieurs études soulignent l'implication du lactate dans le cancer, sa contribution aux pathologies oculaires est peu documentée. Étant donné que la rétine (et possiblement la rétine externe) est l'une des plus grande consommatrice d'énergie parmi toutes les tissus du corps humain et étant donné que son dérèglement métabolique est associé à plusieurs pathologies incluant la dégénérescence maculature liée à l'age (DMLA), la cause principale de cécité chez les personnes âgées dans les pays industrialisés, nous sous sommes intéressés au récepteur de lactate GPR81 et ses fonctions potentielles dans la rétine externe. Curieusement, nous avons observé une expression abondante du GPR81 dans la rétine externe, surtout dans l'épithélium pigmentaire rétinien (EPR), qui est un élément important au maintien de l'homéostasie de la rétine externe incluant la vasculature choroïdienne et les photorécepteurs.

La fonction pro-angiogénique du GPR81 est confirmée par la technique de germination choroïdienne (*ex vivo*) et l'injection intravitréenne de lactate aux souris (*in vivo*). Par contre, en prenant les mesures de l'épaisseur choroïdienne, nous avons observé que les souris GPR81$^{-/-}$ manifestent la dégénération choroïdienne accompagnée par une néovascularisation aberrante.

Les souris GPR81$^{-/-}$ jeunes (<P30) montrent une vasculature choroïdienne plus mince,

résultant de l'activation de la réponse au stress intégré (RSI), qui est un mécanisme élaboré que les cellules adoptent afin de s'adapter aux stress variés. Les essais avec des facteurs de croissance montrent une réduction générale de traduction chez les souris KO, indiquant la présence de stress au niveau du reticulum endoplasmique (RE), que confirme l'augmentation de BiP et PDI. De plus, ces souris ont également manifesté une augmentation du stress oxidatif, suggéré par le niveau accru des dérivés réactifs de l'oxygène (DRO) et de l'isoprostane-8, ainsi que la déficience du système anti-oxidant, indiqué par la réduction de Nrf2 et de l'activité de la SOD. En outre, le stress oxidatif et le stress RE travaillent en synergie afin d'activer la voie de la RSI chez les souris KO, tel que suggéré par le niveau accru de phosphorylation de l'unité alpha du facteur d'initiation 2 chez les eukaryotes (eIF2α), d'ATF4 et de la transcriptions de gênes ciblés. L'inhibition de la voie RSI a éventuellement rétablie l'épaisseur choroïdienne des souris KO à P12, en restaurant partiellement la synthèse des protéines, particulièrement le VEGF A pro-angiogénique et le HGF. La fin de la voie RSI chez les souris KO à P30 est indiquée par l'augmentation de l'arrêt de croissance, le niveau accru de la GADD34 ainsi que la restauration de la traduction générale.

Pourtant, l'augmentation continuelle de traduction globale chez les souris KO déclenchent le développement de la néovascularisation choroïdienne pathologique (NCP), typique à la DMLA humide, à P180. Comparé aux souris WT du même âge, l'épithélium pigmentaire rétinien (EPR) des KO a démontré une dégénérescence suggérée par la

disparition des conmexions d'EPR et l'émergence d'EPR fantôme. À l'âge d'un an, les vaisseaux choroïdiens montrent une croissance dans l'EPR chez les souris KO. Toutes ces données suggèrent que les souris GPR81$^{-/-}$ peuvent être utilisées comme modèle de la néovascularisation choroïdienne.

Globalement, notre étude fournit la première preuve du potentiel thérapeutique de cibler les récepteurs métaboliques GPR81 en DMLA humide via les régulations simultanées du stress oxidant, du stress RE et de la voie RSI.

Mots clés: Récepteur couplé à la protéine G 81 (GPR81); Récepteur d'acide hydroxycarboxylique 1 (HCA1); Lactate; Néovascularisation choroïdienne (NVC); Dégénérescence maculaire liée à l'âge (DMLA); Épaississement choroïdien; Amincissement choroïdien; Stress oxydatif; Stress ER; Réponse au stress intégrée (ISR); dérèglement métabolique; Rétine externe; épithélium pigmentaire rétinien (EPR).

ABSTRACT

Rather than simply a body waste, lactate exhibits various biological activities, including pro-angiogenesis, anti-inflammation, and anti-lipolysis functions, via its receptor G protein-coupled receptor GPR81 (i.e., hydroxycarboxylic acid receptor 1, HCA1). Despite being well studied in cancers, the potential involvement of GPR81 in the eye remains insufficiently investigated. Given that the retina (and perhaps also the outer retina) is one of the most energy-demanding tissues in the human body and that retinal metabolism dysregulation is linked to several pathologies including age-related macular degeneration (AMD), a leading cause of blindness in elderly people in industrialized countries, we are interested in the lactate receptor GPR81 and its potential functions in the outer retina. Intriguingly, GPR81 was abundantly expressed in the retinal pigment epithelium (RPE) layer of the outer retina, which is a key element in maintaining homeostasis of the outer retina including the choroidal vasculature and photoreceptors.

The pro-angiogenic function of GPR81 activation was confirmed by choroid sprout assay (*ex vivo*) and choroidal thickness measurement in mice given intravitreal injections of lactate (*in vivo*). In contrast, by evaluating the choroidal thickness, we found that $GPR81^{-/-}$ (i.e., KO) mice displayed choroidal degeneration followed by aberrant neovascularization.

Compared to age-matched WT mice, young $GPR81^{-/-}$ mice (<P30) displayed a dramatically reduced choroidal vasculature, which was mediated by activation of the

integrated stress response (ISR) pathway, an elaborate mechanism employed by cells to adapt to various stresses. Growth factor microarray analysis revealed a general decrease in translation in GPR81$^{-/-}$ mice, indicating the presence of ER stress, which was further confirmed by the increased levels of ER stress markers (BiP and PDI). Moreover, these mice also showed a significant elevation of oxidative stress evidenced by significantly increased levels of reactive active species (ROS) and 8-isoprostane as well as lower levels of Nrf2 and SOD activity. Therefore, ER stress and oxidative stress in GPR81$^{-/-}$ mice worked synergistically to activate the ISR pathway, as suggested by increased levels of phosphorylation of the alpha subunit of eukaryotic translation initiation factor 2 (eIF2α), ATF4, and transcription of its downstream target genes. Inhibition of the ISR pathway reversed the choroidal thinning in GPR81$^{-/-}$ mice at P12, mediated by a partial restoration of protein synthesis, particularly of the pro-angiogenic factors such as VEGF A and HGF. The termination of the ISR pathway in GPR81$^{-/-}$ mice was at P30, as evidenced by the increased level of growth arrest and DNA damage-inducible protein 34 (GADD34) and the restoration of general translation.

The subsequent increase of global translation in GPR81$^{-/-}$ mice, however, eventually triggered the development of pathological choroidal neovascularization (CNV), the hallmark of “wet” AMD, at P180. Compared to age-matched WT mice, these GPR81$^{-/-}$ RPEs displayed several forms of degeneration manifesting as the disappearance of some RPE junctions as well as the appearance of ghost RPEs. At one year of age, some

choroidal vessels were observed growing into the RPE layer in GPR81$^{-/-}$ mice. All these data suggest that aged GPR81$^{-/-}$ mouse could be a mouse model of CNV.

Taken together, our study provides the first evidence for the therapeutic potential of targeting the metabolic receptor GPR81 in “wet” AMD through the simultaneous regulation of oxidative stress, ER stress, and resultant ISR pathway activation. The GPR81$^{-/-}$ mouse can be used as a mouse model of CNV.

Key words: G protein-coupled receptor 81 (GPR81); Hydroxycarboxylic acid receptor 1 (HCA1); Lactate; Choroidal neovascularization (CNV); Aged-related macular degeneration (AMD); Choroidal thickening; Choroidal thinning; Oxidative stress; ER stress; Integrated stress response (ISR); Metabolism dysregulation; Outer retina; Retinal pigment epithelium (RPE).

TABLE OF CONTENTS

List of Tables

List of Figures

List of Abbreviations

AMD	Aged macular degeneration;
ATF4	The activating translation factor 4;
Asns	Asparagine synthetase;
ATF3	Activating transcriptional factor 3;
Ang II	Angiotensin II;
ApoE	Apolipoprotein E;
BAD	The Bcl2-associated death promoter;
Bcl2	B-cell lymphoma 2;
BiP	The endoplasmic reticulum binding protein;
bFGF2	Basic fibroblast growth factor 2;
beta NGF	Beta nerve growth factor;
Ccl2	Chemokine ligand 2;
CReP	Constitutive repressor of eIF2α phosphorylation;
CHOP	C/EBP homologous protein;
CNV	Choroidal neovascularization;
COX2	Cyclooxygenase 2;
DHBA	3', 5'-Dihydroxybenzoic acid;
eIf2α	Alpha subunit of eukaryotic translation initiation factor 2;
ER	Endoplasmic reticulum;
EGF	Epidermal growth factor;
EGFR	Epidermal growth factor receptor;
FGF7	Fibroblast growth factor 7;
FASL	Fas ligand;
GADD34	Growth arrest and DNA-damage inducible protein 34;
GCN2	General control non-depressible 2;
GPR81	G-protein coupled receptor 81;
GCSF	Granulocyte-colony stimulating factor;
GM-CSF	Granulocyte-macrophage colony-stimulating factor;
HRI	Heme-regulated inhibitor;

HCAs Hydroxycarboxylic acid receptors;

HGF Hepatocyte growth factor;

HGFR Hepatocyte growth factor receptor;

Iba-1 Ionized calcium binding adaptor molecule 1;

ISR The integrated stress response;

ISRIB The integrated stress response inhibitor;

IL-1 beta Interleukin-1 beta;

IL-1 RA Interleukin 1 receptor antagonist;

IL-2 Interleukin-2;

IL-7 Interleukin-7;

IL-8 Interleukin 8 homologue;

IL-10 Interleukin 10;

IGF-1 Insulin growth factor 1;

IGF-1R Insulin growth factor 1 receptor;

IGF-2 Insulin growth factor 2;

IGFBP-2 Insulin like growth factor binding protein 2;

IGFBP-3 Insulin like growth factor binding protein 3;

IGFBP-5 Insulin like growth factor binding protein 5;

IGFBP-6 Insulin like growth factor binding protein 6;

MCP Monocyte colonization protein

M-CSF Macrophage colony-stimulating factor;

MCTs Proton-linked monocarboxylate transporters

MMP Matrix metalloproteinases

NLRP3 NLR family pyrin domain containing 3;

Nrf2 The nuclear factor E2-related factor 2;

OXPHOS Oxidative phosphorylation;

PERK PKR-like endoplasmice reticulum kinase;

PEDF Pigment epithelium derived factor;

PDGF-AA Platelet-derived growth factor-AA;

PDGF-BB Platelet-derived growth factor-BB;

PDI	Protein disulfide isomerase;
PKR	Double-stranded RNA-dependent protein kinase;
PLA2	Phospholipase A2;
PLGF	Placental growth factor;
PRPE	Primary RPE;
ROP	Retinopathy of prematurity;
ROS	Reactive oxygen species;
RAP	Retinal angiomatous proliferation;
RPE	Retinal pigment epithelium;
RIP3	The receptor-interacting protein kinase 3;
SCF	Stem cell factor;
Sema 3F	Semaphoring 3F;
SOD	Superoxide dismutase;
Trib3	Tribbles homolog 3;
TNFα	Tumor necrosis factor α
TIMPs	Tissue inhibitors of metalloproteinases;
TGFβ	Transforming growth factor beta;
TSP-1	Thrombospondin 1;
VEGF A	Vascular endothelial growth factor A;
VEGF-D	Vascular endothelial growth factor D;
VEGFR-1	Vascular endothelial growth factor receptor 1;
VEGFR-2	Vascular endothelial growth factor receptor 2;
VEGFR-3	Vascular endothelial growth factor receptor 3;

Acknowledgments

I would like to express my sincere gratitude to all the people who contributed in some way to the work described in this dissertation. First and foremost, I would like to thank my primary supervisor Dr. Sylvain Chemtob and co-supervisor Dr. Pierre Lachapelle, for their excellent guidance and supervision. During my time in the lab, they have provided me with great patience, numerous supports for my study and professional growth. Their input was invaluable to the completion of my Ph.D. and my growth as a scientist. As I move forward in life, I will definitely carry with me the precious skills, values, lessons, and memories that I have learned/formed during my training.

I also would like to thank my friends and colleagues who assisted me with all the techniques especially at the early stage of this project. Our laboratory manager Dr. Christiane Quiniou was always there for helping me out during difficult times. And thanks for the correction of the Résumé in this thesis**.** Dr. Raphael Rouget and Dr. Tang Zhu, both experts in Biomolecular Science, brought me into a totally different field by their vast knowledge and I was always inspired by the discussions with them. Meanwhile, Dr. Tang Zhu, Dr. Xin Hou, and Isabelle Lahaie, were great team players, and I would never forget their contributions to enrich the data. In addition, Mathieu Nadeau-Vallee, Francois Duhamel, and Baraa Nouiheid established my techniques. Particularly, Dr. Houda Tahiri taught me all the techniques for the choroid-specific studies. Dr. Raphael Rouget and my friends including Xue Li, Lijuan Wang, and Muqing Gu, were always giving me a hand

especially when I had to take care of my little girl. Dr. Nicholas Sitaras elaborated my abstract for ARVO. I also greatly enjoyed the friendship with Dr. Houda Tahiri, Dr. Samy Omri, and Estefania Marin Sierra. Without their support, the completion of my Ph.D. would be “mission impossible”.

The colleagues and friends from my co-supervisor’s laboratory, including Dr. Shasha Lv, Dr. Suna Jung, Dr. Anna Polosa, Dr. Mathieu Gauvin, Dr. Allison Dorfman, and Samaneh Chaychi, are also of great importance to me. I had a great time when working with them. In addition, I also learned a lot when coaching summer students including Alexander Lachapelle, Hamed Mohammed Al-Aamil, and Yoolhoo Lucas Ahn. A special thanks goes to the summer student Shuyi Zhai, who taught me a lot about how to deal with the stress/tough-times and helped me with the translation of the abstract into Résumé in this thesis.

I am grateful for the financial funding from China Scholarship Council and the School of Optometry at the University of Montreal, which consolidate me the opportunity to complete my Ph.D study.

I also would like to acknowledge my friends in life. Lily, Liana, Hong, Qiuxia, and Jane, I am grateful for their encouragement and help to take care of my little girl especially during weekends when I was writing my thesis.

Finally, but not the least, I would like to thank my family. My parents were always helping and encouraging no matter what happened. I also appreciated their visit from

China to Canada in order to look after my girl soon after her birth. My parents-in-law, also reservelessly offered their support to our tiny family. My angel Lina, who is now 4 years old, has given us so much happiness. My husband Pengpeng, without his standing side-by-side with me, I could not be here. Thank you all.

匆匆七年, 历经了换实验室、换导师、换专业（重新入学）、换课题和不被理解等各种痛苦之后，终于即将今年年底毕业。期间的心酸苦辣不可言喻，也许只有经历过才能有所体会。感谢我老公和女儿娜娜的陪伴，他们是我完成学业最坚实的后盾；也很感谢 Pierre 至始至终的支持与理解，让我有勇气去面对一切困难；还有那些生命中结识的有缘人，我很珍惜我所有的一切。这段难忘的经历，磨练了我的意志力，极大的挖掘出了我自己的潜力，也更让我更加明白我是谁。感恩一切，永远铭记！

Chapter 1: INTRODUCTION & LITERATURE REVIEW

1.1 INTRODUCTION

In humans, among the five basic senses (i.e., sight, hearing, smell, taste, and touch), vision is thought to be the predominant sense from which we obtain most information about the world [1]. In general, the formation of vision requires light to pass through the anterior part of the eye including the cornea and lens, which is then focused on the retina where it is received by photoreceptors that generate and then send neuronal signals to the brain via the optic nerve. These processes require precise cooperation between the components of the eye and demand high levels of energy supplied by ocular blood vessels. In fact, the retina has been found to possess the highest metabolic demands and consume the greatest level of oxygen per volume of tissue in the body [2]. More importantly, the main causes of blindness in western countries are a consequence of the dysregulated ocular angiogenesis [3]. Examples include retinopathy of prematurity (ROP), which mainly affects the retinal vessels supplying two-thirds of the retina, and "wet" age-related macular degeneration (AMD), which afflicts the choroidal vasculature that supplies the outer retina. So far, most studies and the main treatment methods of these proliferative ocular pathologies have largely focused on vascular endothelial growth factor (VEGF). However, around 70% of patients are reported to respond poorly to anti-VEGF agents, requiring the urgent development of alternative treatments [4].

As angiogenesis is often associated with ischemia, which provokes a disturbance of cellular metabolism [5, 6], we therefore chose to focus our investigations on the

interplay between angiogenesis and metabolic receptors in these pathologic contexts, due to the discoveries of metabolic receptors in recent decades [7-9]. For example, succinate, an intermediate of the Kreb's cycle, was found to modulate angiogenesis both in normal retinal development and ROP via activation of its receptor G protein-coupled receptor 91 (GPR91) [8].

Of interest, another metabolite called lactate is the main product of ischemia/hypoxia-induced glycolysis and has been demonstrated to possess various biological functions, including pro-angiogenesis, mediated by its receptor G protein-coupled receptor 81 (GPR81) [10, 11]. Intriguingly, our studies have found that GPR81 is abundantly expressed in the retinal pigment epithelium (RPE), which exerts profound effects on the choroidal vasculature. Consequently, herein we will address in detail the effects of lactate activation of its receptor GPR81 on the choroidal vasculature in the context of normal development. By using $GPR81^{-/-}$ mice, we observed that mice lacking GPR81 display choroidal degeneration followed by aberrant neovascularization.

1.2 REVIEW OF THE RELEVANT LITTERATURE

1.2.1 The structure of the eye and its blood supply

The human eye is part of the central nervous system and has a very precise and complex arrangement. It consists of the anterior (including the cornea and lens) and the posterior (including the retina and choroidal vasculature) sections. The retina is a light-sensitive tissue composed of one glial cell type (called Müller cells) and 6 basic

types of cells (cones, rods, bipolar cells, horizontal cells, amacrine cells and ganglion cells). These cells are well organized into layers with photoreceptors (cones and rods) lying back and ganglion cells facing the vitreous (Fig. 1.1). Müller cells lie across the entire retina with their nuclei located in the inner nuclear layer. The inner retina includes the retinal vessels, ganglion cell layer, inner nuclear layer and outer nuclear layer while the **outer retina consists of photoreceptors, the RPE, and choroidal vessels**. Light must pass through the entire retina to reach the photoreceptors where neuronal signals are generated and sent to the brain by ganglion cells via the optic nerve.

Oxygen and nutrients for the inner retina are supplied by dual blood vessels with the primary superficial layer lying at the interface of the nerve fiber layer and ganglion cell layer and the deeper layer located at the border of the inner nuclear layer. In contrast, the outer nuclear layer and photoreceptors, as well as the fovea in humans, remain avascular and receive nutrients and oxygen mainly from the choroidal capillaries.

The choroidal vasculature is a relatively simple arrangement mostly comprising multiple layers of vessel that mainly supply nutrition to the outer retina; these structures are especially important for the photoreceptors, where most of the oxygen from the blood vessels is consumed. Due to its relatively simple structure, researchers have begun to realize the importance of the choroidal vasculature only in recent years, thus making it the main object of this thesis.

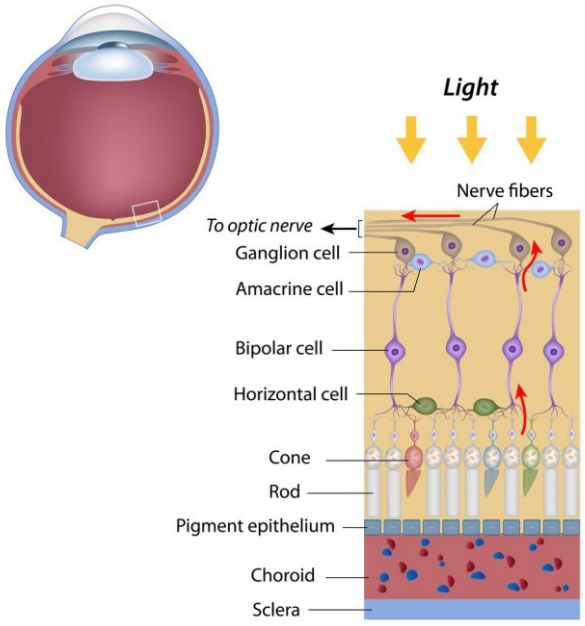

Fig. 1.2.1 The anatomy of the eye. The inner retina includes the retinal vessels, ganglion cell layer, inner nuclear layer and outer nuclear layer, while outer retina consists of photoreceptors (rods and cones), the RPE and choroidal vessels. The figure was reproduced from the website https://discoveryeye.org/layers-of-the-retina/.

1.2.2 Choroid: the blood supply of the outer retina

1.2.2.1 Development of the Choroid in the embryo

Because the choroidal vasculature is the prominent blood supply of the outer retina, it is not surprising that embryonic formation of human choroidal vessels begins much earlier than that of the retinal vasculature. The former commences at about the 4th week of gestation and ends at around the 11th week, whereas the latter is absent until the 16th week of gestation and finishes a few weeks before birth in humans. In newborn mice, the choroidal vasculature is almost complete while the retina is avascular until the first few

weeks after birth [12].

Normal development of human choroid begins at the 4th week of gestation with the formation of the optic cup and the invagination of the lens vesicle [13]. At this moment, the optic cup derived from the neural crest is composed of two layers. The outer layer comprises the future retinal pigment epithelium (RPE), and the inner layer is the progenitor of the neural retina. The surrounding tissue called the mesoderm begins to differentiate into endothelial cells, which are the precursors of the choroidal capillaries, followed by a rapid condensation of the mesoderm at the site of the future choroid and scleral stroma. At the 5th week of gestation, the vascular plexus covers the entire optic cup branching from the posterior pole to the optic rim and is in close contact with the developing RPE in order to differentiate. Until around 8 weeks of gestation, the organization of choroidal structure completes. Therefore, in other words, the choroid derives from different types of cells while the retina and the RPE both derive from the neural ectoderm [14].

The development of the choroidal vasculature continues with long and short posterior ciliary arteries (LPCAs and SPCAs) showing extensive ramifications throughout the choroid. Most of the choroidal structure is formed around the 3rd to 4th months of gestation [15]. Beginning with its formation in uterus, the choroid continues to mature after birth, making it vulnerable to damages when there are defects in the neighboring RPE layer. Thus, in this thesis, we continued to explore the susceptibility of

choroidal vasculature in this scenario.

Table 1.2.1 Differences between retinal and choroidal vasculatures

	Functions	**Embryonic development**	**Flow rate (μL/min)**	**Vasculture resistance**	**Arteriovenous oxygen extract[1]**	**Atery**	**Vein**
Retinal vasculature	Supply the inner retina (2/3)	16th~ 36th week of gestation	Low 40-80	High	High 35-40%	Central retinal artery	Central retinal vein
Choroidal vasculature	Supply the outer retina (1/3)	4th~11th week of gestation	High 1,200~2,000	Low	Low 3-5%	LPCA[2] and SPCA[3]	Vortex vein

[1] The arteriovenous oxygen extract is the difference in oxygen content between the artery and the venous. The value indicates how much oxygen is removed the capillaries to the circulation of the body. [2] LPCA, the lateral posterior choroidal arteries, comprises a branch of the ophthalmic artery that penetrates through the sclera near the equator to supply the choroid, ciliary body and iris [16]. [3]SPCA, the short posterior choroidal arteries, arises from the ophthalmic artery upon crossing the optic nerve to supply the choroid and ciliary processes.

1.2.2.2 Anatomy of the Choroid

The choroid is supplied by 10 to 20 short post-ciliary arteries and 2 long post-ciliary arteries, which penetrate the sclera near the optic nerve and branch out towards the periphery of the eye. Following the curvature of the eyecup, it extends from the margins of the optic nerve to the pars plana, where it continues anteriorly to become the ciliary body. At the cellular level, it is composed mostly of blood vessels, fibroblasts, melanocytes, resident immunocompetent cells, supporting collagenous and elastic

connective tissue. Histologically, the choroid is composed of 5 layers: starting from the inner (retinal) side, these include Bruch's membrane, the choriocapillaris, the two vascular layers (Haller's and Sattler's), and suprachoroidea (Fig. 1.2) [17]. In humans, the thickness of the choroidal vasculature is about 200 μm at birth and decreases to approximately 80 μm by age 90 [18]. Interestingly, the human choroid is the sole blood supply to the fovea. Thus, the choroidal vasculature under the fovea is thickest, ranging between 200~400 μm [19].

Compared to other vessels, choriocapillaris are highly fenestrated with a relatively large diameter (20-40 μm) in humans, which allows proteins to pass through from the retinal side, thereby leading to a high oncotic pressure in the extravascular stroma that facilitates the movement of fluids from the retina to the choroid to maintain homeostasis of the retina [17]. However, these "pores" in the capillaries may also lead to various safety problems especially with treatment applications. For example, in ROP patients receiving bevacizumab (an anti-VEGF agent), serum VEGF levels are found to be low for two weeks, suggesting that this drug is able to penetrate the choriocapillaris and reach the systemic circulation [20].

In addition, the choroid has other unique anatomic features. First, it has a large membrane-lined lacunae, which is able to drain part of the lymph of the eye and change their own volume dramatically, thus altering the thickness of the choroid. Second, it also contains non-vascular smooth muscle cells, mostly under the macular, and the contraction

of this tissue can reduce the thickness of choroid, hence counteracting the thickening caused by the expansion of the lacunae [17, 21, 22]. Finally, by receiving sympathetic, parasympathetic and nitrergic innervation, the choroid contains intrinsic neurons, especially behind the fovea, which control these muscle cells to modulate the choroidal blood-flow [17]. Taken together, all these features can work synergistically to protect the choroidal architecture during accommodation.

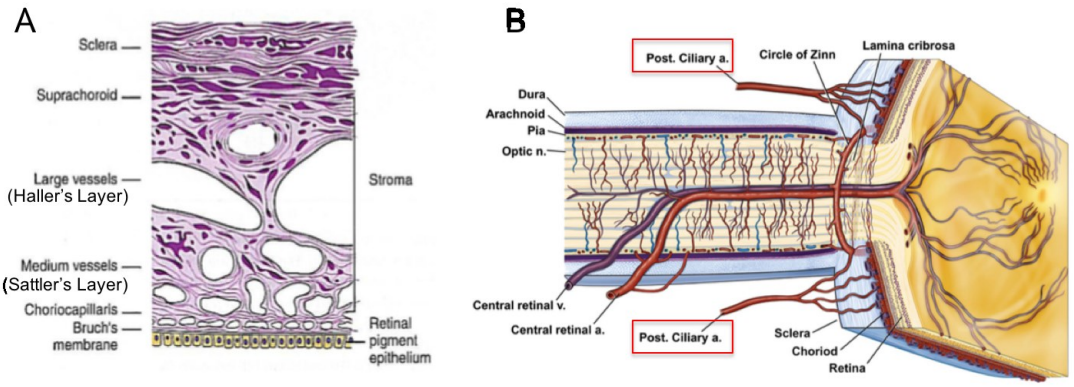

Fig. 1.2.2 Histology of the Choroid and its blood supply. Reproduced from references [17, 23].

1.2.2.3 Functions of the Choroid

As one of the most highly vascularized tissues in our body, the choroid has several functions. First, in species with pigmented choroid, it can absorb excess light, thus protecting the retina against potential damage from excess light. Second, the choroid also participates in around 35% of the aqueous humor drainage from the anterior chamber by the uveoscleral pathway in humans [24]. Third, the choroid is a secretory tissue that synthesizes a number of growth factors necessary for the development, growth, and

maintenance of its vasculature, as well as for ocular growth by influencing the biosynthetic activity of the sclera [17, 25]. Other functions include thermoregulation via heat dissipation and modulation of intraocular pressure (IOP) via vasomotor control of blood flow.

However, the main function of the choroid has traditionally been considered as the sole supplier of oxygen and nutrients to the outer retina, especially to the photoreceptors, which are extremely metabolically active, particularly in darkness when light-gated channels are open [26]. Accordingly, more than 90% of oxygen delivered to the retina is consumed by photoreceptors, among which 90% is supplied by the choroidal vasculature [27]. Intriguingly, the choroid is able to maintain a high oxygen tension with an arterial/venous value of only 3% versus 35% for retinal blood flow, and it is probably one of the highest tissue in terms of oxygen content per unit tissue weight, ten-fold higher than the brain [17, 28]. In general, intraretinal oxygen tension decreases rapidly as the tissue-choroid distance increases. The RPE and outer segments of photoreceptors have the highest oxygen tension, which drops quickly to almost zero at inner segments of the photoreceptors [29]. Moreover, intimate contact between the choroid, RPE, and photoreceptors is very important for sufficient energy supply to the latter. In addition, choroidal circulation has one of the highest perfusion rates in the body (1,200 ~ 2,000 μl/min), while retinal blood flow has a low rate of 40 ~ 80 μl/min [28].

1.2.2.4 Pathologies of the Choroid

With the development of optical coherence tomography (OCT), our understanding of the choroid and its role in diseases has significantly improved. As the most vascularized tissue in the eye, the choroid plays a critical role in the pathologies of various ocular diseases. Given that the choroid is a dynamic tissue, it can be afflicted (thinning or thickening) by many factors in diseases. A detailed pathology-disease list is provided in Table 1.2.1.

Table 1.2.2 Summary of associated choroidal disorders in diseases

Pathologies	Diseases
Choroidal thinning	1. Retinopathy of prematurity (ROP)[30]; 2. Diabetic retinopathy [31]; 3. Myopia [32, 33]; 4. Alzheimer's disease [34]; 5. Geographic atrophy [35]; 6. Non-arteritic anterior ischemic optic neuropathy [36]; 7. Retinitis pigmentosa [37].
Choroidal neovascularization (CNV)	1. "Wet" Age-related macular degeneration (AMD); 2. Vogt-Koyanagi-Harada (VKH) disease [38]; 3. Central serous chorioretinopathy (CSC)[39]; 4. Pathologic Myopia (PM) [40] ; 5. Uveitis [41]; 6. Ocular trauma [42]; 7. Ocular histoplasmosis syndrome (OHS) [43]; 8. Idiopathic disease [44]; 9. Malignant melanoma [45].

1.2.2.5 Choroidal neovascularization (CNV) and its animal models

As a major cause of vision loss, choroidal neovascularization (CNV) results from many diseases such as "wet" AMD, which is the leading cause of blindness in individuals 65 years or older in developed countries [46]. Although retinal angiogenesis contributes

to about 6% of CNV cases [47], CNV mainly results from abnormal new vessels from the choroid growing through the Bruch's membrane into the retinal pigment epithelium (type 1), sub-retinal space (type 2), or both (type 3) [48], where these blood vessels may leak fluid and ultimately lead to the detachment of the retina.

Although etiologically heterogeneous, major sequela results from the dynamic process of choroidal angiogenesis, which depends on the balance of angiogenic promoters and inhibitors. In general, the mechanisms involved in the formation of CNV fall into three categories: inflammation, angiogenesis, and proteolysis [49]. In the "classical" mechanism of CNV, macrophages are considered to be a key initiating factor. At the very early initiation period, the RPE increases its secretion of VEGF, a major stimulator of CNV [50], as well as monocyte chemoattractant protein (MCP) and IL-8 [51, 52]. These latter factors attract monocytes (macrophages) from the choriocapillaris along the outer surface of the Bruch's membrane. Aggregating around the site of vessel growth and defected areas in the Bruch's membrane, these macrophages produce tumor necrosis factor α (TNFα), stimulating RPEs to secrete more IL-8, MCP, and VEGF. Though counteracted by inhibitory factors including pigment epithelium-derived factor (PEDF), a higher level of VEGF promotes the proliferation and migration of vascular endothelial cells to form new vessels, which may penetrate the Bruch's membrane.

After initiation, however, the CNV is able to maintain a certain size despite the active inflammation. At this moment, macrophages and the vascular endothelium release

matrix metalloproteinases (MMP), which are a family of extracellular matrix-digesting enzymes that enables CNV to degrade tissue planes [53]. Meanwhile, the MMPs can be inhibited by tissue inhibitors of metalloproteinases (TIMPs) secreted by RPEs [53]. During this process, MMP9 and TIMP3 in particular are abundantly expressed. In addition, macrophages are capable of producing tissue factor, which is a protein that modulates fibrinogenesis to form a fibrin scaffold upon which CNV grows [54]. Moreover, angiopoietins (Ang I and Ang II) and their receptors (Tie1 and Tie2) as well as other growth factors such as fibroblast growth factor (FGF) are expressed by RPEs and vascular endothelium. In particular, transforming growth factor beta (TGFβ), which limits the margin of CNV, is also produced by RPEs at the site of CNV. As a result, the balance among Ang I and Ang II, VEGF and PEDF, MMPs and TIMPs, fibrin and other factors lead to a stable CNV in the active stage.

Later on, at one point, the balance shifts towards an anti-angiogenic, anti-proteolytic and anti-migratory phenotype, leading to the formation of a disciform scar as observed by Holloway and Verhoeff [55] in 1928. These changes are mostly mediated by RPEs, which decrease production of the factors mentioned above and shift towards the production of TGFβ and TIMP3 [48], both of which have profound effects during fibrosis [56]. Taken together, it is the RPE that initiates, stabilizes and involutes CNV, acting as a “traffic cop” in these process [48]. **Consequently, this study primarily focuses on the role of RPEs in the development of CNV.**

Currently, CNV treatments include anti-VEGF drugs (such as RhuFABV), thermal laser treatment and photodynamic therapy (PDT), among which intravitreal injection of anti-VEGF drugs has been considered as the main therapy in disease management. However, only 30% of patients respond well to recover partial vision following treatment of the anti-VEGF drug (Ranibizumab or Bevacizumab)[4]. Moreover, undesired side effects are also observed, such as atrophy of the retina and RPE cells [57, 58] as well as reduced choriocapillaris size [59]. In general, all these treatments are targeting the consequence (neovascularization) in the development of associated diseases, rather than the causative event underlying the diseases. Even worse, they are of high cost both to the family and the society. For these reasons, it is crucial to improve our understanding of CNV and explore new treatments that target its causative events.

Animal models are of great value for enhancing our understanding of various pathologies. After the first model of CNV was developed in primates [60], various models have been developed in rodents, pigs, and rabbits. Herein, we mainly focus on the rodent models. Currently, the most widely used model is laser-induced CNV. Depending on the specific experiments, the laser treatment parameters may vary. In general, adult mice are anesthetized and their pupils dilated. Laser photocoagulation is administered to the posterior retina through a slit lamp. The criteria of laser treatment include a spot size of 50 μm, a power of 350-400 mW, and 0.05s of exposure. The formation of bubbles demonstrates that Bruch's membrane is successfully ruptured along with all the layers of

the choroidal vasculature within the burn site. One week after laser treatment, over 80% of the lesions contain CNV characterized by large lumens and fenestrations. These new vessels continue to grow into the subretinal space, where some are enveloped by the RPE. Despite its wide experimental use, this model also has its limitations. For example, the mouse eyes are otherwise healthy, thus the environment of the retina and the choroid does not mimic the pathological changes in humans. Moreover, injury-induced angiogenesis does not necessarily reflect the same mechanisms of angiogenesis occurring in human diseases [61]. Other models of CNV include various surgically induced models as well as several knockout and transgenic mouse models (Table 1.2.2).

Though various animal models have been found to develop CNV with different underlying mechanisms (Table 1.2.2), it is noteworthy that there is no perfect animal model, and none of these models accurately reproduce all the clinical features of CNV. Nevertheless, they have been employed successfully to vastly increase our knowledge of this pathology and potentially enrich the treatment options. **In this thesis, a novel model of CNV will be described in detail: aged mice deficient in the lactate receptor GPR81 display choroidal neovascularization.**

Table 1.2.3 Summary of current rodent models for CNV

Categories	Mice	Description
Surgically induced	Matrigel	Subretinal injection of Matrigel induces various degrees of CNV as well as RPE and photoreceptor degeneration in mice [62].
	PEG-8 injection	Subretinal injection of polyethylene glycol (PEG-8) leads to the formation of CNV by activating the complement cascade in mice [63].
	Macrophage injection	Subretinal injection of macrophages in mice results in the fibrosis of choroidal vessels in CNV [64].
	Lipid hydroperoxide injection	Subretinal injection of HpODE, an oxidized lipid isolated from old humans, leads to CNV in rats after 3 weeks [65].
	VEGF transgenic	Subretinal injection of adenovirus vectors expressing VEGF induces CNV in rats after 4 weeks following injection [66]. The transient CNV can be sustained as late as 20 months after injection [67]. It is worth noting that the rupture of Bruch's membrane was included in this protocol.
	$VEGF_{164}$RPE65	Mice with overexpression of $VEGF_{164}$ in the RPE develop intrachoroidal neovascularization [68], supporting the idea that overexpression of VEGF by the retina or RPE is not sufficient to elicit CNV in these models because of the key role of a compromised Bruch's membrane in the development [69, 70].
	TGF β deletion	Transforming growth factor (TGF)-β plays important roles in a variety of changes in tissues including angiogenesis and fibrosis. Conditional deletion of TGF β signaling in the entire eye, the RPE, or the vascular endothelium induces CNV, both in newborns and in 3-week-old mice [71].
	Prokineticin 1 (hPK1) transgenic	Recently, hPK1 was found to be a mitogen of fenestrated endothelium. While the choriocapillaris is the only set of fenestrated

	mice	vessels in the eye, overexpression of hPK1 in mice was found to lead to CNV at 8 months [72].
Chemokines	$Ccl2^{-/-}$ and $Ccr2^{-/-}$	Double knockout of Ccl2 and its receptor Ccr2 in mice enables macrophages to be recruited to the area of the RPE and Bruch's membrane, leading to approximately 25% of the mice to develop CNV [73].
	$Cx3cr1^{-/-}$	Cx3cr1 is found to be expressed only in microglial cells in the retina. Spontaneous CNV is not found in $Cx3cr1^{-/-}$ mice. However, laser-induced CNV in $Cx3cr1^{-/-}$ mice leads to a larger area of neovascularization (two-fold greater) than in controls [49, 74].
Oxidative damage	$SOD1^{-/-}$	10% of Cu, Zn-superoxide dismutase (SOD1)-deficient mice show occurrence of CNV, which appears to connect with retinal vessels at 16 months old [75].
	$NRF2^{-/-}$	Nuclear factor erythroid-related factor 2 (NRF2) is a key transcription factor that plays an important role in antioxidant and detoxification in the body. After 12 months, $NRF2^{-/-}$ mice display spontaneous CNV as well as drusen-like deposits [76].
	$Cp^{-/-}Heph^{-/-}$	Ceruloplasmin (Cp) and its homolog hephaestin (Heph) are important for retinal iron homeostasis. $Cp^{-/-}Heph^{-/-}$ mice display iron overload in the retina as well as RPE hypertrophy, photoreceptor degeneration, and subretinal neovascularization [77].
Lipid metabolism	ApoE overexpression with high fat	ApoE overexpression transgenic mice fed a high-fat diet develops CNV (19% of males and 18% of females) in addition to drusen [78].
	$Vldr^{-/-}$	The very-low-density lipoprotein receptor (vldr) is found to be abundant in RPE [79], which is important for digesting shed-membrane of photoreceptors. $Vldr^{-/-}$ mice develop retinal angiomatous proliferation (RAP) with new blood vessels originating from the outer plexiform layer of the retina and formation of choroidal anastomoses by 3 months [80].

Genetic mutation	sCNV mouse (JR5558 line)	Spontaneous CNV mice (mutant JR5558 line) carry a mutation in rd8, manifesting multifocal, bilateral spontaneous CNV as early as P10 [81].

1.2.2.6 Choroidal thinning in ROP and its animal models

Every year, about 15 million babies globally are born premature (i.e., less than 37 weeks of gestational age) [82], leading to the prevalence of retinopathy of prematurity (ROP). In fact, ROP is the primary cause of visual impairment and blindness in neonates and young children in developed countries [83]. It is mainly characterized by aberrant blood vessel growth in the retina, leading to blindness due to retinal detachment in severe cases.

However, another key component of ROP--choroidal thinning (i.e., choroidal involution) has been ignored for many years. In 2011, for the first time, our lab discovered that in contrast to proliferative retinal vessels, the choroidal vasculature underpins degeneration in rats [30]. Subsequent studies have demonstrated that choroidal thinning is persistent throughout life [84]. Moreover, these findings have been confirmed by clinical research [85]. **Given the prevalence of choroidal thinning (in ROP) and the location of GPR81 in the RPE, it will be very interesting to investigate whether hyperoxia has effects on the choroid in GPR81-deficient mice. Thus, in this study, we applied oxygen exposure as a prolonged stress to exacerbate the pathological progress of CNV.**

Regarding the animal models, oxygen-induced retinopathy (OIR) is the most

common animal model of ROP. Because of our need for genetic manipulations, we utilized the mice. Briefly, neonatal mice are exposed to 75% oxygen from P7 to P12, triggering the loss of immature retinal vessels and reducing the pace of normal retinal vessels developments, leading to the formation of a central avascular zone of vaso-obliteration [86]. After mice are returned to room air at P12, the central avascular area becomes hypoxic, inducing the abundant production of VEGF as well as the formation of extraretinal neovascularization (NV). NV reaches its maximum severity at P17, and then starts to regress and vanishes by P25. In our studies, the same protocol (OIR mice) is applied to induce thinning of the choroid in mice, while age-matched controls are maintained at room air throughout the studies.

1.2.3 The retinal pigment epithelium (RPE): the outer blood-retinal barrier (BRB)

As described in section 1.2.2.4, it is the RPE that initiates, stabilizes and involutes CNV. Thus, in the following sections, the RPE will be introduced.

1.2.3.1 Anatomy of the RPE

As a key component of the blood-retinal barrier (BRB), the RPE appears as a single layer of hexagonal cells shaped like a honey-comb when viewed en face (as shown in flat mounts). Pigmented RPE contains melanin that can absorb excess light entering the retina. The RPE has two types of microvilli [87]: long microvilli that maximize the apical surface for epithelial transport and short microvilli that participate in the phagocytosis of photoreceptor outer segments. Meanwhile, distribution of RPEs is anatomically variable

in terms of number and morphology. For example, macular RPEs are smaller at 14 μm in diameter and a height of 12 μm compared with those in the periphery at 60 μm in diameter with variable heights. In contrast, the number of photoreceptors per RPE and the RPE phagocytic load are higher in the macula compared to that in the periphery.

Given the absence of a macula in mice and the pivotal role of the RPE in macular associated diseases such as AMD, questions may be raised regarding the rationality of using mice in this research. Though mice do not have a macula, their central retinas do share some similarities with human macula. For example, like the human macula, the central retina of the mouse has a higher photoreceptor density and a thicker Bruch's membrane as well as a smaller size of RPE, compared to the periphery [88]. Moreover, the mouse RPE actually has a higher phagocytic load than human RPEs. In addition, both tissues contain bi-nucleated RPEs [89]. In humans, around 3% of RPE cells in the area of perifovea are binucleated [90, 91], while in the central region of the retina, around 60%-75% of RPE cells are binucleated in newborn pups.

Thus, these features of mice make them a reasonable model to perform associated studies.

1.2.3.2 Function of the RPE

Due to its polarity, the RPE is a multifunctional and critical layer in the eye. For example, the RPE together with Bruch's membrane establish the blood-retinal barrier, which plays critical roles in strictly controlling the fluids and solutes that cross the BRB

as well as preventing toxins and plasma components from entering the retina, thus ensuring the integrity of the retina. Other functions [87] include 1) light absorbance and protection of the retina against photo-oxidation; 2) transport of nutrients, water, iron, and oxygen; 3) maintenance of glial cells function by shuttling K^+; 4) uptake of all-*trans*-retinal (vitamin A) from the choroid and its isomerization into 11-*cis*-retinal to maintain the visual cycle; 4) phagocytosis of the outer segments of photoreceptors; 5) secretion of growth factors that maintain the integrity of both photoreceptors and choroidal vasculature, as well as various chemokines that modulate the immune response. Given the vital role of the RPE in the integrity of the choroid, we mainly focus on its "secretory" function, which that has been extensively studied in AMD.

1.2.4 Interplay between the choroid, RPE, and photoreceptors

The choroid, RPEs, and photoreceptors are intimately connected and together maintain homeostasis in the outer retina. Thus, it is not surprising that any change in one component can affect the rest.

As the sole supplier of oxygen and nutrients to the RPE and photoreceptors, any dramatic changes in choroidal blood vessels may exert profound effects on the RPE and photoreceptors. For example, significant choroidal thinning in ROP results in RPE atrophy and photoreceptor disruption in aged rats [84]. Complementarily, defects in the RPE affect the status of choroidal vasculature and photoreceptors, a phenomenon which has been well documented in AMD [92]. In addition, it is also known that photoreceptors

may exert some toxic effects on RPE cells. For example, expression of a mutant human ELOVL4 gene in photoreceptors impairs the phagolysosomal maturation in RPE cells prior to photoreceptor loss [93].

Consequently, in our studies, all of these three elements, the choroidal vasculature, RPE morphology and photoreceptor thickness, were examined.

1.2.5 L-lactate: an emerging critical signaling molecule

Once considered as a waste product of glycolysis, L-lactate has recently been recognized as an emerging critical signaling molecular with multiple functions including energy regulation, memory formation [94], immune tolerance [95], ischemic tissue injury [10], wound healing, as well as cancer growth and metastasis [96, 97]. As mentioned above, the retina is one of the most energy-demanding tissues per unit mass. Surprisingly, aerobic glycolysis is found to be the main pathway for producing energy both in the retina and outer retina [98-100]. In fact, aerobic glycolysis accounts for 80-96% of glucose consumption in the retina [99, 101]. Given that lactate is the main aerobic glycolysis metabolite and is found primarily in photoreceptors, where oxygen tension declines dramatically [99], **its effects in the outer retina are of particular interest in our study.**

1.2.5.1 The production of lactate and its shuttle

As one of the main energy sources, lactate is **normally** produced from glucose in the absence of oxygen (anaerobic condition). At the very beginning of this process, glucose is

metabolized to the intermediate metabolite pyruvate in the cytoplasm. Under aerobic conditions, pyruvate enters the mitochondria and is converted to acetyl CoA, which enters the Kreb's cycle to produce ATP. Under anaerobic conditions, however, pyruvate is converted into lactate by lactate dehydrogenase (LDH), although this process is reversible.

Interestingly, lactate can also be produced by aerobic glycolysis (**abnormally produced**). The term aerobic glycolysis was proposed by Otto Warburg in the early 19th century to describe the special metabolism found in tumor cells. He noticed that cancer cells preferred to convert glucose into lactate even in the presence of oxygen, in contrast to normal cells, where the conversion of glucose to lactate mainly occurred under hypoxic conditions. Thus, he defined the metabolism of tumor cells as aerobic glycolysis to indicate that the conversion of glucose to lactate is not determined by a lack of oxygen [102]. The effects of aerobic glycolysis, apparently, go beyond energy production. In fact, through its transporters (MCTs, monocarboxylate transporters) and receptor (GPR81), lactate has been identified as a signaling molecule with diverse functional effects (Table 2.3).

In the human body, the level of blood lactate is usually maintained between 1-20 mM [103], most of which is produced within muscles, especially during intensive exercise. Some tissues and cells, such as adipocytes [104] and astrocytes [105], are capable of producing higher levels of lactate under physiological conditions. High levels

of lactate can be converted to glycogen in the liver for energy storage. This process is known as the Cori cycle. In the outer retina, as mentioned in section 2.5, lactate is mainly produced in photoreceptors, and subsequently taken up by RPE cells before entering the blood flow via the choroidal vasculature.

1.2.5.2 The monocarboxylate transporters (MCTs): transporters of lactate

The proton-linked monocarboxylate transporters (MCTs) are a class of important transporters that facilitate the shuttling of short-chain monocarboxylates such as L-lactate, pyruvate and ketone bodies across the plasma membrane. To date, 14 members have been identified [106], among which the most well studied are MCT1-4, which include 12 transmembrane proteins. Though their distributions, functions, and affinities to lactate are cell- and tissue- dependent, MCT1-4 all follow some general rules. For example, in general, the most universally distributed MCT1 is preferentially responsible for lactate uptake, while MCT4 is the most highly expressed in muscle and mainly functions to export intracellular lactate. MCT2 and MCT3 show more restricted expression patterns and shuttle lactate bidirectionally.

MCTs are essential in the regulation of many fundamental cellular processes including pH maintenance, respiration, glycolysis, and gluconeogenesis. Inhibition of MCTs ultimately leads to decreases in glycolytic metabolism, migration, and invasion, affecting proliferation and inducing cell death [107, 108]. So far, several MCT inhibitors are in clinical trial. **The effects of lactate transport via MCTs are not the study focus**

in this thesis, because lactate can also activate its receptor G protein-coupled receptor 81 (GPR81), triggering a series of cascades that could represent attractive therapeutic targets for the treatment of diseases. Moreover, drugs targeting G-protein-coupled-receptors GPCRs (108 in total) account for about 34% of FDA-approved drugs (475 in total) in the market [109].

1.2.5.3 G protein-coupled receptor 81 (GPR81): the lactate receptor

1.2.5.3.1 Importance of G protein-coupled receptors (GPCRs)

G protein-coupled receptors (GPCRs) are one of the largest and most ubiquitously expressed families of receptors in humans and animals [110]. Accounting for about 4% of the human protein-coding genome, they are intimately involved in the functions of daily life by regulating a variety of physiological processes, including vision, smell, hearing, taste, endocrine, cardiovascular and reproductive homeostasis [111]. Though more than half of the GPCRs are associated with odor, around 210 receptors have so far been identified with their ligands, while the ligands and biological functions of more than 100 orphan receptors remain unknown [112]. Interestingly, the identified ligands activating GPCRs are very diverse, including proteins, peptides, lipids, small molecules, ions, and photons [113]. For example, in recent decades, basic energy metabolism substrates, such as free fatty acids and the Kreb's cycle intermediate succinate, have been found to activate GPCRs [114, 115]. Malfunctions of GPCRs are involved in many diseases such as diabetes, cancer, hypertension, and obesity [116]. Thus, GPCRs are relevant drug

targets, with GPCRs-targeted drugs (108 in total) accounting for about 34% of FDA-approved drugs (475 in total) in the market [109].

Characterized by a central core composed of seven transmembrane alpha helices with an extracellular N- and intracellular C-termini [117], most GPCRs share a common mechanism of action: receptor activation initiates signal transduction across the cell membrane, which then activates the intracellular heterotrimeric GTP-binding proteins (G protein, Gα, Gβ/Gγ subunits), followed by the Gα and/or Gβ/Gγ subunits transducing these signals to appropriate downstream effectors [116]. In addition, some GPCRs can also transduce signals through pathways independent of G proteins. For example, activation of GCR1 (a GPCR found in plants) can act independently of G proteins in response to brassinosteroids and gibberellins in Arabidopsis seed germination [118].

Given the importance of GPCRs and their involvement in metabolism, we focused on the lactate receptor GPR81.

1.2.5.3.2 G-protein-coupled receptor 81 (GPR81)

GPR81 was discovered in 2001 [119] and was deorphanized with the identification of lactate as its endogenous ligand in 2008 [120]. Also known as HCA1, GPR81 is a member of the hydroxycarboxylic acid receptors family (HCAs, the other members are GPR109A and GPR109B) [121]. Like other classical GPCRs, it is a seven-transmembrane protein but is coupled with G_i protein (a type of Gα subunit protein) [122]. Several agonists have been identified, including lactate (EC50: 5mM) [120] and

3,5-Dihydroxybenzoic acid (DHBA, EC50:~150 μM) [123]. Activation of GPR81 displays a wide variety of fundamental biological functions (Table 2.3). For example, exercise produces abundant lactate, which activates its receptor GPR81, resulting in elevation of cerebral VEGF and thereby angiogenesis [124], thus improving brain function, especially in the elderly [125]. In particular, GPR81 plays a pivotal role in pathological conditions, especially in cancers [96, 97, 126-129]. Interestingly, although both GPR81 and its homologue GPR109A suppress lipolysis in mice, GPR81 does not have the side effect of cutaneous flushing, making it a potential drug target for the treatment of dyslipidemia [130]. Given the diverse functions and importance of GPR81, it has recently received increasing attention in various research fields.

Our preliminary data suggested that GPR81 is abundantly expressed in RPE cells in the outer retina (data not shown here). Thus, **we mainly focus on the function of GPR81 activation in RPE and its effects on choroidal vascular and photoreceptors.**

Table 1.2.4 Biological functions of L-lactate via GPR81 or MCTs

Functions	Tissues and references
Anti-inflammation	In hepatic and pancreatic inflammation[131], the female productive tract to prevent HIV acquisition [132], intestinal inflammation [133], chronic inflammation by inhibition of T cell migration [134];
Anti-lipolysis	In fat cells [135], in a mouse model of obesity [136, 137], improving the sensitivity of insulin in mouse models of type 2 diabetes [137];
Pro-angiogenesis	Promoting wound healing [10, 138], enhancing collagen accumulation [138]; promoting angiogenesis in breast cancer [127];
Proliferation	In ischemic brain injury, low levels of lactate (1-3 mM) promote apoptosis

/Apoptosis	while higher concentrations (~20 mM) promote survival [139]; targeting MCTs* selectively kills hypoxic tumor cells in mice [136]; in cancer around 40 mM lactate induce cancer cell growth and metastasis [129, 140];
Hypertension	Activating GPR81 lowers the level of free fatty acid, but simultaneously induces hypertension in mice [137];
Modulating the function of neurons	Lactate stimulates the release of neurotransmitters between synapses [141] and mediates glia-neuronal signaling in the brain [142]; aerobic glycolysis is pivotal in the brain and mediates memory formation [143];
DNA repair	Activating GPR81 enhances DNA repair and modulates the resistance of cervical carcinoma cells to anticancer drugs via inhibition of histone deacetylase [128]; stimulation of GPR81 affects DNA repair capacity in breast cancer cells via activation of protein kinase C [126];

* effects via MCTs, otherwise via GPR81

1.2.6 The integrated stress response (ISR) pathway

Cellular homeostasis is a dynamic process that maintains both intrinsic and extrinsic environments in relatively steady states, which demands that cells continuously adapt to various fluctuations including temperature, pH, iron concentration, oxygen tension, redox potential, chemical cues, metabolite concentrations, hormones, cytokines, neurotransmitters and microbial pathogens [144]. Over a certain “threshold”, however, these fluctuations are recognized as “stresses” by cells, and the cellular response to such stresses determines the fate of the cells: survival or death [144].

In response to stress, cells attempt to protect themselves against potential damages by undertaking prompt changes to accommodate metabolic requirements. This adaptation can be controlled by multiple stress pathways [144]. In eukaryotic cells, one key stress

pathway is the integrated stress response, which is a complex and common adaptive signaling pathway in response to diverse stresses, including extrinsic factors (e.g. amino acid deprivation, glucose deprivation, hypoxia and viral infection) and intrinsic factors (e.g. endoplasmic reticulum (ER) stress and oxidative stress) [145]. Depending on the intensity and duration of the stress, activation of the ISR pathway can function either to protect the cells or lead to cellular death. In the scenario of mild or short-term stress that is within a cell's capacity, ISR pathway activation facilitates cellular protection and restores cellular homeostasis, while intense or prolonged stress leads to pathological conditions, such as cancer [146, 147] and Alzheimer's disease [148].

The core event of the ISR pathway is phosphorylation of the alpha subunit of eukaryotic translation initiation factor 2 (eIF2α) at serine 51, which can be activated by one of the four kinases, namely: general control non-depressible 2 (GCN2), double-stranded RNA-dependent protein kinase (PKR), heme-regulated inhibitor (HRI) and PKR-like endoplasmic reticulum kinase (PERK), each of which serve as a sensor of different stress stimuli [145]. Phosphorylated eIF2α leads to the transcriptional enhancement of a cohort of genes, accompanied by a global decrease in protein synthesis with the exception of activating translation factor 4 (ATF4), which then induces the expression of its target genes, thereby promoting cellular survival during stress. At some point, it is necessary for cells to restore protein synthesis and normal functioning by terminating the ISR pathway (i.e. eIF2α dephosphorylation) [149], which can be achieved

via the constitutive repressor of eIF2α phosphorylation (CReP) and the growth arrest and DNA damage-inducible protein (GADD34) (Fig. 1.3) [145].

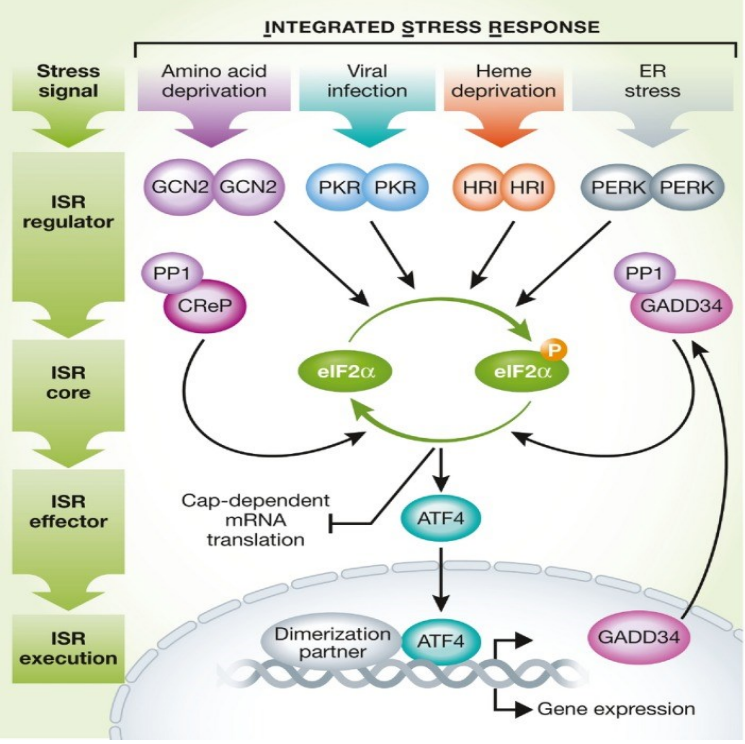

Fig. 1.2.3 The integrated stress response signaling pathway. Adapted from reference [145].

1.2.6.1 The core of the ISR pathway: eIF2α

Under the unstressed conditions, the eIF2 complex plays a critical role in initiating mRNA translation and recognizing AUG start codon [145]. It has 3 subunits (eIF2α, eIF2β, eIF2γ), among which eIF2α is the primary regulatory subunit, as it comprises both the phosphorylation and mRNA binding site. Along with GTP, Met-tRNA$_i$ that binds the

40S ribosome subunit and two small initiation factors, eIF1 and eIF1A, the eIF2 complex forms the 43S pre-initiation complex (PIC), which is then recruited to the 5′methylguanine cap of mRNA mainly by the eIF4 complex. The PIC is stabilized by the interaction between eIF4 complex and eIF3 and then migrates to the AUG start codon and begins the translation until the Met-tRNAi anticodon binds to the AUG start codon, followed by the dissociation of eIF1 from the complex and GTP hydrolysis on the eIF2 complex. As a result, the eIF2-GDP complex dissociates from the 40S ribosomal complex and is recycled for another round of mRNA translation initiation with the conversion to its active form eIF2-GTP complex, a process catalyzed by eIF2B.

In the ISR pathway, phosphorylation of eIF2α prevents the eIF2B-mediated exchange of GDP for GTP, thus blocking the formation of the 43S PIC, which then leads to a global arrest of 5′Cap-dependent protein synthesis except for the translation of certain mRNAs that have a short upstream open reading frame in their 5′ untranslated region. Examples of such examples include ATF4, ATF5, CHOP, and GADD34, as these mRNA translations deploy mechanisms other than the cap recognition by the eIF4 complex [150, 151].

Phosphorylation of eIF2α usually occurs at serine 51 [145]. Mice with mutations at that site (i.e., a residue unable to be phosphorylated) die shortly after birth due to hypoglycemia, suggesting that phosphorylation of eIF2α is necessary for the induction of gluconeogenic enzymes and insulin to maintain glucose homeostasis [152]. In addition,

phosphorylation of eIF2α has been shown to protect cells against ER stress and oxidative stress, as demonstrated by the fact that maintaining eIF2α S51A/S51A MEF cells (which are hypersensitive to ER stress) requires supplementation with amino acids and a reductive agent [152]. Therefore, selective enhancement of eIF2α phosphorylation, either by activating upstream kinases in the absence of stress or by inhibiting eIF2α dephosphorylation using phosphatase inhibitors, may produce beneficial effects in some pathological conditions. For example, halofuginone, an activator of the GCN2 kinase, is a potent inhibitor of angiogenesis [153] that can increase the chemosensitivity of cancer cells and reduce the fibrosis and tissue regeneration in cancer [154, 155]. In contrast, an inhibitor of GADD34 and CReP, salubrinal, protects cells against ER stress [156] and causes attenuation of β-amyloid-induced neuronal death in a mouse model of Alzheimer's disease [157]. Inhibition of ISR signaling, represents another strategy to treat neurodegenerative diseases, resistant cancers and diabetes [145]. For instance, GSK inhibitors (i.e., GSK2606414 and GSK2656157) that inhibit eIF2α kinases, have been found to exhibit antitumor activity mediated by trapping PERK and preventing its autophosphorylation, as the active form of the latter is involved in the proliferation of cancer cells [158, 159]. **The integrated stress response inhibitor (ISRIB), a small molecule that will be used in our project, decreases cellular sensitivity in response to phosphorylated eIF2α, thereby attenuating the synthesis of ATF4 and restoring protein synthesis capacity, impairing cellular adaption to chronic ER stress** [160].

More importantly, ISRIB seems to be a promising drug for the treatment of memory disorders in particular, as it can significantly increase cognitive memory [161-164].

1.2.6.2 ATF4: the best-characterized effector of the ISR

In stressed cells, phosphorylated eIF2α regulates ATF4, a basic leucine zipper (bZIP) transcription factor and a member of the activating transcription factor/cyclic AMP response element binding protein (AFE/CREB family) [165]. Levels of ATF4 are transcriptionally, translationally and post-translationally regulated. In fact, ATF4 plays a critical role in deciding the cellular fate upon ISR activation. By transcribing its target genes selectively, ATF4 tailors cellular outcomes depending on the stress and the cellular context.

In normal cells, ATF4 is usually maintained at a low level due to its instability with a half-life of < 1 h [166]. Upon ISR activation, more ATF4 mRNA is transcribed and translated with some post-translational modifications (e.g., phosphorylation) enhancing its protein stability [145]. Elevated ATF4 then enters the nucleus, selectively activating downstream gene expression for cellular adaptation depending on the context. Such target genes include asparagine synthetase (Asns), tribbles homolog 3 (Trib3), C/EBP homologous protein (CHOP), activating transcriptional factor 3 (ATF3) and others.

Notably, these adaptive genes have different functions regarding cellular fate. For instance, Asns, a suppressor of apoptosis, promotes survival in cancer [167, 168], and Trib3, together with ATF4, prevents ATF4-induced apoptosis in prostate cancer cells

[169]. In contrast, ATF3 enhances apoptosis in ovarian cancer cells [170] and Hela cells [171]. ATF4/CHOP exerts a dual effect depending on cell type. For example, ATF4/CHOP induces apoptotic effects during prolonged ER stress in cancers and diabetes, through induction of pro-apoptotic genes [172-174] while inducing proliferation in vascular smooth muscle cells [175] and hepatocellular carcinoma [176]. Taken together, the levels of these adaptive genes vary to tune the cellular outcome in response to ISR activation.

As ATF4 is a critical element of the ISR, it is important to elucidate its essential functions in addition to its transcriptional activity. $ATF4^{-/-}$ mice are mostly used for this purpose, and studies suggest that AFT4 actually has a pivotal role in normal development as well as pathological conditions. It regulates normal metabolic and redox processes [177] to mediate glucose homeostasis [178], obesity, energy expenditure [179] and neural plasticity [180]. Moreover, ATF4 also regulates normal cellular proliferation. For instance, null $ATF4^{-/-}$ mice display severe anemia with pale and hypoplasic livers due to growth retardation during fetal-liver hematopoiesis [181]. Deficiency of ATF4 in mice also leads to a malformed embryonic lens that can develop into severe microphthalmia in adults [182, 183]. Recently, investigators have found that aging increases the level of ATF4 [184], and the latter is proposed to mediate age-related muscle weakness and atrophy [185], making it a promising target for muscular atrophy.

Though ATF4 is implicated in many diseases, its role in ocular diseases is our main

study focus [186]. Several studies have reported that ATF4 is significantly elevated in inheritable diseases and degenerative retina with particular effects on photoreceptor death in several diseases [187-189]. For example, Bhootada, Y., et al., have observed that overexpression of ATF4 leads to photoreceptor loss while its knockout prolongs photoreceptor survival in autosomal dominant retinitis pigmentosa [190]. Moreover, ATF4 has been proposed as a marker for proliferative diabetic retinopathy as well as a new therapeutic target, as the inhibition of ATF4 attenuates high-glucose-induced-inflammation and vascular leakage [191]. In hypoxic retina, deficiency of ATF4 in a mouse model of retinopathy of prematurity (ROP) dramatically attenuates neovascularization [192], suggesting that ATF4 is a key promoter of angiogenesis [193, 194]. ATF4 also seems to be involved in dry age-related macular degeneration (AMD), as drusen (the hallmark of dry AMD) induces ATF4 production [195].

Taken together, ATF4 is necessary for normal cellular function, but its over-expression aggravates pathological conditions, thus making it a potential therapeutic target. **The present study found young GPR81$^{-/-}$ mice showed choroidal degeneration due to ATF4 elevation induced by ISR activation in response to oxidative stress and ER stress. Such stress in the long term leads to choroidal neovascularization in aged GPR81$^{-/-}$ mice.**

Chapter 2: HYPOTHESIS & OBJECTIVES

Hypothesis

Intravitreal injection of anti-VEGF agents remains one of the main treatments of "wet" AMD. However, around 70% of patients do not respond well, suggesting that urgent development of alternative treatments is required.

Given the fact that the retina is one of the most energy-demanding tissues and consumes the most oxygen per tissue weight, metabolism disturbance is considered as a key contributor to ocular pathological conditions. Therefore, it is of great importance to elucidate the interplays between metabolic receptors and ocular pathologies.

Recently, a substantial amount of studies have unveiled that lactate, rather than simply a "body waste", is a signaling molecule that via GPR81 triggers tremendous cellular signaling cascades that are involved in inflammation, angiogenesis, apoptosis, glucose homeostasis, and lipid metabolism. It also plays a pivotal role in many pathological conditions, especially in cancers. Therefore, the main focus of this study is to investigate the functions of GPR81 in the eye. Our preliminary studies have shown that GPR81 is abundantly expressed in the RPE layer, which is a key element for maintaining homeostasis of the outer retina. As the choroidal vasculature is the sole provider of nutrients and oxygen for the RPE and photoreceptors, its defects (i.e., thinning, or thickening) are associated with several diseases, and may significantly affect the survival of the RPE and photoreceptors.

Taken together, **we hypothesized that lactate via RPE-resident GPR81 has significant effects on the integrity of choroidal vasculature, which in turn affects**

survival of the RPE and photoreceptors and may lead to pathological conditions.

Objectives

General objectives:

1. To understand the effects of GPR81 on the integrity of the choroidal vasculature both in the short- and long-term and its consequences on the survival of the RPE and photoreceptors;
2. To further explore the observation by elucidating the underlying mechanisms;
3. To identify potential therapeutic targets;

Specific aims:

1. Identify the location of GPR81 in the outer retina, measure its expression and the levels of its endogenous agonist;
2. Confirm the pro-angiogenic effect of GPR81 activation using choroid sprout assay (*ex vivo*) and by measuring choroidal thickness from mice that are intravitreally injected with lactate (*in vivo*);
3. Observe the phenotype regarding choroidal thickness in GPR81$^{-/-}$ mice, both in the short- and long-term, as well as the function of the eye by using ERG;
4. Identify potential factors involved in the observed phenotype using q-PCR and western blot;
5. Uncover the potential mechanisms that explain the phenotype;
6. Demonstrate the potential therapeutic value of GPR81 for treatment options for outer retina disorders;

Chapter 3: MATERIALS & METHODS

3.1 Animal care

All the animal experiments were strictly performed in compliance with the ARVO statement for the Use of Animals in Ophthalmic and Vision Research and approved by the Animal Care Committee of the Sainte-Justine Hospital according to guidelines established by the Canadian Council on Animal Care. Briefly, GPR81$^{-/-}$ mice were purchased from Lexicon Pharmaceuticals (Texas, USA), and their wild-type littermates were generated on a background of C57BL/6J mice. They were maintained in an environmentally controlled breeding room (temperature: 20 ± 2 °C, humidity: 60 ± 5%, 12 h dark/light circle). Food and water were taken *ad libitum.*

3.2 Chemical preparations

L-lactate (L7022, Sigma-Aldrich, USA) was prepared with PBS, and its pH value was adjusted to 6.5-7.5 with HCl and NaOH solutions. The same procedure was performed for 3', 5'-DHBA (D110000, Sigma-Aldrich, USA). ISRIB (SML0843, Sigma-Aldrich, USA) was dissolved in DMSO.

3.3 Choroidal/RPE complex collection

Eyes were rapidly enucleated and kept in cold PBS for a short time. After removing the cornea and lens, the posterior eyecups underwent peeling of the retina under a microscope. In some cases, sterile procedures were performed for cell isolation. The obtained choroid/RPE complex was then dried for several seconds on delicate wipes before being frozen rapidly on dry ice if applicable. Two eyes from one mouse were

pooled together to perform RNA extraction while eyes from a cohort of mice were prepared for experiments including Western blot, growth factor microarray, lactate detection, ROS/RNS detection, and 8-isoprostane detection.

3.4 Primary RPE cell culture

Primary RPE cells were obtained from 12-day old mice according to a previously described method [196] with some modifications. Briefly, mice were sacrificed with eyes enucleated. After the external tissue was removed, the obtained eyes were then washed and maintained overnight at room temperature in DMEM media (Invitrogen, Carlsbad, CA) supplemented with 10% FBS and 0.2% Fungizone [197]. In order to sufficiently dissociate RPE from the retina, they were kept in darkness overnight. On the following day, after washing with PBS several times, these eyes were digested by a cold mixture containing 2 mg/ml trypsin (T9201, Sigma, USA)/collagenase I (C0130, Sigma, USA) in DMEM media for 28 min at 37 °C [198]. After washing with DMEM media containing 10% FBS and 1% penicillin/streptomycin, the RPE layers were then harvested by peeling from the retina and the choroid. The solution of single RPE cells from one eye was gently pipetted up and down and placed in 24-well plates that were freshly pre-coated with attachment factor (S006100, Gibco, Fisher Scientific, USA) at a rate of one eye per well. Cells were maintained for 7 days before any treatments. The purity of the obtained RPE cells was determined by staining with an RPE marker RPE-65.

3.5 RNA extraction and Quantitative RT-PCR

Total RNA was extracted from choroidal/RPE complexes and primary RPE cells using Ribozol RNA Extraction Reagent, followed by DNase I treatment to remove any contaminating genomic DNA and subsequent conversion into cDNA using M-MLV reverse transcriptase (Invitrogen). A SYBR Green Master mix kit (Thermofisher) and Stratagene Mx3000p detection system were used to perform quantitative analysis of gene expression. Triplicate samples were analyzed and their threshold cycle numbers were averaged. Primer sequences (Table 3.1) were designed using the Primer-Blast program and produced by the company Alpha DNA (Montreal, Quebec, Canada). Gene expressions were normalized to 18S expression using the ΔC method.

3.6 Immunohistochemistry

Eyes were enucleated and fixed in 4% paraformaldehyde on ice for 1.5 h. After removing the cornea and lens, the posterior eyecups were further dehydrated by 30% sucrose overnight at 4 °C, and subsequently embedded in optimal cutting temperature (O.C.T) medium, which was rapidly frozen on dry ice and then kept at -80 °C. Sagittal sections of 12-µm thickness were obtained (model CM3050S cryostat; Leica Microsystems, Wetzlar, Germany) and kept at -80°C until further processing. Cryosections were stained with antibodies followed by a second antibody staining if necessary (Table 3.2). Slides were mounted with the gold antifade medium (P36961, ThermoFisher Scientific, USA), and then assessed by epifluorescent microscopy (E800;

Nikon Eclipse, Melville, NY), slide scanner (Axio Scan.Z1, ZEISS, Germany), or confocal microscope (SP8, Leica, Germany).

3.7 Quantification of Choroidal Thickness

Lectin staining was used to indicate the choroidal endothelium. Only slides that contained sections with the optic nerve head were subjected to the scanner. Thickness of the choroidal vasculature was measured on digital images taken by the scanner under 40X amplifications using the software Zen Blue Lite. The average of both sides around the optic nerve head was considered as the mean thickness. To minimize artifacts, all the samples followed the same procedures.

3.8 Choroidal sprout assay

Choroidal explants were prepared using adult mice (around one month old) according to a previously described method [199]. Enucleated eyes were obtained under aseptic conditions and kept in EBM-2 media (CC-3156, Lonza, USA). After removal of the external connective tissue, blood vessels and fatty tissue, the eye was then removed of the cornea, lens, retina and the optic nerve head. The harvested choroid/RPE complex was further cut into 1- to 2- mm sections, each of which was placed in 30 μL Matrigel (Corning life science, USA) in a 24 well plate. After solidifying the Matrigel in the incubator for 30 min, choroidal explants were kept in EGM-2 media. All these procedures were performed in the cell culture hood to maintain sterility.

Choroid-alone complexes (with the removal of RPE) were prepared based on a

previous method [200]. In general, the procedure was similar to preparation of the choroid/RPE complex, except for the digestion. Briefly, after removal of the external connective tissue, blood vessels and fatty tissue, the eyes were incubated at 37 °C for 30 min with 2% Dispase II (neutral protease; Roche Applied Science, Indianapolis, IN) in Hank's balanced salt solution (HBSS, Invitrogen). The choroid layer was obtained by peeling off the RPE with fine forceps and then subjected to the same procedure as described for choroid/RPE explants.

Before any treatments, explants were kept in the media for 3 days until the growth of vessels was observed. On the 4th day, explants were treated with vehicle (PBS), 10 mM lactate or 80 μM DHBA until the 6th day. Photographs were taken prior to the treatment and daily until the 6th day. Using ImageJ1.42q, the angiogenesis response was determined by measuring the vessel area and normalized to the control groups.

3.9 Western blot analysis

Collected choroid/RPE complexes in RIPA buffer supplemented with 0.1 mg/ml PMSF and proteinase inhibitor cocktail (11697498001, Roche, USA), were homogenized thoroughly (Precellys 24 Tissue Homogenizer System, Bertin Technologies, France) and then kept on ice for 1 h. After centrifuging at 10,000xg for 15 min, the supernatant was harvested and subjected to protein concentration measurement by the Bradford method [201]. Around 50 μg total lysate was loaded on an SDS-PAGE gel, and then electroblotted onto a nitrocellulose membrane (BioRad) according to a previously

described method [202]. After blocking with 10% milk or 10% BSA, the membrane was incubated overnight with primary antibodies (Table 3.2) at 4 °C. After washing, membranes were incubated with 1:1000 horseradish peroxidase (HRP)-conjugated anti-mouse or anti-rabbit secondary antibodies (Millipore). Membranes were imaged with the LAS-3000 imager. The analysis was performed with ImageJ1.42q.

3.10 Growth factor microarray

The levels of various growth factors including those involved in angiogenesis were detected by using a commercial kit (mouse growth factor array C3, RayBiotech, USA). Briefly, after blocking the membrane at room temperature, 500 μg of total protein was loaded and incubated overnight at 4 °C. After several washes, a prepared biotinylated antibody cocktail was added to each well and incubated overnight at 4 °C, followed by incubation with HRP-streptavidin and chemiluminescence detection. Membranes were imaged with the LAS-3000 imager. The analysis was performed with ImageJ1.42q.

3.11 Choroidal flat mount

Eyes were enucleated and fixed in 4% paraformaldehyde on ice for 1.5 h. After removing the cornea, lens, external connective tissue, blood vessels and fatty tissue, the posterior eyecups were subjected to delicate removal of the retina with fine forceps under a dissecting microscope. The remaining eyecup (RPE/choroid complex) was then incubated with blocking solution (PBS containing 0.5% BSA, 0.5% Triton-X) for 1 h at room temperature, followed by simultaneous incubation with Rhodamine phalloidin

(1:400) and FITC-conjugated lectin (1:400) at 4 °C overnight. On the following day, after washing with PBS, 4-5 cuts were made to unfold the eyecup, which was then mounted with a coverslip. Slides were then subjected to epifluorescent microscopy (E800; Nikon Eclipse, Melville, NY), slide scanner (Axio Scan.Z1, ZEISS, Germany), or confocal microscopy (SP8, Leica, Germany).

3.12 Oxidative stress measurement by carboxy-H2DCFDA (CM-H2DCFDA)

Isolated primary RPE cells were further subjected to measurement of oxidative stress levels by incubation with the dye CM-H2DCFDA according to the manual (C6827, ThermoFisher Scientific, USA) with some modifications. CM-H2DCFDA is a general oxidative indicator that retains in live cells. After several reaction steps, it is finally converted to a fluorescent adduct inside cells with an E_x/E_m: ~492–495/517–527 nm. Briefly, 10,000 cells per well were placed in a 96-well black plate until reaching 80-90% confluence. Primary RPE cells were then incubated with 10 μM CM-H2DCFDA for 45 min followed by treatment with either L-lactate, 3', 5'-DHBA or vehicle. The fluorescence was measured at a series of time points with E_x/E_m: 485/515 nm. Blank wells with medium alone were used as the background reference. T-BHT was used as the positive control.

3.13 L-lactate detection

The level of endogenous lactate was determined using a kit (Sku1200011002, Eton Bioscience, USA) according to the manual with some modifications. Fresh dry

choroid/RPE complexes from a cohort of mice were obtained, followed by thorough homogenization (Precellys 24 Tissue Homogenizer System, Bertin Technologies, France) and subsequent extraction of cold 80% ethanol with a tissue weight/ethanol ratio of 1:8 for 1 h at 4 °C. The supernatant was obtained by centrifuging at 10,000x g, followed by condensation with a spin column (Z677108, Sigma-Aldrich, USA). Subsequent procedures were performed according to the manual. The standard curve was established with a series of concentrations of L-lactate. Absorbance was recorded at 490 nm. Lactate levels were then calculated based on the pre-configured standard curve.

3.14 Superoxide dismutase (SOD) detection

SOD is one of the most important anti-oxidative enzymes. Its activity was measured with a detection kit (19160, Sigma-Aldrich, USA) with some modifications. Briefly, fresh dry choroid/RPE complexes from a cohort of mice were prepared and homogenized in ice-cold buffer 0.1 M Tris/HCl (pH 7.4) containing 5 mM β-ME, 0.5% Triton X-100 and 0.1 mg/ml PMSF with a tissue weight/buffer ratio of 1:8 at 4 °C. After centrifuging at 14,000x g for 5 min at 4 °C, supernatants were collected and subjected to the assay according to the manual. Absorbance was read at 450 nm. SOD activity was then calculated based on the formula provided by the kit.

3.15 ROS/RNS detection

Reactive oxygen species (ROS) and reactive nitrogen species (RNS) are responsible for the deleterious outcomes of oxidative stress that are implicated in many diseases.

Their levels were determined using a kit (STA-347-5, Cell Biolabs, USA). Briefly, fresh dry choroid/RPE complexes from a cohort of mice were prepared and homogenized. After centrifuging, 80 μg of lysate was added to each well of a 96-well plate with a black wall and transparent bottom. Subsequent procedures were performed according to the manual. Fluorescence was read at 480 nm Ex/530 nm Em. Samples were run in quadruplicate. H_2O_2 was used to construct the standard curve. Accordingly, levels of ROS/RNS were calculated and normalized to the amount of protein.

3.16 8-Isoprostane detection

As one of the major products arising from lipid oxidation, 8-isoprostane is considered as a marker of oxidative stress. Its level was determined using an ELISA kit (516351, Cayman Chemical, USA). Briefly, fresh dry choroid/RPE complexes from a cohort of mice were prepared and homogenized. After centrifuging, 80 μg of lysate was added to each well, followed by addition of the reagents required for the reaction according to the manual. After 18 h of incubation at 4 °C, the wells were further rinsed, and solutions were added according to the manual to develop fluorescence. Absorbance was obtained at 410 nm. 8-Isoprostane was used to construct the standard curve. Accordingly, calculations were made and normalized to the amount of protein.

3.17 Electroretinography (ERG)

Full-field flash ERGs were recorded to measure retinal functions at different ages, using a recording system (AcqKnowledge®; Biopac MP100; Biopac Systems Inc.,

Goleta, CA, USA) as previously described [203, 204]. Briefly, after overnight dark-adaption, the mice were anesthetized with an intramuscular injection of a mixed solution containing ketamine, 85 mg/kg and xylazine, 5 mg/kg. Following pupil dilation with 1-2 drops of 1% tropicamide (Mydriacyl®; Alcon Canada Inc., Mississauga, ON, Canada), the corneas were then anesthetized with proparacaine hydrochloride (Alcaine®; Alcon Canada Inc., Mississauga, ON, Canada). With a recording electrode on the cornea (DTL fiber electrode), a reference electrode in the mouth and a ground reference in the tail, respectively, the mouse was placed inside a recording chamber. All these procedures were performed under a dim red light. Scotopic ERGs were recorded with a flash of 0.9 $\log \cdot cd \cdot s \cdot m^{-2}$ (averages, 3–5 flashes; bandwidth, 1–1000 Hz).

3.18 Statistical analysis

Statistical analysis was carried out by Prism software (GraphPad Software). One-way or two-way ANOVA was used for data analysis. Significance between groups was calculated with Bonferroni post-hoc analysis. For between two-group comparisons, a two-tailed Student's t-test was applied to calculate the significance. Data were presented as means ± SEM with statistical significance at $p=0.05$.

Chapter 4: RESULTS

Part 1: Young mice maintained in normal air

4.1.1 In the outer retina, the lactate receptor GPR81 is exclusively expressed in the retinal pigment epithelium (RPE) layer

We investigated the location of GPR81 in the outer retina by immunohistochemistry. As shown in Fig. 4.1A, GPR81 (red) perfectly overlapped with RPE 65 (green), a marker of the RPE layer. These data suggest that in the outer retina, GPR81 is abundantly located at the RPE layer. To confirm our observation, we sought to examine the mRNA levels of GPR81 both in the isolated choroid and extracted primary RPE cells (PRPE, purity is 100%, Fig. 4.1D). In line with our staining observations, GPR81 was not detected in the isolated choroids, but was abundantly expressed in primary RPE cells (Fig. 4.1B), suggesting that GPR81 is exclusively expressed in the RPE layer in the outer retina.

Noticeably, the physical level of GPR81 mRNA reached a peak at P12, followed by a dramatic decrease at P15 (Fig. 4.2A), while the level of its endogenous ligand lactate increased as well until P12 (Fig. 4.2B), suggesting that P12 may be a critical time-point worthy of investigation.

4.1.2 Activating GPR81 promotes angiogenesis *in vivo* and *ex vivo*

Activating GPR81 has been found to promote angiogenesis [124, 127, 205]. To confirm its pro-angiogenic function, we performed the choroidal sprout assay where tissues were cultured in Matrigel and the increased areas of angiogenesis were then measured following different treatments. After treatment with 10 mM lactate or 80 μM

DHBA for 48 h, neither lactate-treated nor DHBA-treated "choroid only" showed a significantly increased angiogenic area compared to vehicle treatment, confirming the absence of GPR81 in the choroidal vasculature. In contrast, both lactate- and DHBA-treated "WT RPE/choroid complex" had dramatically increased choroidal sprouting compared to their controls, while treated KO RPE/choroid complex did not show any significant difference (Fig. 4.3A-B). All these data indicate that GPR81 is present in the RPE and that its activation results in angiogenesis *ex vivo*.

These observations were further confirmed by a thickening of the choroidal vasculature caused by intravitreal injection of its endogenous ligand lactate in mice. Lactate was intravitreally injected at a final concentration of 10 mM in P9 mice, which were then sacrificed at P12 and measured for choroidal thickness as shown by lectin staining (Fig. 4.3C). Lactate-injected WT mice had almost two-fold increased choroidal thickness compared to the vehicle group, while intravitreal injection of lactate in KO mice did not show the same pattern (Fig. 4.3D), indicating that lactate-activating GPR81 enhances angiogenic responses *in vivo*.

These data clearly demonstrate that lactate via GPR81 promotes angiogenesis in the outer retina, further suggesting that knockout of GPR81 in mice may lead to a thinner choroidal vasculature.

4.1.3 Young GPR81$^{-/-}$ mice display thinner choroidal vasculature

GPR81$^{-/-}$ mice were successfully generated (Fig. 4.1C). The thickness of the

choroidal vasculature both in WT and KO mice was measured by lectin staining. In line with our prediction, KO mice displayed a significantly thinner choroidal vasculature at P15, especially in the central region (Fig. 4.4B), compared to their WT counterparts. Moreover, this reduction in KO mice was sustained until P30 compared to their WT mates (Fig. 4.4C-D), indicating that GPR81 activation may play an important role in angiogenesis of the choroid *in vivo*. We subsequently sought to screen for potential factors implicated in the observed choroidal thinning in KO mice.

4.1.4 A discrepancy regarding gene and protein profiles is present in the developing outer retina of GPR81$^{-/-}$ mice

In order to elucidate possible underlying mechanisms, quantitative RT-PCR was first performed. As noted in the " **INTRODUCTION**", GPR81 has been found to possess various biological effects, including anti-inflammation [206-209], anti-lipolysis [120, 210, 211], pro-angiogenesis [124, 127] and anti-apoptosis [139, 212] functions. Accordingly, factors that promote and inhibit these functions were screened, including VEGF A and IL-1β. A total of 22 genes were assayed (Fig. 4.5A). Surprisingly, all of these genes in the KO mice showed increased expressions to various extents at P9 compared to their age-matched WT mice (Fig. 4.5A). Such a tendency in the KO mice was observed both at P12 and P15 (Fig. 4.5B-C), suggesting that a general process may occur in the KO outer retina at these ages. Furthermore, comparable observations were also found in primary RPE cells (Fig. 4.5D) with higher gene expression in KO primary RPE cells compared to

their WT controls.

The protein profiles in KO mice, however, displayed a broad reduction. Growth factor microarrays capable of detecting a total of 30 factors involved in cellular growth were performed at P9 and P12. These data showed that compared to age-matched WT groups, the reduction of these growth factors in KO mice began with the most pronounced decrease in hepatocyte growth factor (HGF, a major pro-angiogenic factor) at P9 (Fig. 4.6A), followed by a general pattern of dramatic decreases with the exception of 2 factors at P12 (Fig. 4.6B). Moreover, this pattern was shared in the microarray of primary KO RPE cells (Fig. 4.6D). However, the microarray of P30 KO mice revealed a general restoration of translation (Fig. 4.6C), and these mice showed a similar choroidal thickness compared to age-matched WT mice (Fig. 4.4D).

Intriguingly, such a discrepancy between gene expression and translation can be caused by global processes [213] including oxidative stress [214-216], ER stress [217], and inflammation [218]. Among these, activation of ER stress is capable of arresting global protein synthesis; if applicable in this scenario, this process could explain our observations. Thus, the potential presence of the above-mentioned stresses in KO mice was then examined.

4.1.5 Rather than inflammation, elevated oxidative stress and ER stress are simultaneously present in the outer retina of young GPR81$^{-/-}$ mice.

Accordingly, levels of oxidative stress and ER stress were fully investigated both in

WT and KO mice.

Nuclear factor E2-related factor 2 (Nrf2), a major transcription factor that facilitates the expression of various anti-oxidants, showed a substantial decrease in KO mice, particularly at P9, P12, and P15 (to nearly 10%) (Fig. 4.7A, G) compared to age-matched controls. Its downstream enzyme superoxide dismutase (SOD), a major anti-oxidative enzyme, was also found to exhibit noticeably lower activity in KO mice at P12 (Fig. 4.7D), suggesting that defense against oxidants is comparatively lower in KO mice. Thus, it was postulated that a higher level of oxidative stress was present in KO mice. In line with our observation, levels of oxidative stress including ROS and RNS were significantly higher in KO outer retina at P9, P12, and P15 (Fig. 4.7H), and one ROS marker 8-isoprostane, also showed a dramatic increase at P9 (around 6-fold) (Fig. 4.7J), but then rapidly decreased due to its fast entry into the circulation [219]. Furthermore, *in vitro* (Fig. 4.7I), DHBA treatment in primary RPE cells that were previously incubated with the general oxidative indicator CM-H2DCFDA dramatically lowered the basal level of oxidative stress in WT primary RPE cells, while greatly enhancing the level of the latter in KO cells, a phenomenon that might be caused by the metabolism of DHBA by cytochrome P450 enzymes [220], especially since inflammation (linked with oxidative stress) is augmented in GPR81 KO mice [208]. All of these observations indicate that GPR81 deficiency in mice leads to elevated oxidative stress.

Since there is a tight link between oxidative stress and ER stress, we then sought to evaluate levels of ER stress in mice. Consequently, the endoplasmic reticulum binding protein BiP (also termed GPR78), a classic ER stress marker [221], was investigated to determine the levels of ER stress in WT and KO mice at different ages. Western blots (Fig. 4.7B, E) showed that compared to their age-matched WT mice, KO mice displayed significantly elevated levels of BiP, particularly at P9 and P12 (approximately three -fold), implying that a higher level of ER stress is present in KO mice. In agreement with this observation, another ER stress marker called protein disulfide isomerase (PDI) (Fig. 4.7 B, F) also showed the same pattern as BiP in western blot studies. In addition, PDI staining (red) (Fig. 4.7 C) showed that a significantly stronger fluorescence was present in KO mice compared to their WT counterparts, especially at P12, demonstrating the presence of pronounced ER stress in young KO mice. All of these data suggest that GPR81 deficiency in mice leads to ER stress.

Lastly, the inflammatory response was further examined in mice using a microglia marker (Iba-1) as GPR81 activation has been found to hinder global inflammation. Iba-1 staining (green) (Fig. 4.7K) from WT and KO mice at P12 did not show any dramatic difference, demonstrating that inflammation is not a critical element of the choroidal degeneration observed in KO mice.

Interestingly, ER stress and oxidative stress can work synergistically to activate the integrated stress response pathway. Thus, we further focused our investigations on this

pathway.

4.1.6 Oxidative stress and ER stress synergistically activate the ISR pathway in the developing outer retina of GPR81$^{-/-}$ mice

As mentioned above, the ISR pathway can be activated due to intracellular stresses including ER stress and oxidative stress. The core event of ISR activation is the phosphorylation of the alpha subunit of eukaryotic translation initiation factor 2 (eIF2α). As shown in Fig. 4.8A-B, compared to age-matched WT mice, the KO outer retina displayed increased phosphorylated eIF2α with a peak at P15 (around 2.5-fold) followed by a decrease until P30, where no significant difference was found between the two groups, indicating that the ISR pathway is initially activated at 9 days of life and terminated around 30 days of life in KO mice. Meanwhile, its effector ATF4 followed the same pattern as p- eIF2α as shown in western blot studies (Fig. 4.8 A, C). In line with these observations, the target genes of ATF4 also showed multitude increase in transcriptions. For example, at P12 when the ISR pathway was activated, gene expression of pro-survival gene factors including asparagine synthetase (Asns) and tribbles homolog 3 (Trib3) were noticeably enhanced, while the pro-death gene activating transcriptional factor 3 (ATF3) significantly decreased (Fig. 4.8E). At P30, the ISR pathway was terminated by an elevated level of growth arrest and DNA-damage inducible protein 34 (GADD34) (Fig. 4.8A, D), coupled with decreased levels of p- eIF2α (Fig. 4.8 A, B) and ATF4 (Fig. 4.8 A, C) and a return of its target genes to normal levels with the exception

of Asns (Fig. 4.8F), indicating that the ER stress is resolved around P30. As a result, global protein levels were restored, and the ISR pathway was terminated (Fig. 4.6C).

4.1.7 The reduced choroidal thickness in young GPR81$^{-/-}$ mice is reversed by an ISR inhibitor

To confirm the involvement of the ISR pathway in KO mice, we used the ISR pathway inhibitor ISRIB, which was intravitreally injected (the final concentration in the eye was 200 nM) in P9 mice. Choroidal thickness was then evaluated at P12. As shown in Fig. 4.9A-B, ISRIB significantly increased choroidal thickness in KO mice (approximately two-fold), compared to the vehicle group, while no significant difference was found in WT mice, demonstrating that the choroidal thinning in young KO mice was mediated by activation of the ISR pathway. To further support our hypothesis, the ability of ISRIB to reverse the attenuation of global protein translations was investigated. Compared to the vehicle group, inhibition of the ISR pathway in KO mice at P12 partially restored the protein profile (Fig. 4.9C), especially VEGF-A. This is in line with other investigations showing partial restoration of the protein profile by ISRIB [222]. Compared to the ISRIB-treated WT group (Fig. 4.9D), ISRIB-treated KO mice at P12 showed a restored protein profile with a noticeable increase of VEGF-A, indicating that VEGF-A in particular mediates the neovascularization observed in ISRIB-treated KO mice.

Taken together, these results collectively suggest that the choroidal thinning in

young GPR81$^{-/-}$ mice is mediated by activation of the ISR pathway, which is induced by simultaneous ER stress and oxidative stress. Given the fact that termination of the ISR pathway restored global protein translation (Fig. 4.6C), it is postulated that aged KO mice might display choroidal neovascularization (CNV), as evidenced by the smaller difference in choroidal vasculature thickness between WT and KO groups at P30 (Fig. 4.4D).

Part 2: Characterization of aged mice that are maintained in normal air

4.2.1 Aged GPR81- deficient mice display choroidal neovascularization (CNV)

As mentioned above, the thinning choroidal vasculature in young KO mice was due to intracellular stresses that activated the ISR pathway, which is a transient adaptive stress response. Termination of the ISR pathway leads to a restoration of global protein production including growth factors (Fig. 4.6C). Hence, it is worth investigating the choroidal vasculature in aged mice. As shown in Fig. 4.10, the choroidal vasculature in KO mice began to catch up with that in WT mice at P30, and eventually dramatically surpassed the latter after P180 (6 months old, around 1.5-fold), which was sustained until 1Y7M of age (approximately two-fold); these data demonstrate that aged KO mice develop CNV that mimics the hallmark of "wet" aged macular degeneration (AMD). Accordingly, it was worth further investigating whether these mice displayed other features of AMD.

4.2.2 Retina function

To evaluate retinal function, scotopic electroretinography (ERG) was performed. Of interest, the a-wave (the trough, Fig. 4.11A) of the scotopic ERG represents the retinal response that is mediated by photoreceptors. As shown in Fig. 4.11B, the amplitude of the a-wave was significantly increased in P180 KO mice compared to their controls, a finding that could be attributed to the choroidal neovascularization that provides more

nutrients and oxygen to the photoreceptors from which the a-wave originates. However, the amplitude of a-wave was significantly decreased at 1Y7M in KO mice compared to their controls (Fig. 4.11B), which could suggest that these choroidal neovessels may have invaded the RPE layer at this point and caused consequent damage to the functions of the photoreceptors. To investigate this claim, we examined the morphology of the RPE, the results of which are presented in the following section.

As shown in Fig. 4.11C, the amplitudes of b wave were also measured at different ages. Though there were no significant difference between the WT and KO groups at P30 and P180, KO mice at 1Y7M had dramatically lower amplitudes compared to age-matched WT mice, which was consistent with the pattern of a wave.

4.2.3 Aged GPR81$^{-/-}$ mice display RPE degeneration

To confirm the above-mentioned hypothesis, RPE/choroid complex flat mount was performed. After labeling with the RPE cell membrane marker phalloidin (Fig. 4.12A), we found that GPR81$^{-/-}$ mice displayed RPE degeneration with aging. Specifically, no obvious difference was found between WT and KO mice at P30, while the latter began to show vague junctions between RPE cells at P90. These vague junctions vanished at P120 and some ghost RPE appeared at P180, suggesting that RPEs degenerate in KO mice with aging (Fig. 4.12A). The histogram (Fig. 4.12B) revealed a significant increase in the number of abnormal RPE cells in the flat mounts in KO mice at P180 compared to the WT group (Fig. 4.12B).

Further, flat mounts that were double-stained with phalloidin and lectin (green), showed that some KO mice displayed choroidal vessels penetrating the RPE at 1 year of age and that these punctures were progressive with aging (Fig. 4.12C).

4.2.4 Aged GPR81$^{-/-}$ mice display photoreceptor degeneration

As mentioned in the "**INTRODUCTION"**, the RPE layer is critical for maintaining photoreceptor survival. Given that aged GPR81$^{-/-}$ mice displayed RPE degeneration, we investigated the thickness of photoreceptors. As shown in Fig. 4.13, KO mice at P180 began to show a dramatic decrease in photoreceptors thickness (around 70%) compared to their controls.

As an aside, young mice at P12 that have thinner choroidal vasculature also show smaller photoreceptor thickness (about 84%) compared to age-matched WT mice.

4.2.5 Drusen was not found in GPR81$^{-/-}$ mice

Drusen is mainly composed of proteins and lipids and has been recognized as the hallmark of "dry" AMD. Given the fact that activating GPR81 inhibits lipolysis, we sought to investigate whether drusen was present in KO mice. Cryosections at P180 were stained with a drusen marker CD46 (a complement regulatory protein) [223] and showed that rather than a stronger staining, a weaker signal in KO mice was found compared to their WT controls, demonstrating that no drusen was present in KO mice at P180 (Fig. 4.14). More studies are needed to further substantiate this observation as drusen can also be reliably identified with several alternatives.

Taken together, these studies suggest that aged GPR81$^{-/-}$ mice display CNV, which is the hallmark of "wet" AMD. In other words, the aged GPR81$^{-/-}$ mouse is a model of "wet" AMD.

Chapter 5: DISCUSSION & CONCLUSION

Vision impairment is a considerable health problem that significantly affects the quality of life worldwide. In elderly people of Western countries, the leading cause of blindness is age-related macular degeneration, which is a heterogeneous disease. The "wet" AMD subtype is a proliferative ocular disorder with the hallmark of choroidal neovascularization. Although extensive efforts have been undertaken to better understand this pathology, current treatment outcomes remain unsatisfactory. Given that the retina is one of the most energy-demanding tissues in the human body and that dysregylation of its metabolism provokes several pathologies including AMD [224], our study provides the first evidence for the therapeutic potential of targeting a metabolic receptor, GPR81, in CNV through simultaneous regulations of oxidative stress and ER stress. Specifically, we report that GPR81-deficient mice eventually develop CNV with aging (Appendix 1A). Such involvement of a metabolic receptor in the pathologies of AMD is in line with a previous study showing that deficiency of the succinate receptor GPR91 in mice leads to "dry" AMD [224].

Animal models are essential for pathological research. To date, dozens of animal models have been developed to facilitate the study of choroidal neovasculature (CNV), including several lines of knockout mice as described in the "**INTRODUCTION"**. Compared to these animal models, aged GPR81$^{-/-}$ mice spontaneously develop the pathology without any manipulation such as lipid supplementation. Similar to other transgenic mouse model of CNV [69, 73, 75] (e.g., 25% of Ccr2/Ccl2 deficient mice

develop CNV [73]), not all of the GPR81$^{-/-}$ mice (4 out of 8 mice) display the growth of choroidal vessels into RPE layer, which is simply due to the thickening of Bruch's membrane with aging [225].

Intriguingly, several studies have shown that application of intensive stresses (e.g., oxygen exposure) could accelerate spontaneous pathological formation. Examples include: application of a chronic stress can successfully accelerate ligature-induced periodontitis in rats [226] as well as enhance the onset and progression of the Alzheimer's disease phenotype in mice [227-229], while hyperoxia exposure accelerates the progression of hepatic fibrosis in rats [230]. Since the spontaneous development of CNV in KO mice is mediated by stress-induced ISR pathway activation, we sought to investigate whether oxygen exposure application (a model of retinopathy of prematurity [ROP]) could accelerate spontaneous pathological progression. Consequently, the following OIR model was generated: 7-day-old pups were subjected to a daily regimen of 75% oxygen (controlled by an oxygen monitor; 24 hours) for 5 consecutive days, after which they were returned to normal air. Control groups were maintained in normal room air (i.e., 21%) throughout the experiments. Then, thickness of the choroidal vasculature was evaluated, and the choroidal flat mount staining was also performed. In line with previous reports [30, 84], hyperoxic insult led to choroidal thinning at P15 both in WT and KO mice (Appendix 2 C). With aging, however, the OIR KO mice at P30 displayed significant CNV (Appendix 2 A and D), in contrast to the spontaneous model that

develops CNV at P180, thus confirming that hyperoxic insult can accelerate the spontaneous progression of CNV.

Overall, these investigations indicate that GPR81 deficiency increases ocular susceptibility in mice. Accordingly, we postulate that GPR81 deficiency in mice may exacerbate the development of laser-induced CNV. Nevertheless, this is the first report that reveals the essential involvement of a metabolic receptor in the development of CNV.

In accordance with previous studies (mentioned in the **"INTRODUCTION"**), GPR81 activation exhibits various biological activities, including pro-angiogenesis, anti-inflammation, and anti-lipolysis functions. In this study, we observed its pro-angiogenic function as demonstrated by the choroidal sprout assay and increased choroidal thickness upon intravitreal injection of lactate in WT mice. Though no direct evidence of substantial inflammation was found in GPR81$^{-/-}$ mice (Iba-1 staining) that were maintained in normal room air, KO mice previously exposed to oxygen from P7 to P12 showed signs of macrophage infiltrations at P30 (Appendix 2 B), while age-matched WT mice did not show any sign of macrophages, confirming the anti-inflammatory activity of GPR81.

The anti-lipolysis function was not a target in our study. However, as an aside, we examined the body weight and found that KO mice suffered a significant loss in body weight (Appendix 3) with a higher level of plasmatic fatty acids at P180 (data not shown here), confirming its anti-lipolysis role. However, despite this enhancement in plasmatic

level, fatty acids did not seem to accumulate under the RPE to form the drusen (mainly composed of lipids and proteins [231]), as demonstrated in our preliminary study (CD46 staining). Such an observation is consistent with other studies [232-236] that found no significant relationship between AMD and higher levels of plasmatic lipids, though the link between the two remains controversial [237, 238]. Nonetheless, drusen (the hallmark of "dry" AMD) contains a number of plasmatic proteins such as vitronectin [239] and clusterin [240], suggesting the presence of systematic elements in its formation. Moreover, the succinate receptor GPR91, which like GPR81 also exhibits anti-lipolysis properties, decreases in expression with aging and its deficiency in mice results in a higher plasmatic level of fatty acids and eventual formation of drusen in "dry" AMD as early as 5 months of life [224], suggesting a possible role of GPR81 in "dry" AMD. Although lipofuscin (CD46 staining) was not detected at 6 months of life in our settings, further studies are necessary to examine its presence in the KO mice using older mice, alternative staining markers or a high-fat diet to exacerbate the pathology. In addition, more refined techniques such as electron microscopy are needed to obtain more details about the morphological changes in Bruch's membranes as well as the RPE.

Novel functions of GPR81 activation identified in this study include anti-oxidative stress, anti-ER stress, and an overall anti-integrated stress response. Oxidative stress is defined as an imbalance between the production of reactive oxygen species (ROS) and anti-oxidant defense that favors oxidants [241, 242]. Though the generation of ROS by

oxidation phosphorylation (OXPHOS) is unavoidable during normal aerobic metabolism, a defective antioxidant system results in oxidative stress. Of note, the major antioxidant transcription nuclear factor E2-related factor 2 (Nrf2) has been reported to be associated with levels of G-protein linked signal proteins [243]. Such an observation is confirmed by our data that GPR81 modulates cellular redox status via Nrf2, and its deficiency in mice leads to increased level of oxidative stress both *in vivo* (ROS/RNS detection and 8-isoprostane detection) and *in vitro* (CM-H2DCFDA incubation with primary RPE cells). In addition, the application of exogenous stimuli generating oxidative stress also provides an alternative method to examine antioxidant activity. For instance, prolonged hyperoxia (a condition that produces massive oxidative stress [242]) in KO mice leads to a thinner choroidal vasculature (Appendix 2) compared to their WT OIR mates, demonstrating the anti-oxidant role of GPR81 activation. Noticeably, increased cellular oxidative stress is usually associated with high levels of lactate [244-246], at least, some of which can activate its receptor GPR81 to promote cellular protection by enhancing the defense mechanism to counteract the potential damage of elevated ROS, according to our study. Although monocarboxylate transporters (MCTs) appear to contribute to ROS generation [247-250], their potential effects have been excluded in this study by using KO mice and the GPR81 selective agonist DHBA.

As a source of ROS production [251, 252], the endoplasmic reticulum (ER) is an intracellular organelle with multiple functions including mRNA translation and protein

folding. Intriguingly, its lumen presents a redox system that is simultaneously both in reduced and oxidative states [253], which is of vital importance for the formation of disulfide bonds and proper protein folding. Disturbances including changes in cellular redox status, nutrient deprivation, and pathogen infections result in ER stress and thereby activate its adaptive pathway - the unfolded protein response (UPR). Accumulating studies [251, 254, 255] have demonstrated that oxidative stress and ER stress are in fact tightly linked events, and thus it is not surprising to observe that ER stress (increased BiP and PDI) and oxidative stress coexist in the KO mice. These two stresses synergistically induce the activation of the integrated stress response (ISR) (phosphorylation of eIF2α, ATF4, and its downstream target genes), leading to a transient attenuation of global protein synthesis (as demonstrated by protein microarray, resulting in a thinner choroidal vasculature in KO mice) to adapt to alterations in homeostasis, manifesting as the choroidal thinning. Once these stresses are relieved at around P30 (as suggested by the significant elevation of GADD34), protein synthesis is restored (protein microarray), ultimately leading to the development of CNV as the animal age.

With a profound effect on mRNA translation, activation of the ISR pathway is usually associated with changes in gene profiles. Depending on the cellular setting, ISR activation may differentially affect translation and transcription. For example, a multi-omics analysis of the ISR activation induced by mitochondrial stress [214] revealed that 59 genes and 17 proteins were up-regulated while 4 genes and 101 proteins were

down-regulated. In line with the above data, 21 out of 157 analyzed genes were increased more than two-fold while no significant gene was found to be down-regulated upon stimulation with the ISR activator [256]. In addition, in the frontal cortex of rats given chronic morphine treatment, 14 of 8000 total genes were elevated two-fold or mote, with only one gene reduced more than two-fold, upon activation of the ISR pathway [257, 258]. Collectively, these studies demonstrate that activation of the ISR pathway tends to increase gene expression, especially for those genes involved in adaptive responses including those regulating angiogenesis, inflammation, and death. Consequently, it is not surprising that in our study, young KO mice displayed elevated gene expression concomitant with a global decrease in translation.

Accordingly, questions may be raised regarding whether this general increase in gene expression is associated with an epigenetic modification, as oxidative stress can alter global gene transcription by the crosstalk with various epigenetic processes including histone acetylation [259-261], one of the most common epigenetic modifications. Thus, levels of histone acetylation were further examined. Briefly, histone acetylation is a reversible process balanced by two types of modulating enzymes, including histone acetyltransferases (HATs) and histone deacetylases (HDACs). Acetylated chromatin is more relaxed and accessible to enhance gene expression while de-acetylation leads to lower levels of gene expression. Thus, the levels of both histone acetylation and HDAC activity were examined in our studies. As shown in Appendix

4A-B, the level of histone acetylation in KO RPE/choroid complexes was significantly elevated compared to age-matched WT mice (two-fold at P9 and 1.5-fold at P12, respectively). In contrast, HDAC activity was found to be dramatically lower in the KO group compared to the WT group (Appendix 4C). Consequently, with the elevation in histone acetylation and the decrease of HDAC activity, the KO RPE/choroid complex possesses higher levels of gene expression, as observed here. Such evidence agrees with data from other studies. For example, amino acid deprivation leading to ISR activation recaptures latent HIV expression via the inhibition of histone deacetylase 4 (HDAC4) [262], and decreases expression of HDAC1-3 in U1 monocytes that harbor the latent HIV genome [263] while increasing transcription via acetylation of histone 3 and 4 in yeast [264]. Moreover, HDAC 6 is reported to regulate sensitivity to cell death in response to stresses including ER stress [265]. Furthermore, cellular redox status is reported to play a critical role in genome stability that affects gene expression, as it is involved in multiple essential signaling pathways including proliferation and apoptosis [266]. Taken together, these pieces of evidence suggest that epigenetic modification contributes to the general elevation of gene expressions via ISR activation during oxidative stress and ER stress [266].

Of note, a closer examination of the protein profiles at different ages reveals that different phenotypes are in fact mediated by different growth factors. For example, during ISR activation in which KO mice display choroidal degeneration, translation in

KO choroid/RPE complexes began to decline at P9, with a significant decrease of hepatocyte growth factor (HGF), while at P12, it progressed to a general pattern of attenuation including common essential factors such as VEGF A and IGF. Among these, HGF is a potent angiogenic inducer independent of VEGF A and is involved in the initial phase of neovascularization, whereas VEGF A mediates the later phases [267]. Meanwhile, as a mitogen for RPE cells, HGF regulates the barrier function of these cells [268] and is associated with proliferative vitreoretinopathy [269]. Accordingly, we postulate that lower levels of HGF and its receptor (HGFR, which also resides exclusively in the RPE layer [269]) may indicate morphological changes of the RPE, which was confirmed by RPE flat mount at different ages.

In contrast, when stresses were relieved at P30, only a small difference in choroidal thickness between KO and WT mice was found. Termination of the ISR pathway initiated the restoration of translation with a pronounced increase of macrophage colony-stimulating factor (M-CSF), a cytokine necessary for the differentiation of monocytes during development [270]. Moreover, it is reported to act as an "angiogenic switch" to facilitate the formation of a high density of vessel networks in cancers [271-273]. Thus, M-CSF may be a therapeutically relevant anti-angiogenic target in CNV development, given the unsatisfactory outcome of anti-VEGF treatment.

Finally, the immunoactivity of GPR81 has been investigated. As shown in Appendix 5, the presence of GPR81 in WT RPE cells but not in GPR81$^{-/-}$ was confirmed by PCR

and western blot (A-D). Meanwhile, antibody also showed immunoactivity of GPR81 in the WT retina but not in GPR81$^{-/-}$ (E). Lastly, this was confirmed in brain as well (F).

To summarize, the main findings of our study are as follows: 1) Aged GPR81 KO mouse is the spontaneous model of CNV; 2) GPR81 KO mouse that exposed to oxygen serves as the accelerated model of CNV; 3) Novel functions of GPR81 have been identified: anti-oxidative stress, anti-ER stress, and anti-integrated stress response. In addition, the scheme of cellular and molecular effects of GPR81 is described in Appendix 6.

In conclusion, our study provides the first evidence for the therapeutic potential of targeting a metabolic receptor GPR81 in "wet" AMD through simultaneous regulation of oxidative stress and ER stress. GPR81-deficient mice serve as a mouse model of spontaneous CNV, while hyperoxia in GPR81-deficient mice accelerates the pathology to as early as P30. Consequently, it is worth investigating the levels of GPR81 in CNV patients in the near future.

References

1. Wade, N. and M. Swanston, *Visual perception: An introduction*. 2013: Psychology Press.
2. Flammer, J., et al., *The eye and the heart.* Eur Heart J, 2013. **34**(17): p. 1270-8.
3. Sapieha, P., et al., *Proliferative retinopathies: angiogenesis that blinds.* The international journal of biochemistry & cell biology, 2010. **42**(1): p. 5-12.
4. Fernández-Robredo, P., et al., *Current treatment limitations in age-related macular degeneration and future approaches based on cell therapy and tissue engineering.* Journal of ophthalmology, 2014. **2014**.
5. Brahimi-Horn, M.C. and J. Pouyssegur, *Hypoxia in cancer cell metabolism and pH regulation.* Essays Biochem, 2007. **43**: p. 165-78.
6. Murray, A.J., et al., *Metabolic adjustment to high-altitude hypoxia: from genetic signals to physiological implications.* Biochem Soc Trans, 2018.
7. Schoors, S., et al., *Partial and transient reduction of glycolysis by PFKFB3 blockade reduces pathological angiogenesis.* Cell metabolism, 2014. **19**(1): p. 37-48.
8. Sapieha, P., et al., *The succinate receptor GPR91 in neurons has a major role in retinal angiogenesis.* Nat Med, 2008. **14**(10): p. 1067-76.
9. Joyal, J.S., et al., *Neovascularization in retinopathy of prematurity: opposing actions of neuronal factors GPR91 and semaphorins 3A.* Acta Paediatr, 2012. **101**(8): p. 819-26.
10. Porporato, P.E., et al., *Lactate stimulates angiogenesis and accelerates the healing of superficial and ischemic wounds in mice.* Angiogenesis, 2012. **15**(4): p. 581-92.
11. Polet, F. and O. Feron, *Endothelial cell metabolism and tumour angiogenesis: glucose and glutamine as essential fuels and lactate as the driving force.* J Intern Med, 2013. **273**(2): p. 156-65.
12. Stone, J., et al., *Development of retinal vasculature is mediated by hypoxia-induced vascular endothelial growth factor (VEGF) expression by neuroglia.* J Neurosci, 1995. **15**(7 Pt 1): p. 4738-47.

13. Hartnett, M.E., *Pediatric retina*. 2005: Lippincott Williams & Wilkins.
14. Nickla, D.L. and J. Wallman, *The multifunctional choroid.* Prog Retin Eye Res, 2010. **29**(2): p. 144-68.
15. Pansky, B., *Review of medical embryology*. 1982: Macmillan New York.
16. Gray, H., *Henry Gray's Anatomy of the Human Body.* Lea and Febiger, Philadelphia, 1918.
17. Nickla, D.L. and J. Wallman, *The multifunctional choroid.* Progress in retinal and eye research, 2010. **29**(2): p. 144-168.
18. Ramrattan, R.S., et al., *Morphometric analysis of Bruch's membrane, the choriocapillaris, and the choroid in aging.* Investigative ophthalmology & visual science, 1994. **35**(6): p. 2857-2864.
19. Gray, H., *Anatomy of the human body*. Vol. 8. 1878: Lea & Febiger.
20. Sato, T., et al., *Serum concentrations of bevacizumab (avastin) and vascular endothelial growth factor in infants with retinopathy of prematurity.* American journal of ophthalmology, 2012. **153**(2): p. 327-333. e1.
21. Flugel-Koch, C., C.A. May, and E. Lutjen-Drecoll, *Presence of a contractile cell network in the human choroid.* Ophthalmologica, 1996. **210**(5): p. 296-302.
22. May, C.A., *Non-vascular smooth muscle cells in the human choroid: distribution, development and further characterization.* J Anat, 2005. **207**(4): p. 381-90.
23. Kur, J., E.A. Newman, and T. Chan-Ling, *Cellular and physiological mechanisms underlying blood flow regulation in the retina and choroid in health and disease.* Prog Retin Eye Res, 2012. **31**(5): p. 377-406.
24. Alm, A. and S.F. Nilsson, *Uveoscleral outflow–a review.* Experimental eye research, 2009. **88**(4): p. 760-768.
25. Summers, J.A., *The choroid as a sclera growth regulator.* Exp Eye Res, 2013. **114**: p. 120-7.
26. Okawa, H., et al., *ATP consumption by mammalian rod photoreceptors in darkness and in light.* Curr Biol, 2008. **18**(24): p. 1917-21.
27. Linsenmeier, R.A. and R.D. Braun, *Oxygen distribution and consumption in the cat retina during normoxia and hypoxemia.* The Journal of general physiology,

1992. **99**(2): p. 177-197.

28. Alm, A. and A. Bill, *Ocular and optic nerve blood flow at normal and increased intraocular pressures in monkeys (Macaca irus): a study with radioactively labelled microspheres including flow determinations in brain and some other tissues.* Experimental eye research, 1973. **15**(1): p. 15-29.
29. Linsenmeier, R.A. and L. Padnick–Silver, *Metabolic dependence of photoreceptors on the choroid in the normal and detached retina.* Investigative ophthalmology & visual science, 2000. **41**(10): p. 3117-3123.
30. Shao, Z., et al., *Choroidal involution is a key component of oxygen-induced retinopathy.* Investigative ophthalmology & visual science, 2011. **52**(9): p. 6238-6248.
31. Esmaeelpour, M., et al., *Choroidal thinning in diabetes type 1 detected by 3-dimensional 1060 nm optical coherence tomography.* Investigative ophthalmology & visual science, 2012. **53**(11): p. 6803-6809.
32. Ikuno, Y. and Y. Tano, *Retinal and choroidal biometry in highly myopic eyes with spectral-domain optical coherence tomography.* Investigative ophthalmology & visual science, 2009. **50**(8): p. 3876-3880.
33. Wang, S., et al., *Choroidal thickness and high myopia: a cross-sectional study and meta-analysis.* BMC ophthalmology, 2015. **15**(1): p. 70.
34. Gharbiya, M., et al., *Choroidal thinning as a new finding in Alzheimer's disease: evidence from enhanced depth imaging spectral domain optical coherence tomography.* Journal of Alzheimer's Disease, 2014. **40**(4): p. 907-917.
35. Adhi, M., et al., *Analysis of the thickness and vascular layers of the choroid in eyes with geographic atrophy using spectral-domain optical coherence tomography.* Retina, 2014. **34**(2): p. 306-312.
36. Schuster, A.K., et al., *Choroidal thickness in nonarteritic anterior ischemic optic neuropathy.* American journal of ophthalmology, 2014. **158**(6): p. 1342-1347. e1.
37. Ayton, L.N., R.H. Guymer, and C.D. Luu, *Choroidal thickness profiles in retinitis pigmentosa.* Clin Exp Ophthalmol, 2013. **41**(4): p. 396-403.

38. Maruko, I., et al., *Subfoveal choroidal thickness after treatment of Vogt-Koyanagi-Harada disease.* Retina, 2011. **31**(3): p. 510-7.
39. Kuroda, S., et al., *Choroidal thickness in central serous chorioretinopathy.* Retina, 2013. **33**(2): p. 302-8.
40. Chan, W.-M., et al., *Intravitreal bevacizumab (Avastin) for myopic choroidal neovascularization: six-month results of a prospective pilot study.* Ophthalmology, 2007. **114**(12): p. 2190-2196. e2.
41. D'Ambrosio, E., P. Tortorella, and L. Iannetti, *Management of uveitis-related choroidal neovascularization: from the pathogenesis to the therapy.* 2014. **2014**: p. 450428.
42. Ament, C.S., et al., *Predictors of visual outcome and choroidal neovascular membrane formation after traumatic choroidal rupture.* Archives of ophthalmology, 2006. **124**(7): p. 957-966.
43. Saxe, S., et al. *ULTRASTRUCTURAL FEATURES OF SURGICALLY-EXCISED SUBRETINAL NEOVASCULAR MEMBRANES IN THE PRESUMED OCULAR HISTOPLASMOSIS SYNDROME*. in *INVESTIGATIVE OPHTHALMOLOGY & VISUAL SCIENCE*. 1992. LIPPINCOTT-RAVEN PUBL 227 EAST WASHINGTON SQ, PHILADELPHIA, PA 19106.
44. Thomas, J.W., et al., *Ultrastructural features of surgically excised idiopathic subfoveal neovascular membranes.* Retina (Philadelphia, Pa.), 1993. **13**(2): p. 93-98.
45. LUBIN, J.R., E.S. GRAGOUDAS, and D.M. ALBERT, *Choroidal neovascularization associated with malignant melanoma: a case report.* Acta ophthalmologica, 1982. **60**(3): p. 412-418.
46. Klein, R., B.E. Klein, and K.L. Linton, *Prevalence of age-related maculopathy: the Beaver Dam Eye Study.* Ophthalmology, 1992. **99**(6): p. 933-943.
47. Green, W.R. and C. Enger, *Age-related macular degeneration histopathologic studies: the 1992 Lorenz E. Zimmerman Lecture.* Ophthalmology, 1993. **100**(10): p. 1519-1535.
48. Grossniklaus, H.E. and W.R. Green, *Choroidal neovascularization.* Am J

Ophthalmol, 2004. **137**(3): p. 496-503.

49. Grossniklaus, H.E., S.J. Kang, and L. Berglin, *Animal models of choroidal and retinal neovascularization.* Progress in retinal and eye research, 2010. **29**(6): p. 500-519.
50. Kwak, N., et al., *VEGF is major stimulator in model of choroidal neovascularization.* Investigative ophthalmology & visual science, 2000. **41**(10): p. 3158-3164.
51. Elner, S., et al., *Monocyte chemotactic protein gene expression by cytokine-treated human retinal pigment epithelial cells.* Laboratory investigation; a journal of technical methods and pathology, 1991. **64**(6): p. 819-825.
52. Elner, V., et al., *Neutrophil chemotactic factor (IL-8) gene expression by cytokine-treated retinal pigment epithelial cells.* The American journal of pathology, 1990. **136**(4): p. 745.
53. Steen, B., et al., *Matrix metalloproteinases and metalloproteinase inhibitors in choroidal neovascular membranes.* Investigative ophthalmology & visual science, 1998. **39**(11): p. 2194-2200.
54. Grossniklaus, H.E., et al., *Macrophage and retinal pigment epithelium expression of angiogenic cytokines in choroidal neovascularization.* Mol Vis, 2002. **8**(8): p. 119-126.
55. Holloway, T. and F. Verhoeff, *Disc-like degeneration of the macula with microscopic report concerning a tumor-like mass in the macular region.* Transactions of the American Ophthalmological Society, 1928. **26**: p. 206.
56. Roberts, A.B., et al., *Transforming growth factor type beta: rapid induction of fibrosis and angiogenesis in vivo and stimulation of collagen formation in vitro.* Proc Natl Acad Sci U S A, 1986. **83**(12): p. 4167-71.
57. Rofagha, S., et al., *Seven-year outcomes in ranibizumab-treated patients in ANCHOR, MARINA, and HORIZON: a multicenter cohort study (SEVEN-UP).* Ophthalmology, 2013. **120**(11): p. 2292-2299.
58. Lally, D.R., A.T. Gerstenblith, and C.D. Regillo, *Preferred therapies for*

neovascular age-related macular degeneration. Current opinion in ophthalmology, 2012. **23**(3): p. 182-188.

59. Schraermeyer, U. and S. Julien, *Effects of bevacizumab in retina and choroid after intravitreal injection into monkey eyes.* Expert opinion on biological therapy, 2013. **13**(2): p. 157-167.
60. Ryan, S.J., *The development of an experimental model of subretinal neovascularization in disciform macular degeneration.* Trans Am Ophthalmol Soc, 1979. **77**: p. 707-45.
61. Shah, R.S., et al., *A Mouse Model for Laser-induced Choroidal Neovascularization.* J Vis Exp, 2015(106): p. e53502.
62. Shen, D., et al., *Exacerbation of retinal degeneration and choroidal neovascularization induced by subretinal injection of Matrigel in CCL2/MCP-1-deficient mice.* Ophthalmic Res, 2006. **38**(2): p. 71-3.
63. Lyzogubov, V.V., et al., *Polyethylene glycol (PEG)-induced mouse model of choroidal neovascularization.* J Biol Chem, 2011. **286**(18): p. 16229-37.
64. Jo, Y.J., et al., *Establishment of a new animal model of focal subretinal fibrosis that resembles disciform lesion in advanced age-related macular degeneration.* Invest Ophthalmol Vis Sci, 2011. **52**(9): p. 6089-95.
65. Baba, T., et al., *A rat model for choroidal neovascularization using subretinal lipid hydroperoxide injection.* Am J Pathol, 2010. **176**(6): p. 3085-97.
66. Baffi, J., et al., *Choroidal neovascularization in the rat induced by adenovirus mediated expression of vascular endothelial growth factor.* Invest Ophthalmol Vis Sci, 2000. **41**(11): p. 3582-9.
67. Wang, F., et al., *AAV-mediated expression of vascular endothelial growth factor induces choroidal neovascularization in rat.* Invest Ophthalmol Vis Sci, 2003. **44**(2): p. 781-90.
68. Schwesinger, C., et al., *Intrachoroidal neovascularization in transgenic mice overexpressing vascular endothelial growth factor in the retinal pigment epithelium.* Am J Pathol, 2001. **158**(3): p. 1161-72.
69. Elizabeth Rakoczy, P., et al., *Mouse models of age-related macular degeneration.*

Exp Eye Res, 2006. **82**(5): p. 741-52.

70. Grossniklaus, H.E., S.J. Kang, and L. Berglin, *Animal models of choroidal and retinal neovascularization.* Prog Retin Eye Res, 2010. **29**(6): p. 500-19.
71. Schlecht, A., et al., *Deletion of Endothelial Transforming Growth Factor-beta Signaling Leads to Choroidal Neovascularization.* Am J Pathol, 2017. **187**(11): p. 2570-2589.
72. Tanaka, N., et al., *Choroidal neovascularization in transgenic mice expressing prokineticin 1: an animal model for age-related macular degeneration.* Mol Ther, 2006. **13**(3): p. 609-16.
73. Ambati, J., et al., *An animal model of age-related macular degeneration in senescent Ccl-2- or Ccr-2-deficient mice.* Nat Med, 2003. **9**(11): p. 1390-7.
74. Combadiere, C., et al., *CX3CR1-dependent subretinal microglia cell accumulation is associated with cardinal features of age-related macular degeneration.* J Clin Invest, 2007. **117**(10): p. 2920-8.
75. Imamura, Y., et al., *Drusen, choroidal neovascularization, and retinal pigment epithelium dysfunction in SOD1-deficient mice: a model of age-related macular degeneration.* Proc Natl Acad Sci U S A, 2006. **103**(30): p. 11282-7.
76. Zhao, Z., et al., *Age-related retinopathy in NRF2-deficient mice.* PLoS One, 2011. **6**(4): p. e19456.
77. Hahn, P., et al., *Disruption of ceruloplasmin and hephaestin in mice causes retinal iron overload and retinal degeneration with features of age-related macular degeneration.* Proc Natl Acad Sci U S A, 2004. **101**(38): p. 13850-5.
78. Malek, G., et al., *Apolipoprotein E allele-dependent pathogenesis: a model for age-related retinal degeneration.* Proc Natl Acad Sci U S A, 2005. **102**(33): p. 11900-5.
79. Hu, W., et al., *Expression of VLDLR in the retina and evolution of subretinal neovascularization in the knockout mouse model's retinal angiomatous proliferation.* Invest Ophthalmol Vis Sci, 2008. **49**(1): p. 407-15.
80. Heckenlively, J.R., et al., *Mouse model of subretinal neovascularization with choroidal anastomosis.* Retina, 2003. **23**(4): p. 518-22.

81. Nagai, N., et al., *Spontaneous CNV in a novel mutant mouse is associated with early VEGF-A-driven angiogenesis and late-stage focal edema, neural cell loss, and dysfunction.* Invest Ophthalmol Vis Sci, 2014. **55**(6): p. 3709-19.
82. Blencowe, H., et al., *Born too soon: the global epidemiology of 15 million preterm births.* Reproductive health, 2013. **10**(1): p. S2.
83. Gilbert, C., et al., *Characteristics of infants with severe retinopathy of prematurity in countries with low, moderate, and high levels of development: implications for screening programs.* Pediatrics, 2005. **115**(5): p. e518-e525.
84. Zhou, T.E., et al., *Choroidal involution is associated with a progressive degeneration of the outer retinal function in a model of retinopathy of prematurity: early role for IL-1β.* The American journal of pathology, 2016. **186**(12): p. 3100-3116.
85. Moreno, T.A., et al., *Choroid development and feasibility of choroidal imaging in the preterm and term infants utilizing SD-OCT.* Investigative ophthalmology & visual science, 2013. **54**(6): p. 4140-4147.
86. Stahl, A., et al., *The mouse retina as an angiogenesis model.* Investigative ophthalmology & visual science, 2010. **51**(6): p. 2813-2826.
87. Strauss, O., *The retinal pigment epithelium in visual function.* Physiological reviews, 2005. **85**(3): p. 845-881.
88. Volland, S., et al., *A comparison of some organizational characteristics of the mouse central retina and the human macula.* PLoS One, 2015. **10**(4): p. e0125631.
89. Al-Hussaini, H., et al., *Mature retinal pigment epithelium cells are retained in the cell cycle and proliferate in vivo.* Molecular vision, 2008. **14**: p. 1784.
90. Ts'o, M.O. and E. Friedman, *The retinal pigment epithelium: I. Comparative histology.* Archives of ophthalmology, 1967. **78**(5): p. 641-649.
91. Starnes, A.C., et al., *Multi-nucleate retinal pigment epithelium cells of the human macula exhibit a characteristic and highly specific distribution.* Visual neuroscience, 2016. **33**.
92. Bhutto, I. and G. Lutty, *Understanding age-related macular degeneration*

(AMD): relationships between the photoreceptor/retinal pigment epithelium/Bruch's membrane/choriocapillaris complex. Mol Aspects Med, 2012. **33**(4): p. 295-317.

93. Dejos, C., et al., *Photoreceptor-induced RPE phagolysosomal maturation defects in Stargardt-like Maculopathy (STGD3).* Sci Rep, 2018. **8**(1): p. 5944.
94. Suzuki, A., et al., *Astrocyte-neuron lactate transport is required for long-term memory formation.* Cell, 2011. **144**(5): p. 810-23.
95. Nasi, A., et al., *Dendritic cell reprogramming by endogenously produced lactic acid.* J Immunol, 2013. **191**(6): p. 3090-9.
96. Doherty, J.R. and J.L. Cleveland, *Targeting lactate metabolism for cancer therapeutics.* The Journal of clinical investigation, 2013. **123**(9): p. 3685-3692.
97. Sun, S., et al., *Lactic Acid: No Longer an Inert and End-Product of Glycolysis.* Physiology (Bethesda), 2017. **32**(6): p. 453-463.
98. Ames, A., 3rd, et al., *Energy metabolism of rabbit retina as related to function: high cost of Na+ transport.* J Neurosci, 1992. **12**(3): p. 840-53.
99. Hurley, J.B., K.J. Lindsay, and J. Du, *Glucose, lactate, and shuttling of metabolites in vertebrate retinas.* J Neurosci Res, 2015. **93**(7): p. 1079-92.
100. Rueda, E.M., et al., *The cellular and compartmental profile of mouse retinal glycolysis, tricarboxylic acid cycle, oxidative phosphorylation, and ~P transferring kinases.* Mol Vis, 2016. **22**: p. 847-85.
101. Winkler, B.S., *Glycolytic and oxidative metabolism in relation to retinal function.* The Journal of general physiology, 1981. **77**(6): p. 667-692.
102. Warburg, O., *On the origin of cancer cells.* Science, 1956. **123**(3191): p. 309-314.
103. Kuei, C., et al., *Study of GPR81, the lactate receptor, from distant species identifies residues and motifs critical for GPR81 functions.* Mol Pharmacol, 2011. **80**(5): p. 848-58.
104. DiGirolamo, M., F. Newby, and J. Lovejoy, *Lactate production in adipose tissue: a regulated function with extra-adipose implications.* The FASEB Journal, 1992.

6(7): p. 2405-2412.

105. Kasischke, K.A., *A new pathway for lactate production in the CNS.* The Journal of physiology, 2008. **586**(5): p. 1207-1208.
106. Halestrap, A.P. and D. Meredith, *The SLC16 gene family—from monocarboxylate transporters (MCTs) to aromatic amino acid transporters and beyond.* Pflügers Archiv, 2004. **447**(5): p. 619-628.
107. Le Floch, R., et al., *CD147 subunit of lactate/H+ symporters MCT1 and hypoxia-inducible MCT4 is critical for energetics and growth of glycolytic tumors.* Proc Natl Acad Sci U S A, 2011. **108**(40): p. 16663-8.
108. Polański, R., et al., *Activity of the monocarboxylate transporter 1 inhibitor AZD3965 in small cell lung cancer.* Clinical cancer research, 2013.
109. Hauser, A.S., et al., *Pharmacogenomics of GPCR drug targets.* Cell, 2018. **172**(1-2): p. 41-54. e19.
110. Pierce, K.L., R.T. Premont, and R.J. Lefkowitz, *Signalling: seven-transmembrane receptors.* Nature reviews Molecular cell biology, 2002. **3**(9): p. 639.
111. Berry, J., et al., *Effect of rhodopsin phosphorylation on dark adaptation in mouse rods.* Journal of Neuroscience, 2016. **36**(26): p. 6973-6987.
112. Wise, A., S.C. Jupe, and S. Rees, *The identification of ligands at orphan G-protein coupled receptors.* Annu. Rev. Pharmacol. Toxicol., 2004. **44**: p. 43-66.
113. Black, J.B., R.T. Premont, and Y. Daaka. *Feedback regulation of G protein-coupled receptor signaling by GRKs and arrestins*. in *Seminars in cell & developmental biology*. 2016. Elsevier.
114. Briscoe, C.P., et al., *The orphan G protein-coupled receptor GPR40 is activated by medium and long-chain fatty acids.* Journal of Biological chemistry, 2002.
115. He, W., et al., *Citric acid cycle intermediates as ligands for orphan G-protein-coupled receptors.* Nature, 2004. **429**(6988): p. 188.
116. Vilardaga, J.-P., et al., *G-protein-coupled receptor heteromer dynamics.* J Cell Sci, 2010. **123**(24): p. 4215-4220.
117. Hanson, M.A. and R.C. Stevens, *Discovery of new GPCR biology: one receptor*

structure at a time. Structure, 2009. **17**(1): p. 8-14.

118. Chen, J.-G., et al., *GCR1 can act independently of heterotrimeric G-protein in response to brassinosteroids and gibberellins in Arabidopsis seed germination.* Plant Physiology, 2004. **135**(2): p. 907-915.
119. Lee, D.K., et al., *Discovery and mapping of ten novel G protein-coupled receptor genes.* Gene, 2001. **275**(1): p. 83-91.
120. Liu, C., et al., *Lactate inhibits lipolysis in fat cells through activation of an orphan G-protein-coupled receptor, GPR81.* Journal of Biological Chemistry, 2009. **284**(5): p. 2811-2822.
121. Ahmed, K., *Biological roles and therapeutic potential of hydroxy-carboxylic Acid receptors.* Frontiers in endocrinology, 2011. **2**: p. 51.
122. Ge, H., et al., *Elucidation of signaling and functional activities of an orphan GPCR, GPR81.* Journal of lipid research, 2008. **49**(4): p. 797-803.
123. Liu, C., et al., *3, 5-Dihydroxybenzoic acid, a specific agonist for hydroxycarboxylic acid 1, inhibits lipolysis in adipocytes.* Journal of Pharmacology and Experimental Therapeutics, 2012. **341**(3): p. 794-801.
124. Morland, C., et al., *Exercise induces cerebral VEGF and angiogenesis via the lactate receptor HCAR1.* Nature Communications, 2017. **8**: p. 15557.
125. Barnes, J.N., *Exercise, cognitive function, and aging.* Advances in physiology education, 2015. **39**(2): p. 55-62.
126. Wagner, W., K.D. Kania, and W.M. Ciszewski, *Stimulation of lactate receptor (HCAR1) affects cellular DNA repair capacity.* DNA Repair (Amst), 2017. **52**: p. 49-58.
127. Lee, Y.J., et al., *G-protein-coupled receptor 81 promotes a malignant phenotype in breast cancer through angiogenic factor secretion.* Oncotarget, 2016. **7**(43): p. 70898.
128. Wagner, W., W.M. Ciszewski, and K.D. Kania, *L-and D-lactate enhance DNA repair and modulate the resistance of cervical carcinoma cells to anticancer drugs via histone deacetylase inhibition and hydroxycarboxylic acid receptor 1 activation.* Cell Communication and Signaling, 2015. **13**(1): p. 36.

129. Roland, C.L., et al., *Cell surface lactate receptor GPR81 is crucial for cancer cell survival.* Cancer Res, 2014. **74**(18): p. 5301-10.
130. Sakurai, T., et al., *Identification of a novel GPR81-selective agonist that suppresses lipolysis in mice without cutaneous flushing.* European journal of pharmacology, 2014. **727**: p. 1-7.
131. Lerch, M.M., D.L. Conwell, and J. Mayerle, *The anti-inflammasome effect of lactate and the lactate GPR81-receptor in pancreatic and liver inflammation.* Gastroenterology, 2014. **146**(7): p. 1602-5.
132. Hearps, A.C., et al., *Vaginal lactic acid elicits an anti-inflammatory response from human cervicovaginal epithelial cells and inhibits production of pro-inflammatory mediators associated with HIV acquisition.* Mucosal Immunol, 2017. **10**(6): p. 1480-1490.
133. Iraporda, C., et al., *Local Treatment with Lactate Prevents Intestinal Inflammation in the TNBS-Induced Colitis Model.* Front Immunol, 2016. **7**: p. 651.
134. Haas, R., et al., *Lactate Regulates Metabolic and Pro-inflammatory Circuits in Control of T Cell Migration and Effector Functions.* PLoS Biol, 2015. **13**(7): p. e1002202.
135. Liu, C., et al., *Lactate inhibits lipolysis in fat cells through activation of an orphan G-protein-coupled receptor, GPR81.* J Biol Chem, 2009. **284**(5): p. 2811-22.
136. Dvorak, C.A., et al., *Identification of Hydroxybenzoic Acids as Selective Lactate Receptor (GPR81) Agonists with Antilipolytic Effects.* ACS Med Chem Lett, 2012. **3**(8): p. 637-9.
137. Wallenius, K., et al., *Involvement of the metabolic sensor GPR81 in cardiovascular control.* JCI insight, 2017. **2**(19).
138. Constant, J.S., et al., *Lactate elicits vascular endothelial growth factor from macrophages: a possible alternative to hypoxia.* Wound Repair Regen, 2000. **8**(5): p. 353-60.
139. Shen, Z., et al., *Inhibition of G protein-coupled receptor 81 (GPR81) protects*

against ischemic brain injury. CNS Neurosci Ther, 2015. **21**(3): p. 271-9.

140. Sonveaux, P., et al., *Targeting lactate-fueled respiration selectively kills hypoxic tumor cells in mice.* J Clin Invest, 2008. **118**(12): p. 3930-42.
141. Lauritzen, K.H., et al., *Lactate receptor sites link neurotransmission, neurovascular coupling, and brain energy metabolism.* Cerebral cortex, 2013. **24**(10): p. 2784-2795.
142. Tang, F., et al., *Lactate-mediated glia-neuronal signalling in the mammalian brain.* Nature communications, 2014. **5**: p. 3284.
143. Lynch, M.A., *Long-term potentiation and memory.* Physiological reviews, 2004. **84**(1): p. 87-136.
144. Kroemer, G., G. Mariño, and B. Levine, *Autophagy and the integrated stress response.* Molecular cell, 2010. **40**(2): p. 280-293.
145. Pakos‐Zebrucka, K., et al., *The integrated stress response.* EMBO reports, 2016: p. e201642195.
146. Ali, M.U., et al., *Eukaryotic translation initiation factors and cancer.* Tumor Biology, 2017. **39**(6): p. 1010428317709805.
147. Chu, J., et al., *Translation initiation factors: reprogramming protein synthesis in cancer.* Trends in cell biology, 2016. **26**(12): p. 918-933.
148. Erguler, K., M. Pieri, and C. Deltas, *A mathematical model of the unfolded protein stress response reveals the decision mechanism for recovery, adaptation and apoptosis.* BMC systems biology, 2013. **7**(1): p. 16.
149. Novoa, I., et al., *Feedback inhibition of the unfolded protein response by GADD34-mediated dephosphorylation of eIF2α.* The Journal of cell biology, 2001. **153**(5): p. 1011-1022.
150. Chan, C.-P., et al., *Internal ribosome entry site-mediated translational regulation of ATF4 splice variant in mammalian unfolded protein response.* Biochimica et Biophysica Acta (BBA)-Molecular Cell Research, 2013. **1833**(10): p. 2165-2175.
151. Rzymski, T., et al., *Regulation of autophagy by ATF4 in response to severe hypoxia.* Oncogene, 2010. **29**(31): p. 4424.

152. Scheuner, D., et al., *Translational control is required for the unfolded protein response and in vivo glucose homeostasis.* Molecular cell, 2001. **7**(6): p. 1165-1176.

153. Elkin, M., et al., *Halofuginone: a potent inhibitor of critical steps in angiogenesis progression.* The FASEB Journal, 2000. **14**(15): p. 2477-2485.

154. Pines, M., *Halofuginone for fibrosis, regeneration and cancer in the gastrointestinal tract.* World Journal of Gastroenterology: WJG, 2014. **20**(40): p. 14778.

155. Tsuchida, K., et al., *Halofuginone enhances the chemo-sensitivity of cancer cells by suppressing NRF2 accumulation.* Free Radical Biology and Medicine, 2017. **103**: p. 236-247.

156. Boyce, M., et al., *A selective inhibitor of eIF2α dephosphorylation protects cells from ER stress.* Science, 2005. **307**(5711): p. 935-939.

157. Huang, X., et al., *Salubrinal attenuates beta-amyloid-induced neuronal death and microglial activation by inhibition of the NF-kappaB pathway.* Neurobiol Aging, 2012. **33**(5): p. 1007.e9-17.

158. Axten, J.M., et al., *Discovery of 7-methyl-5-(1-{[3-(trifluoromethyl) phenyl] acetyl}-2, 3-dihydro-1 H-indol-5-yl)-7 H-pyrrolo [2, 3-d] pyrimidin-4-amine (GSK2606414), a potent and selective first-in-class inhibitor of protein kinase R (PKR)-like endoplasmic reticulum kinase (PERK).* Journal of medicinal chemistry, 2012. **55**(16): p. 7193-7207.

159. Axten, J.M., et al., *Discovery of GSK2656157: an optimized PERK inhibitor selected for preclinical development.* ACS medicinal chemistry letters, 2013. **4**(10): p. 964-968.

160. Sidrauski, C., et al., *Pharmacological brake-release of mRNA translation enhances cognitive memory.* Elife, 2013. **2**: p. e00498.

161. Ma, T., et al., *Suppression of eIF2alpha kinases alleviates Alzheimer's disease-related plasticity and memory deficits.* Nat Neurosci, 2013. **16**(9): p. 1299-305.

162. Chou, A., et al., *Inhibition of the integrated stress response reverses cognitive*

deficits after traumatic brain injury. Proceedings of the National Academy of Sciences, 2017. **114**(31): p. E6420-E6426.

163. Costa-Mattioli, M., et al., *eIF2α phosphorylation bidirectionally regulates the switch from short-to long-term synaptic plasticity and memory.* Cell, 2007. **129**(1): p. 195-206.
164. Pavitt, G.D., *Cell Biology: Less translational control, more memory.* Elife, 2013. **2**: p. e00895.
165. Ameri, K. and A.L. Harris, *Activating transcription factor 4.* The international journal of biochemistry & cell biology, 2008. **40**(1): p. 14-21.
166. Vallejo, M., et al., *C/ATF, a member of the activating transcription factor family of DNA-binding proteins, dimerizes with CAAT/enhancer-binding proteins and directs their binding to cAMP response elements.* Proceedings of the National Academy of Sciences, 1993. **90**(10): p. 4679-4683.
167. Gwinn, D.M., et al., *Oncogenic KRAS Regulates Amino Acid Homeostasis and Asparagine Biosynthesis via ATF4 and Alters Sensitivity to L-Asparaginase.* Cancer cell, 2018. **33**(1): p. 91-107. e6.
168. Ye, J., et al., *The GCN2 ‐ ATF4 pathway is critical for tumour cell survival and proliferation in response to nutrient deprivation.* The EMBO journal, 2010. **29**(12): p. 2082-2096.
169. Örd, D., K. Meerits, and T. Örd, *TRB3 protects cells against the growth inhibitory and cytotoxic effect of ATF4.* Experimental cell research, 2007. **313**(16): p. 3556-3567.
170. Mei, Y., et al., *Activating transcription factor 3 up-regulated by c-Jun NH2-terminal kinase/c-Jun contributes to apoptosis induced by potassium deprivation in cerebellar granule neurons.* Neuroscience, 2008. **151**(3): p. 771-779.
171. Downward, J., *Cell biology: metabolism meets death.* Nature, 2003. **424**(6951): p. 896.
172. Rozpedek, W., et al., *The role of the PERK/eIF2α/ATF4/CHOP signaling pathway in tumor progression during endoplasmic reticulum stress.* Current

molecular medicine, 2016. **16**(6): p. 533-544.

173. Li, Y., et al., *New insights into the roles of CHOP-induced apoptosis in ER stress.* Acta biochimica et biophysica Sinica, 2014. **46**(8): p. 629-640.
174. Marciniak, S.J., et al., *CHOP induces death by promoting protein synthesis and oxidation in the stressed endoplasmic reticulum.* Genes & development, 2004. **18**(24): p. 3066-3077.
175. Zhou, A.-X., et al., *C/EBP-homologous protein (CHOP) in vascular smooth muscle cells regulates their proliferation in aortic explants and atherosclerotic lesions.* Circulation research, 2015: p. CIRCRESAHA. 114.305602.
176. DeZwaan-McCabe, D., et al., *The stress-regulated transcription factor CHOP promotes hepatic inflammatory gene expression, fibrosis, and oncogenesis.* PLoS genetics, 2013. **9**(12): p. e1003937.
177. Lange, P.S., et al., *ATF4 is an oxidative stress–inducible, prodeath transcription factor in neurons in vitro and in vivo.* Journal of Experimental Medicine, 2008. **205**(5): p. 1227-1242.
178. Adams, C.M., *Role of the transcription factor ATF4 in the anabolic actions of insulin and the anti-anabolic actions of glucocorticoids.* Journal of Biological Chemistry, 2007. **282**(23): p. 16744-16753.
179. Seo, J., et al., *Atf4 regulates obesity, glucose homeostasis, and energy expenditure.* Diabetes, 2009.
180. Vernon, E., et al., *GABAB receptors couple directly to the transcription factor ATF4.* Molecular and Cellular Neuroscience, 2001. **17**(4): p. 637-645.
181. Masuoka, H.C. and T.M. Townes, *Targeted disruption of the activating transcription factor 4 gene results in severe fetal anemia in mice.* Blood, 2002. **99**(3): p. 736-745.
182. Tanaka, T., et al., *Targeted disruption of ATF4 discloses its essential role in the formation of eye lens fibres.* Genes to Cells, 1998. **3**(12): p. 801-810.
183. Hettmann, T., K. Barton, and J.M. Leiden, *Microphthalmia due to p53-mediated apoptosis of anterior lens epithelial cells in mice lacking the CREB-2 transcription factor.* Developmental biology, 2000. **222**(1): p. 110-123.

184. Lenox, A.R., et al., *Unfolded protein response is activated in aged retinas.* Neuroscience letters, 2015. **609**: p. 30-35.
185. Ebert, S.M., et al., *Identification and small molecule inhibition of an ATF4-dependent pathway to age-related skeletal muscle weakness and atrophy.* Journal of Biological Chemistry, 2015: p. jbc. M115. 681445.
186. Pitale, P.M., O. Gorbatyuk, and M. Gorbatyuk, *Neurodegeneration: Keeping ATF4 on a Tight Leash.* Frontiers in cellular neuroscience, 2017. **11**: p. 410.
187. Gorbatyuk, M. and O. Gorbatyuk, *Retinal degeneration: Focus on the unfolded protein response.* Molecular vision, 2013. **19**: p. 1985.
188. Zhang, S.X., et al., *Endoplasmic reticulum stress and the unfolded protein responses in retinal degeneration.* Experimental eye research, 2014. **125**: p. 30-40.
189. Ooe, E., et al., *The involvement of ATF4 and S-opsin in retinal photoreceptor cell damage induced by blue LED light.* Molecular vision, 2017. **23**: p. 52.
190. Bhootada, Y., et al., *Limited ATF4 expression in degenerating retinas with ongoing ER stress promotes photoreceptor survival in a mouse model of autosomal dominant retinitis pigmentosa.* PLoS One, 2016. **11**(5): p. e0154779.
191. Chen, Y., et al., *Activating transcription factor 4 mediates hyperglycaemia-induced endothelial inflammation and retinal vascular leakage through activation of STAT3 in a mouse model of type 1 diabetes.* Diabetologia, 2012. **55**(9): p. 2533-2545.
192. Wang, X., et al., *Modulation of angiogenesis by genetic manipulation of ATF4 in mouse model of oxygen-induced retinopathy.* Investigative ophthalmology & visual science, 2013. **54**(9): p. 5995-6002.
193. Liu, C., et al., *Activating transcription factor 4 promotes angiogenesis of breast cancer through enhanced macrophage recruitment.* BioMed research international, 2015. **2015**.
194. Chen, D., et al., *ATF4 promotes angiogenesis and neuronal cell death and confers ferroptosis in a xCT-dependent manner.* Oncogene, 2017. **36**(40): p.

5593.

195. Afonyushkin, T., et al., *Oxidized phospholipids regulate expression of ATF4 and VEGF in endothelial cells via NRF2-dependent mechanism: novel point of convergence between electrophilic and unfolded protein stress pathways.* Arteriosclerosis, thrombosis, and vascular biology, 2010. **30**(5): p. 1007-1013.

196. Picard, E., et al., *CD36 plays an important role in the clearance of oxLDL and associated age-dependent sub-retinal deposits.* Aging (Albany NY), 2010. **2**(12): p. 981-9.

197. Favret, S., et al., *Deficiency in the metabolite receptor SUCNR1 (GPR91) leads to outer retinal lesions.* Aging (Albany NY), 2013. **5**(6): p. 427-44.

198. Tahiri, H., et al., *p75 neurotrophin receptor participates in the choroidal antiangiogenic and apoptotic effects of T-lymphocyte-derived microparticles.* Invest Ophthalmol Vis Sci, 2013. **54**(9): p. 6084-92.

199. Lameynardie, S., et al., *Inhibition of choroidal angiogenesis by calcium dobesilate in normal Wistar and diabetic GK rats.* European journal of pharmacology, 2005. **510**(1-2): p. 149-156.

200. Defoe, D.M. and K.C. Easterling, *Reattachment of retinas to cultured pigment epithelial monolayers from Xenopus laevis.* Investigative ophthalmology & visual science, 1994. **35**(5): p. 2466-2476.

201. Bradford, M.M., *A rapid and sensitive method for the quantitation of microgram quantities of protein utilizing the principle of protein-dye binding.* Analytical biochemistry, 1976. **72**(1-2): p. 248-254.

202. Towbin, H., T. Staehelin, and J. Gordon, *Electrophoretic transfer of proteins from polyacrylamide gels to nitrocellulose sheets: procedure and some applications.* Proceedings of the National Academy of Sciences, 1979. **76**(9): p. 4350-4354.

203. Dorfman, A., et al., *Early manifestations of postnatal hyperoxia on the retinal structure and function of the neonatal rat.* Investigative ophthalmology & visual science, 2008. **49**(1): p. 458-466.

204. Dorfman, A.L., et al., *Functional and structural changes resulting from strain differences in the rat model of oxygen-induced retinopathy.* Investigative ophthalmology & visual science, 2009. **50**(5): p. 2436-2450.
205. Madaan, A., *Regulation of retinal angiogenesis by a novel lactate receptor, GPR81*. 2012: McGill University (Canada).
206. Hoque, R., et al., *Lactate reduces liver and pancreatic injury in Toll-like receptor–and inflammasome-mediated inflammation via GPR81-mediated suppression of innate immunity.* Gastroenterology, 2014. **146**(7): p. 1763-1774.
207. Lerch, M.M., D.L. Conwell, and J. Mayerle, *The anti-inflammasome effect of lactate and the lactate GPR81-receptor in pancreatic and liver inflammation.* Gastroenterology, 2014. **146**(7): p. 1602-1605.
208. Madaan, A., et al., *Lactate produced during labor modulates uterine inflammation via GPR81 (HCA1).* American Journal of Obstetrics & Gynecology, 2017. **216**(1): p. 60. e1-60. e17.
209. Khatib-Massalha, E., et al., *Lactate Release By Bone Marrow Neutrophils Promotes Their Inflammatory Mobilization Via Endothelial GPR81 Signaling*. 2017, Am Soc Hematology.
210. Ahmed, K., et al., *An autocrine lactate loop mediates insulin-dependent inhibition of lipolysis through GPR81.* Cell metabolism, 2010. **11**(4): p. 311-319.
211. Cai, T.-Q., et al., *Role of GPR81 in lactate-mediated reduction of adipose lipolysis.* Biochemical and biophysical research communications, 2008. **377**(3): p. 987-991.
212. Feng, J., et al., *Tumor cell-derived lactate induces TAZ-dependent upregulation of PD-L1 through GPR81 in human lung cancer cells.* Oncogene, 2017. **36**(42): p. 5829-5839.
213. Liu, Y., A. Beyer, and R. Aebersold, *On the Dependency of Cellular Protein Levels on mRNA Abundance.* Cell, 2016. **165**(3): p. 535-50.
214. Quirós, P.M., et al., *Multi-omics analysis identifies ATF4 as a key regulator of the*

mitochondrial stress response in mammals. J Cell Biol, 2017: p. jcb. 201702058.

215. Williams, E.G., et al., *Systems proteomics of liver mitochondria function.* Science, 2016. **352**(6291): p. aad0189.
216. Chick, J.M., et al., *Defining the consequences of genetic variation on a proteome-wide scale.* Nature, 2016. **534**(7608): p. 500.
217. Cheng, Z., et al., *Differential dynamics of the mammalian mRNA and protein expression response to misfolding stress.* Molecular systems biology, 2016. **12**(1): p. 855.
218. Prabhakar, U., et al., *Correlation of protein and gene expression profiles of inflammatory proteins after endotoxin challenge in human subjects.* DNA Cell Biol, 2005. **24**(7): p. 410-31.
219. Milne, G.L., et al., *Isoprostane generation and function.* Chem Rev, 2011. **111**(10): p. 5973-96.
220. Bojic, M., et al., *Aromatic hydroxylation of salicylic acid and aspirin by human cytochromes P450.* Eur J Pharm Sci, 2015. **73**: p. 49-56.
221. Lee, A.S., *The ER chaperone and signaling regulator GRP78/BiP as a monitor of endoplasmic reticulum stress.* Methods, 2005. **35**(4): p. 373-81.
222. Halliday, M., et al., *Partial restoration of protein synthesis rates by the small molecule ISRIB prevents neurodegeneration without pancreatic toxicity.* Cell death & disease, 2016. **6**(3): p. e1672.
223. Imamura, Y., et al., *Drusen, choroidal neovascularization, and retinal pigment epithelium dysfunction in SOD1-deficient mice: a model of age-related macular degeneration.* Proceedings of the National Academy of Sciences, 2006. **103**(30): p. 11282-11287.
224. Favret, S., et al., *Deficiency in the metabolite receptor SUCNR1 (GPR91) leads to outer retinal lesions.* Aging (Albany NY), 2013. **5**(6): p. 427.
225. Bird, A., *Bruch's membrane change with age.* The British journal of ophthalmology, 1992. **76**(3): p. 166.
226. Lu, H., et al., *Chronic stress accelerates ligature-induced periodontitis by*

suppressing glucocorticoid receptor-α signaling. Experimental & molecular medicine, 2016. **48**(3): p. e223.

227. Cuadrado-Tejedor, M., et al., *Chronic mild stress accelerates the onset and progression of the Alzheimer's disease phenotype in Tg2576 mice.* Journal of Alzheimer's Disease, 2012. **28**(3): p. 567-578.
228. Jeong, Y.H., et al., *Chronic stress accelerates learning and memory impairments and increases amyloid deposition in APPV717I-CT100 transgenic mice, an Alzheimer's disease model.* The FASEB Journal, 2006. **20**(6): p. 729-731.
229. Justice, N.J., *The relationship between stress and Alzheimer's disease.* Neurobiology of stress, 2018.
230. Lee, S.H., S.-I. Do, and H.-S. Kim, *Hyperoxia accelerates progression of hepatic fibrosis by up-regulation of transforming growth factor-β expression.* World Journal of Gastroenterology: WJG, 2014. **20**(11): p. 3011.
231. Wang, L., et al., *Abundant lipid and protein components of drusen.* PloS one, 2010. **5**(4): p. e10329.
232. Cougnard-Grégoire, A., et al., *Elevated high-density lipoprotein cholesterol and age-related macular degeneration: the Alienor study.* PloS one, 2014. **9**(3): p. e90973.
233. Cackett, P., et al., *Smoking, cardiovascular risk factors, and age-related macular degeneration in Asians: the Singapore Malay Eye Study.* American journal of ophthalmology, 2008. **146**(6): p. 960-967. e1.
234. Chakravarthy, U., et al., *Clinical risk factors for age-related macular degeneration: a systematic review and meta-analysis.* BMC ophthalmology, 2010. **10**(1): p. 31.
235. Smith, W., et al., *Plasma fibrinogen levels, other cardiovascular risk factors, and age-related maculopathy: the Blue Mountains Eye Study.* Archives of ophthalmology, 1998. **116**(5): p. 583-587.
236. Tomany, S.C., et al., *Risk factors for incident age-related macular degeneration: pooled findings from 3 continents.* Ophthalmology, 2004. **111**(7): p. 1280-1287.

237. Butt, A.L., et al., *Prevalence and risks factors of age-related macular degeneration in Oklahoma Indians: the Vision Keepers Study.* Ophthalmology, 2011. **118**(7): p. 1380-1385.
238. van Leeuwen, R., et al., *Cholesterol and age-related macular degeneration: is there a link?* American journal of ophthalmology, 2004. **137**(4): p. 750-752.
239. Wasmuth, S., et al., *Increased vitronectin production by complement-stimulated human retinal pigment epithelial cells.* Investigative ophthalmology & visual science, 2009. **50**(11): p. 5304-5309.
240. Johnson, L.V., et al., *A potential role for immune complex pathogenesis in drusen formation.* Experimental eye research, 2000. **70**(4): p. 441-449.
241. Betteridge, D.J., *What is oxidative stress?* Metabolism, 2000. **49**(2 Suppl 1): p. 3-8.
242. Birben, E., et al., *Oxidative stress and antioxidant defense.* World Allergy Organization Journal, 2012. **5**(1): p. 9.
243. Cho, H.-Y., et al., *Gene expression profiling of NRF2-mediated protection against oxidative injury.* Free Radical Biology and Medicine, 2005. **38**(3): p. 325-343.
244. Álvarez, Z., et al., *Neuronal progenitor maintenance requires lactate metabolism and PEPCK-M-directed cataplerosis.* Cerebral cortex, 2014. **26**(3): p. 1046-1058.
245. Joulia, F., et al., *Reduced oxidative stress and blood lactic acidosis in trained breath-hold human divers.* Respiratory physiology & neurobiology, 2002. **133**(1-2): p. 121-130.
246. Abbott, D.A., et al., *Catalase overexpression reduces lactic acid-induced oxidative stress in Saccharomyces cerevisiae.* Applied and environmental microbiology, 2009. **75**(8): p. 2320-2325.
247. Yoshimura, K., et al., *Monocarboxylate transporter-1 is required for cell death in mouse chondrocytic ATDC5 cells exposed to interleukin-1β via late-phase activation of nuclear factor κB and expression of phagocyte-type NADPH-oxidase.* Journal of Biological Chemistry, 2011: p. jbc. M111. 221259.
248. Lee, I., et al., *Inhibition of monocarboxylate transporter 2 induces*

senescence-associated mitochondrial dysfunction and suppresses progression of colorectal malignancies in vivo. Molecular cancer therapeutics, 2012.

249. De Saedeleer, C., et al., *Glucose deprivation increases monocarboxylate transporter 1 (MCT1) expression and MCT1-dependent tumor cell migration.* Oncogene, 2014. **33**(31): p. 4060.
250. Petrides, C., et al., *Monocarboxylate transporter 4 as a prognostic biomarker in patients with colorectal cancer and liver metastases.* International Journal of Surgery Open, 2016. **5**: p. 37-43.
251. Cao, S.S. and R.J. Kaufman, *Endoplasmic reticulum stress and oxidative stress in cell fate decision and human disease.* Antioxidants & redox signaling, 2014. **21**(3): p. 396-413.
252. Di Meo, S., et al., *Role of ROS and RNS sources in physiological and pathological conditions.* Oxidative Medicine and Cellular Longevity, 2016. **2016**.
253. Piccirella, S., et al., *Uncoupled redox systems in the lumen of the endoplasmic reticulum pyridine nucleotides stay reduced in an oxidative environment.* Journal of Biological Chemistry, 2006. **281**(8): p. 4671-4677.
254. Malhotra, J.D. and R.J. Kaufman, *Endoplasmic reticulum stress and oxidative stress: a vicious cycle or a double-edged sword?* Antioxidants & redox signaling, 2007. **9**(12): p. 2277-2294.
255. Chong, W.C., M.D. Shastri, and R. Eri, *Endoplasmic reticulum stress and oxidative stress: a vicious nexus implicated in bowel disease pathophysiology.* International journal of molecular sciences, 2017. **18**(4): p. 771.
256. Harding, H.P., et al., *Bioactive small molecules reveal antagonism between the integrated stress response and sterol-regulated gene expression.* Cell metabolism, 2005. **2**(6): p. 361-371.
257. Ammon, S., et al., *Microarray analysis of genes expressed in the frontal cortex of rats chronically treated with morphine and after naloxone precipitated withdrawal.* Molecular brain research, 2003. **112**(1-2): p. 113-125.
258. Fan, R., et al., *Chronic oxycodone induces integrated stress response in rat brain.* BMC neuroscience, 2015. **16**(1): p. 58.

259. Berthiaume, M., et al., *High levels of oxidative stress globally inhibit gene transcription and histone acetylation.* DNA and cell biology, 2006. **25**(2): p. 124-134.

260. Mahalingaiah, P.K.S., L. Ponnusamy, and K.P. Singh, *Oxidative stress-induced epigenetic changes associated with malignant transformation of human kidney epithelial cells.* Oncotarget, 2017. **8**(7): p. 11127.

261. Bhat, A.V., et al., *Stressing the (epi) genome: dealing with reactive oxygen species in cancer.* Antioxidants & redox signaling, 2017.

262. Palmisano, I., et al., *Amino acid starvation induces reactivation of silenced transgenes and latent HIV-1 provirus via down-regulation of histone deacetylase 4 (HDAC4).* Proceedings of the National Academy of Sciences, 2012. **109**(34): p. E2284-E2293.

263. De Vito, A., et al., *Amino acid deprivation triggers a novel GCN2-independent response leading to the transcriptional reactivation of non-native DNA sequences.* PloS one, 2018. **13**(7): p. e0200783.

264. Balasubramanian, M.N., J. Shan, and M.S. Kilberg, *Dynamic changes in genomic histone association and modification during activation of the ASNS and ATF3 genes by amino acid limitation.* Biochemical Journal, 2013. **449**(1): p. 219-229.

265. Ryu, H.-W., et al., *HDAC6 regulates sensitivity to cell death in response to stress and post-stress recovery.* Cell Stress and Chaperones, 2017. **22**(2): p. 253-261.

266. Mikhed, Y., et al., *Redox regulation of genome stability by effects on gene expression, epigenetic pathways and DNA damage/repair.* Redox biology, 2015. **5**: p. 275-289.

267. Hu, W., et al., *Differences in the temporal expression of regulatory growth factors during choroidal neovascular development.* Exp Eye Res, 2009. **88**(1): p. 79-91.

268. Jin, M., et al., *Regulation of RPE intercellular junction integrity and function by hepatocyte growth factor.* Invest Ophthalmol Vis Sci, 2002. **43**(8): p. 2782-90.

269. Lashkari, K., N. Rahimi, and A. Kazlauskas, *Hepatocyte growth factor receptor*

in human RPE cells: implications in proliferative vitreoretinopathy. Invest Ophthalmol Vis Sci, 1999. **40**(1): p. 149-56.

270. Cecchini, M.G., et al., *Role of colony stimulating factor-1 in the establishment and regulation of tissue macrophages during postnatal development of the mouse.* Development, 1994. **120**(6): p. 1357-1372.
271. Lin, E.Y., et al., *Macrophages regulate the angiogenic switch in a mouse model of breast cancer.* Cancer research, 2006. **66**(23): p. 11238-11246.
272. Kubota, Y., et al., *M-CSF inhibition selectively targets pathological angiogenesis and lymphangiogenesis.* Journal of Experimental Medicine, 2009. **206**(5): p. 1089-1102.
273. Lin, E.Y., et al., *Colony-stimulating factor 1 promotes progression of mammary tumors to malignancy.* Journal of Experimental Medicine, 2001. **193**(6): p. 727-740.

TABLES & FIGURES

Table 3.1 Mouse primers used in our study

Primers	Forward (5' to 3')	Reverse (5' to 3')
GPR81	CATCTTGTTCTGCTCGGTCA	GAGGAAGTAGAGCCTAGCCA
VEGF A	GCCCTGAGTCAAGAGGACAG	CTCCTAGGCCCCTCAGAAGT
bFGF2	TGGCTTCTAAGTGTGTTACAG	GTTTCAGTGCCACATACCAAC
Ang II	ATGAGCCCAGGTCCTTTGTT	AGAGGTTAGCTTTCTTTTCACCA
PEDF	GGGGCCCTCCTCTTCATAG	GAGCCCGTTCATGTTACAAGT
ApoE	TTCGGAAGGAGCTGACTGG	TTCTTGTGTGACTTGGGAGC
Sema 3F	TCGCGCACAGGATTACATCTT	ACCGGGAGTTGTACTGATCTG
TSP-1	CAAAGCCTGCAAGAAAGACG	TTGGACAGGCATCCATCAAT
IL-1 β	AGATGAAGGGCTGCTTCCAAA	GGAAGGTCCACGGGAAAGAC
TNF α	GCCTCTTCTCATTCCTGCTTG	CTGATGAGAGGGAGGCCATT
IL-8 homologue	TAGGCATCTTCGTCCGTCC	CAACAGTAGCCTTCACCCAT
COX2	ACGTGCAACACCTGAGCGGTT	CCAGCAACCCGGCCAGCAATC
NLRP3	AGCCAGAGTGGAATGACACG	CGTGTAGCGACTGTTGAGGT
PLA2	TCTTGATCCCCAATGCTTCG	GCTGCATCTCCTTTTTGCTG
Ccl2	GCTCAGCCAGATGCAGTTA	TGTCTGGACCCATTCCTTCT
MMP3	GTGACCCCACTCACTTTCTC	TTGGTACCAGTGACATCCTCT
IL-1 RA	TGGGAAGGTCTGTGCCATA	CCAGATTCTGAAGGCTTGCAT
IL-10	TAACTGCACCCACTTCCCAG	AGGCTTGGCAACCCAAGTAA
Bcl2	TGTGGCCTTCTTTGAGTTCG	TTCCACAAAGGCATCCCAG
BAD	GGCCTCCAGGATCCAAATG	GAACATACTCTGGGCTGCT
Caspase 3	CCTCAGAGAGACATTCATGG	GCAGTAGTCGCCTCTGAAGA
FASL	TGGCTACCGGTGGTATTTTT	GGGTTGGCTATTTGCTTTTC
RIP3	CTGATTGTTCCCTTTGCAGAC	CAGTAGGCCATAACTTGACAG
Asns	GAGAAACTCTTCCCAGGCTTTG	CAAGCGTTTCTTGATAGCGTTGT
Trib3	TGTCTTCAGCAACTGTGAGAGGA	CAGTCATCACGCAGGCATC
Chop	CGGAACCTGAGGAGAGAGTG	CGTTTCCTGGGGATGAGATA
ATF3	ATGATGCTTCAACACCCAGGC	TTAGCTCTGCAATGTTCCTTC

Table 3.2 Antibodies/markers and associated applications in our project

No.	Name	Cat.#	Isotypes	IHC	WB	kD
1.	RPE65	AB13826	Mouse monoclonal	1:250		
2.	ATF4/creb-2 (b3)	Sc-390063	Mouse monoclonal	1:100	1:100 10%gel	40/50kDa
3.	Ace-H3	Millipore 06-599	Rabbit polyclonal	1:1000	1:1000 15%gel	~17 kDa observed
4.	Total H3	Ab1791	Rabbit monoclonal		1:1000 15%gel	17 kDa
5.	eIF2a(D-3)	Sc-133132	Mouse monoclonal		1:100 10%gel	36 kDa
6.	Pho-eIF2a	Ab32157	Rabbit monoclonal		1:500 10%gel	36 kDa
7.	BiP	BD 610978	Mouse monoclonal	n/a	1:1000 10%gel	78 kDa
8.	HSP90 sample	Sc-13119	Mouse monoclonal		1:1000	90 kDa
9.	β-actin (C4)	Sc-47778	Mouse monoclonal		1:1000	43 kDa
10	Lectin green	L2895 sigma			1:400	
11.	Rhodamine phalloindin	Biotium 00027		1:400		
12.	Iba-1	Wako 019-19741	Rabbit polyclonal	1:500		
13	Lectin (red) Rhodamine labeled	RL-1102	Vector laboratories, USA			
14.	Anti-GPR81	Sigma SAB1300790	Rabbit polyclonal	1:400		
15.	Anti-CD46	Ab175397	Rabbit polyclonal	1:100		
16.	Anti-GADD34	PA1-139 (thermo fisher)	Rabbit polyclonal		1:1000	75kD
17.	PDI	Ab2792	Mouse monoclonal	1:100	1:1000	58 kDa

18.	Nrf2	Ab31163	Rabbit polyclonal	1:500

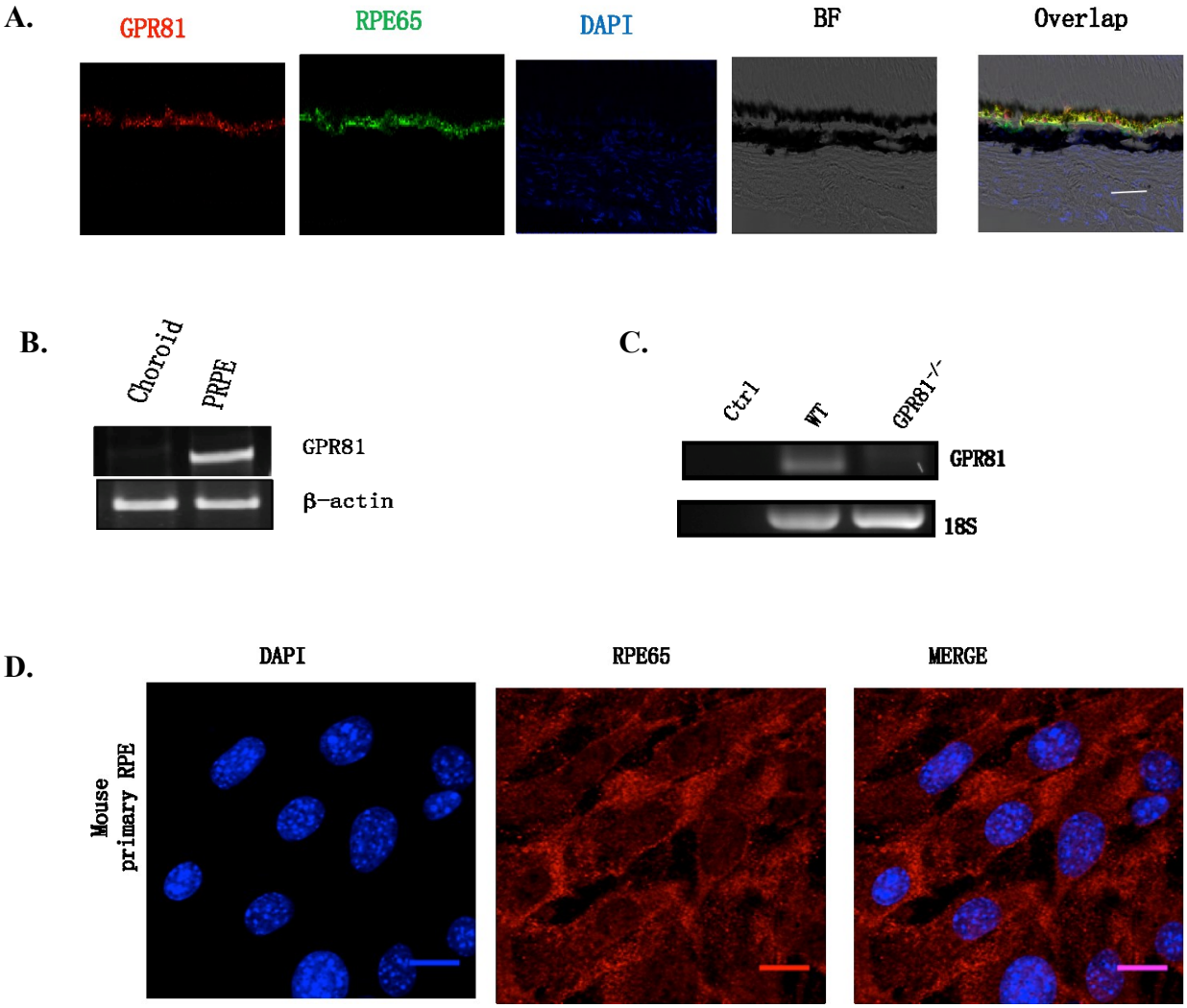

Fig. 4.1 GPR81 is exclusively located in the RPE layer in the outer retina.

(A) Sagittal cryosection of the eye (P12) stained with anti-GPR81 (red) and anti-RPE65 (an RPE marker, green) revealed GPR81 is located in RPE layer. Scale bar: 50 μm; (B) Representative PCR images of mRNA levels of GPR81 in choroid and primary RPE (PRPE) cells, indicating that GPR81 is exclusively expressed in the RPE layer; (C) Examined by PCR, mRNA levels of GPR81 in GPR81 WT and KO mice suggested that GPR81$^{-/-}$ mice was successfully generated; (D) RPE65 staining (red) in isolated PRPE shows that its purity is almost 100%. Scale bar: 5 μm. BF: bright field.

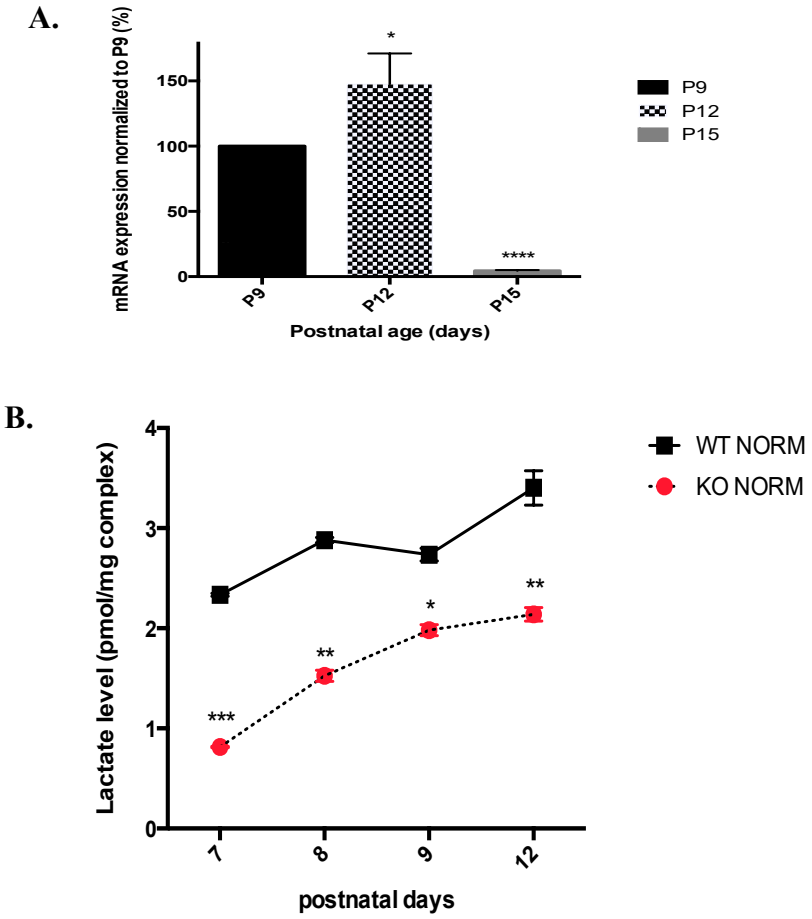

Fig. 4.2 Physical levels of GPR81 and its endogenous ligand lactate in RPE/choroid complex.

(A) mRNA levels of GPR81 in RPE/choroid complex were detected at P9, P12, and P15 by q-PCR, indicating a peak at P12; (B) The level of its endogenous ligand lactate also increased as well until P12 in both WT and KO mice. Data were presented as mean ± SEM. * $p<0.05$, **$p<0.01$ (one way ANOVA and t-test). $n\geq4$.

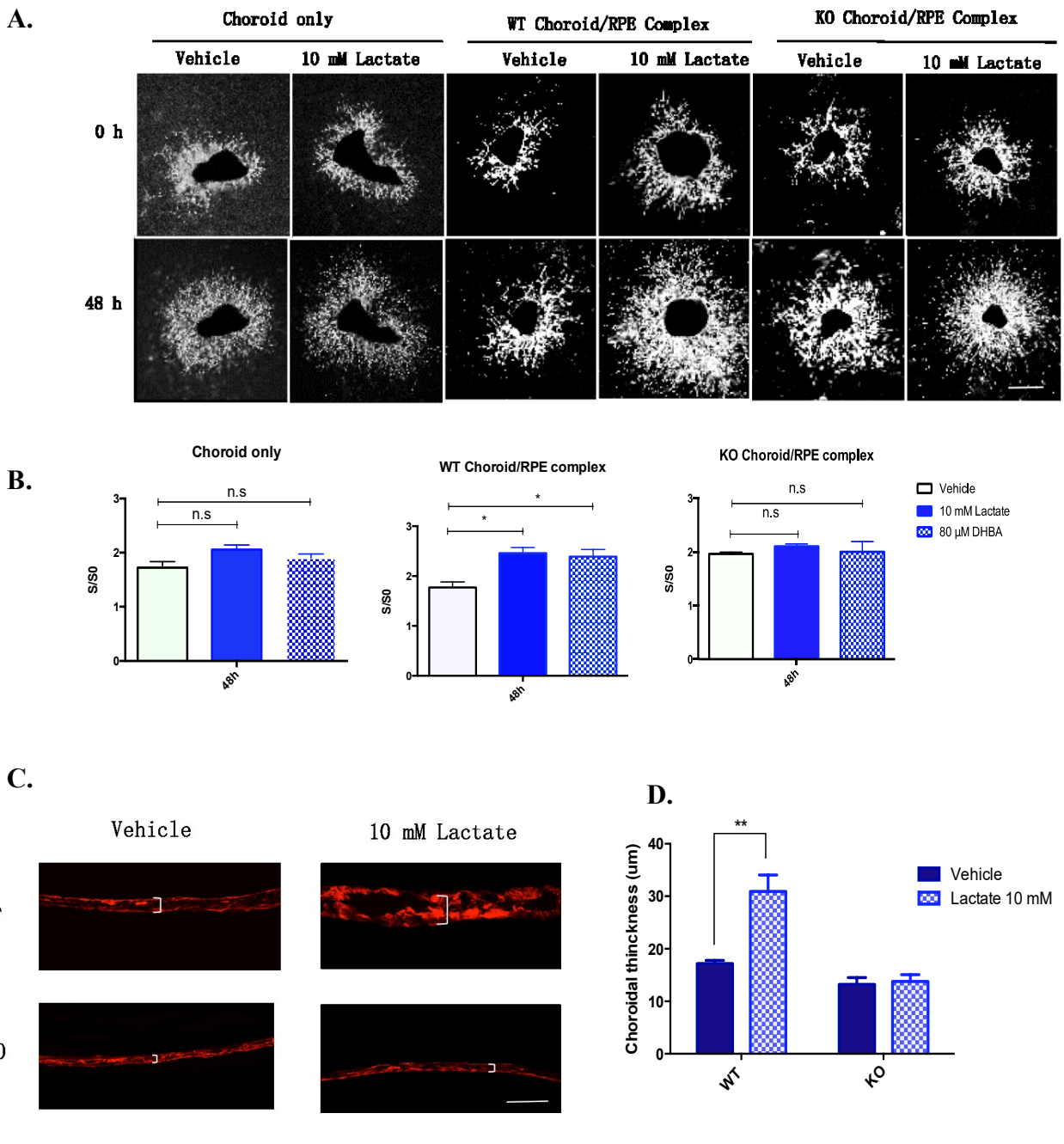
A.
Choroid only
WT Choroid/RPE Complex
KO Choroid/RPE Complex
Vehicle
10 mM Lactate
Vehicle
10 mM Lactate
Vehicle
10 mM Lactate
0 h
48 h
B.
Choroid only
WT Choroid/RPE complex
KO Choroid/RPE complex
n.s
n.s
*
*
n.s
n.s
S/S0
48h
Vehicle
10 mM Lactate
80 μM DHBA
C.
Vehicle
10 mM Lactate
WT
KO
D.
**
Choroidal thinckness (um)
Vehicle
Lactate 10 mM
WT
KO

Fig. 4.3 Activating GPR81 promotes angiogenesis *ex vivo* and *in vivo*.

(A) Representative images of choroid sprout assay. Isolated choroid, WT choroid/RPE complex or KO choroid/RPE complex was treated with vehicle, 10 mM lactate or 80 μM DHBA. (B) Quantification of choroid sprout assay. (C) Representative images of choroidal vasculature thickness stained with lectin (red) from mice that was intravitreal injected with 10 mM lactate at P9 and sacrificed at P12. (D) Quantification of the choroidal vasculature thickness. Data were presented as mean ± SEM. * $p<0.05$, **$p<0.01$. n.s: not significant. $n\geq4$ per group. Scale bar: 50 μm.

A.

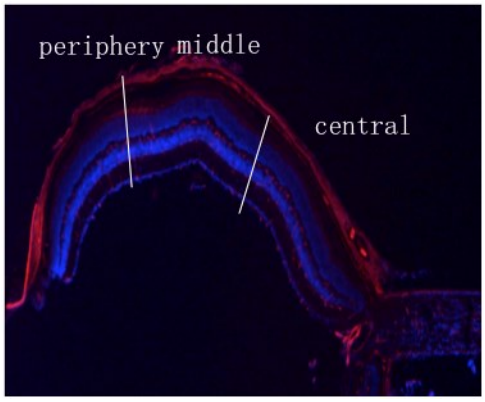
periphery middle
central

B.

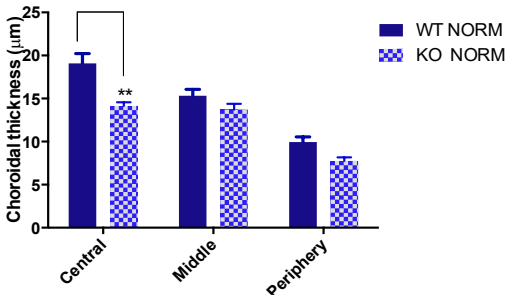
Choroidal thickness (μm)
25
20
15
10
5
0
**
Central
Middle
Periphery
WT NORM
KO NORM

C.

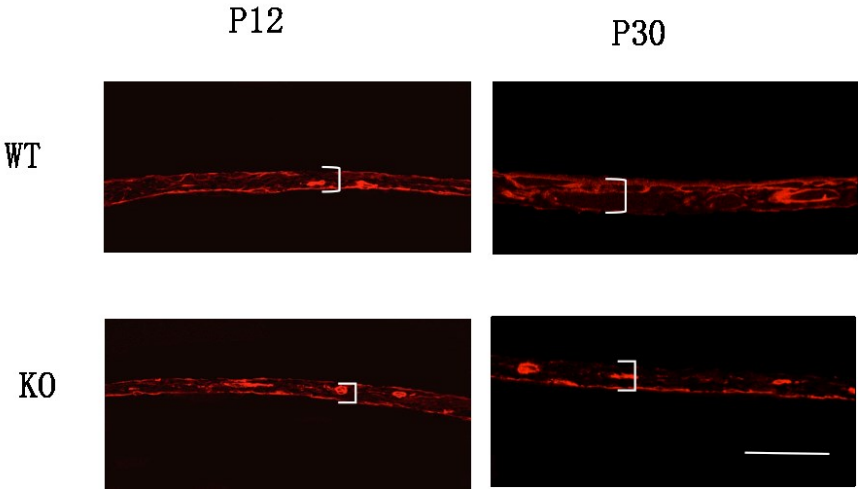
P12
P30
WT
KO

D.

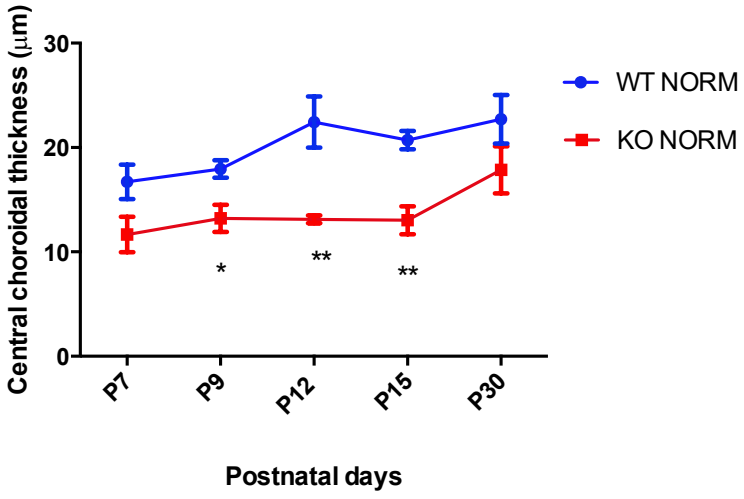
Central choroidal thickness (μm)
30
20
10
0
*
**
**
P7
P9
P12
P15
P30
Postnatal days
WT NORM
KO NORM

Fig. 4.4 The choroidal thinning in young GPR81$^{-/-}$ mice.

(A) Representative image of sagittal cryosection stained with lectin (red) and DAPI (blue). The eyecup was divided into 3 sections: central, middle and periphery, to facilitate the calculations of choroidal thickness. (B) Quantification of choroidal thickness in different regions of the eyecup, indicating the most pronounced affected region in KO mice was the central, compared to their controls. (C) Representative images of choroidal vasculature at young ages. (D) Quantifications of choroidal vasculature at different ages in mice, indicating KO mice have thinner choroidal vasculature at young age. Data were presented as mean ± SEM. * $p<0.05$, **$p<0.01$. n.s: not significant. $n\geq4$ per group. Scale bar: 50 μm.

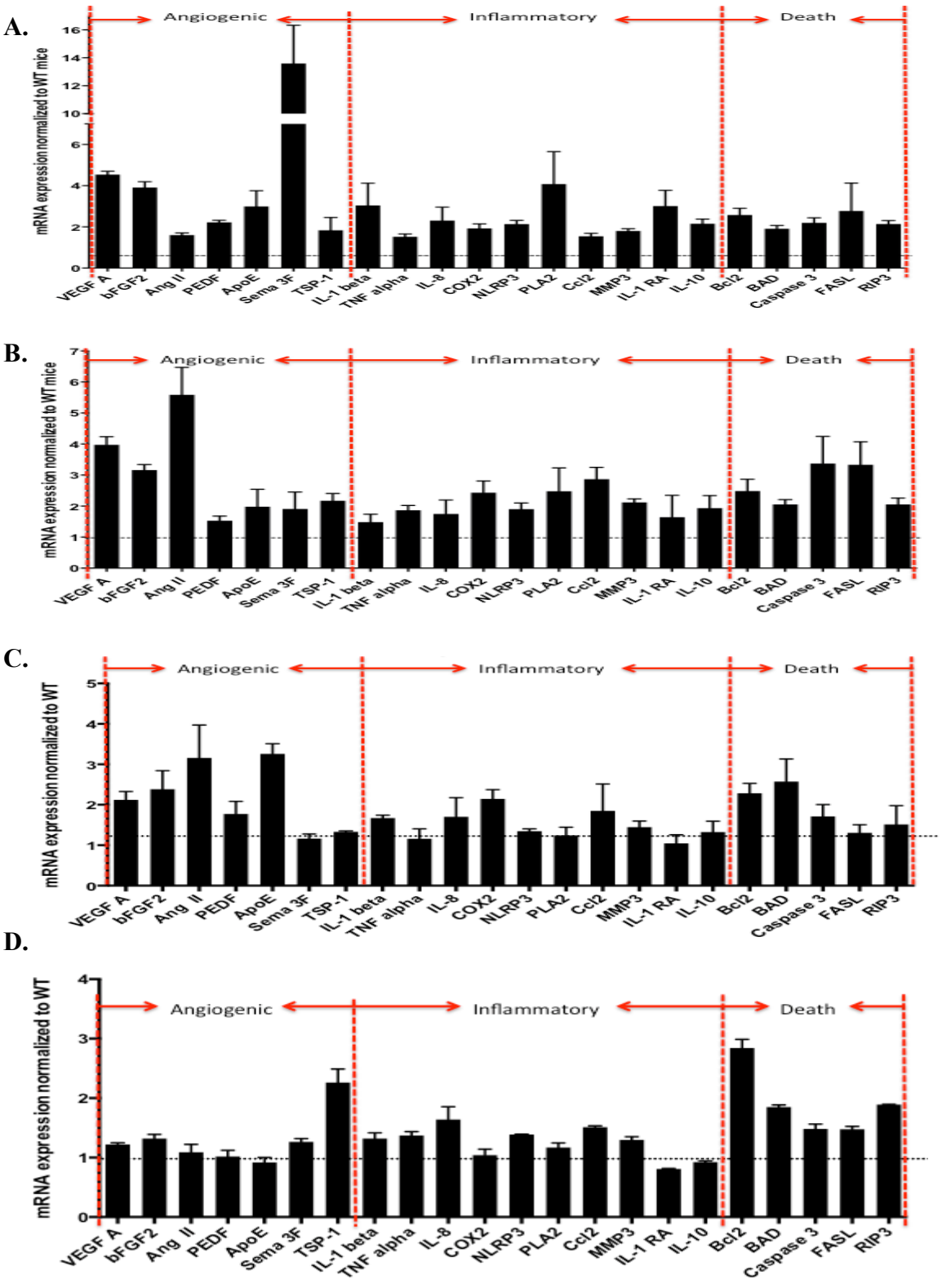
A.
B.
C.
D.
Angiogenic
Inflammatory
Death
mRNA expression normalized to WT mice
mRNA expression normalized to WT
VEGF A
bFGF2
Ang II
PEDF
ApoE
Sema 3F
TSP-1
IL-1 beta
TNF alpha
IL-8
COX2
NLRP3
PLA2
Ccl2
MMP3
IL-1 RA
IL-10
Bcl2
BAD
Caspase 3
FASL
RIP3

Fig. 4.5 Fold changes of gene profiles in GPR81$^{-/-}$ mice normalized to age-matched WT groups.

mRNA levels of 22 factors that are involved in angiogenesis, inflammation and death were screened by quantitative PCR, and were presented as the fold changes of KO versus WT : (A) the fold changes of P9 mice; (B) the fold changes of P12 mice; (C) the fold changes of P15 mice; (D) the fold changes of primary RPE cells. Data were presented as mean ± SEM. n≥4 per group.

VEGF-A: vascular endothelial growth factor A; bFGF2: basic fibroblast growth factor 2; Ang II: angiotensin II; PEDF: pigment epithelium-derived factor; ApoE: apolipoprotein E; Sema 3F: semaphoring 3F; TSP-1: thrombospondin 1; IL-1 beta: interleukin-1 beta; TNF alpha: tumor necrosis factor alpha; IL-8: interleukin 8 homologue; COX2: cyclooxygenase 2; NLRP3: NLR family pyrin domain containing 3; PLA2: Phospholipase A2; Ccl2: Chemokine ligand 2; MMP3: Matrix metalloproteinase 3; IL-1 RA: interleukin 1 receptor antagonist; IL-10: interleukin 10; Bcl2: B-cell lymphoma 2; BAD: the Bcl2-associated death promoter; FASL: Fas ligand; RIP3: the receptor-interacting protein kinase 3.

A.

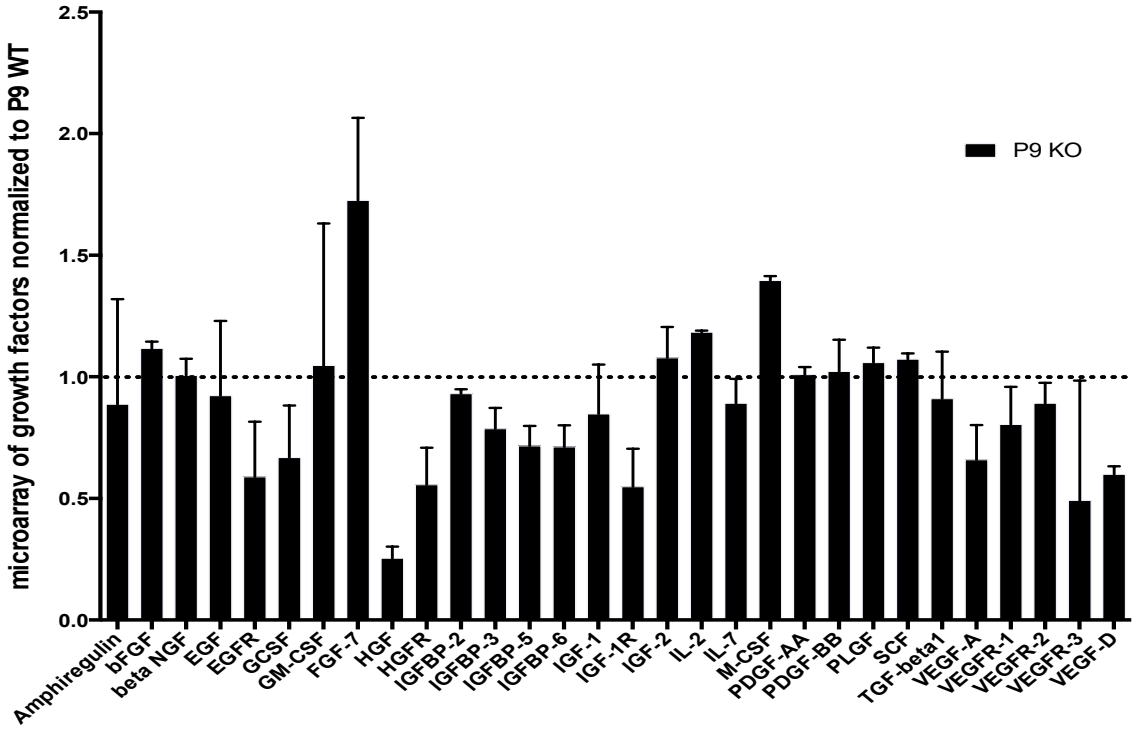
microarray of growth factors normalized to P9 WT
2.5
2.0
1.5
1.0
0.5
0.0
P9 KO
Amphiregulin
bFGF
beta NGF
EGF
EGFR
GCSF
GM-CSF
FGF-7
HGF
HGFR
IGFBP-2
IGFBP-3
IGFBP-5
IGFBP-6
IGF-1
IGF-1R
IGF-2
IL-2
IL-7
M-CSF
PDGF-AA
PDGF-BB
PLGF
SCF
TGF-beta1
VEGF-A
VEGFR-1
VEGFR-2
VEGFR-3
VEGF-D

B.

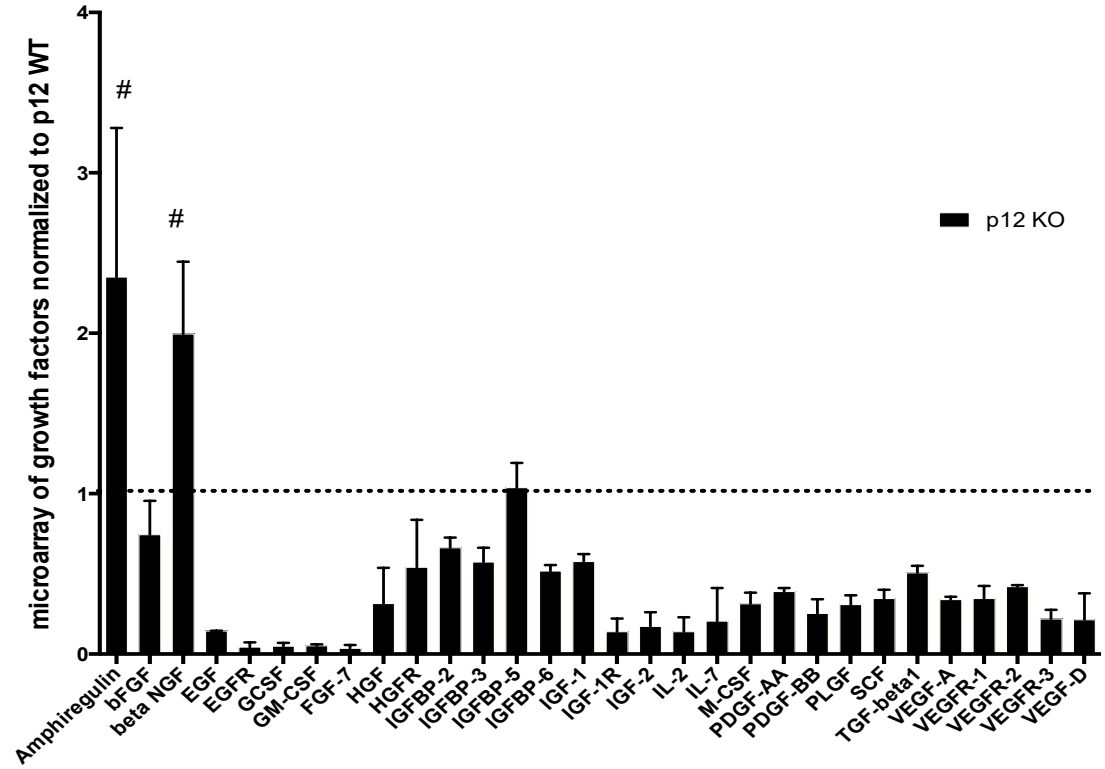
microarray of growth factors normalized to p12 WT
4
3
2
1
0
#
#
p12 KO
Amphiregulin
bFGF
beta NGF
EGF
EGFR
GCSF
GM-CSF
FGF-7
HGF
HGFR
IGFBP-2
IGFBP-3
IGFBP-5
IGFBP-6
IGF-1
IGF-1R
IGF-2
IL-2
IL-7
M-CSF
PDGF-AA
PDGF-BB
PLGF
SCF
TGF-beta1
VEGF-A
VEGFR-1
VEGFR-2
VEGFR-3
VEGF-D

C.

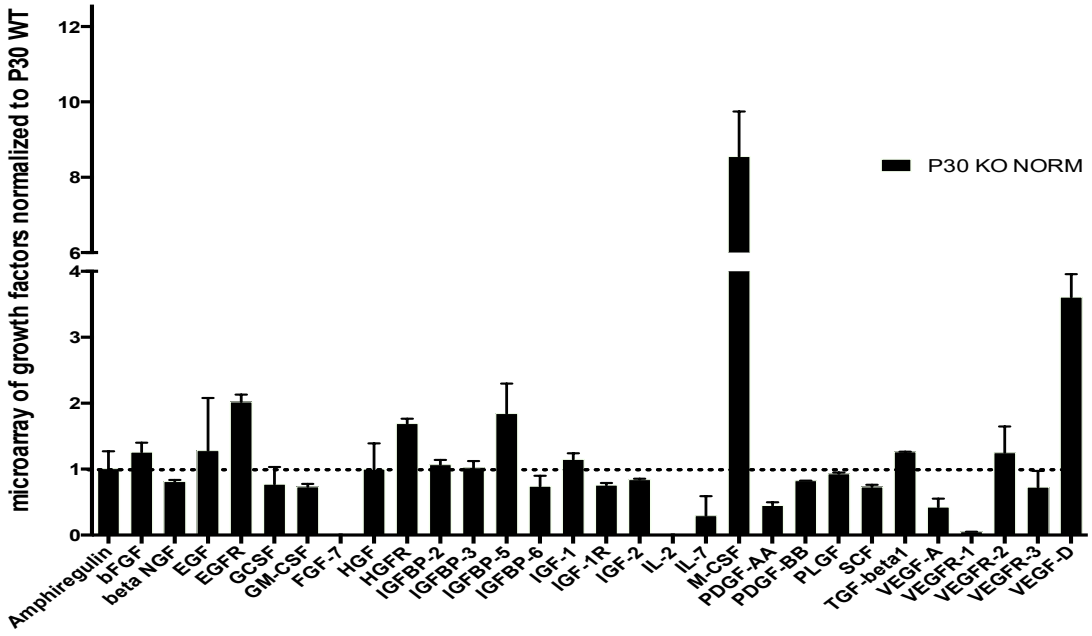
microarray of growth factors normalized to P30 WT
P30 KO NORM
Amphiregulin
bFGF
beta NGF
EGF
EGFR
GCSF
GM-CSF
FGF-7
HGF
HGFR
IGFBP-2
IGFBP-3
IGFBP-5
IGFBP-6
IGF-1
IGF-1R
IGF-2
IL-2
IL-7
M-CSF
PDGF-AA
PDGF-BB
PLGF
SCF
TGF-beta1
VEGF-A
VEGFR-1
VEGFR-2
VEGFR-3
VEGF-D

D.

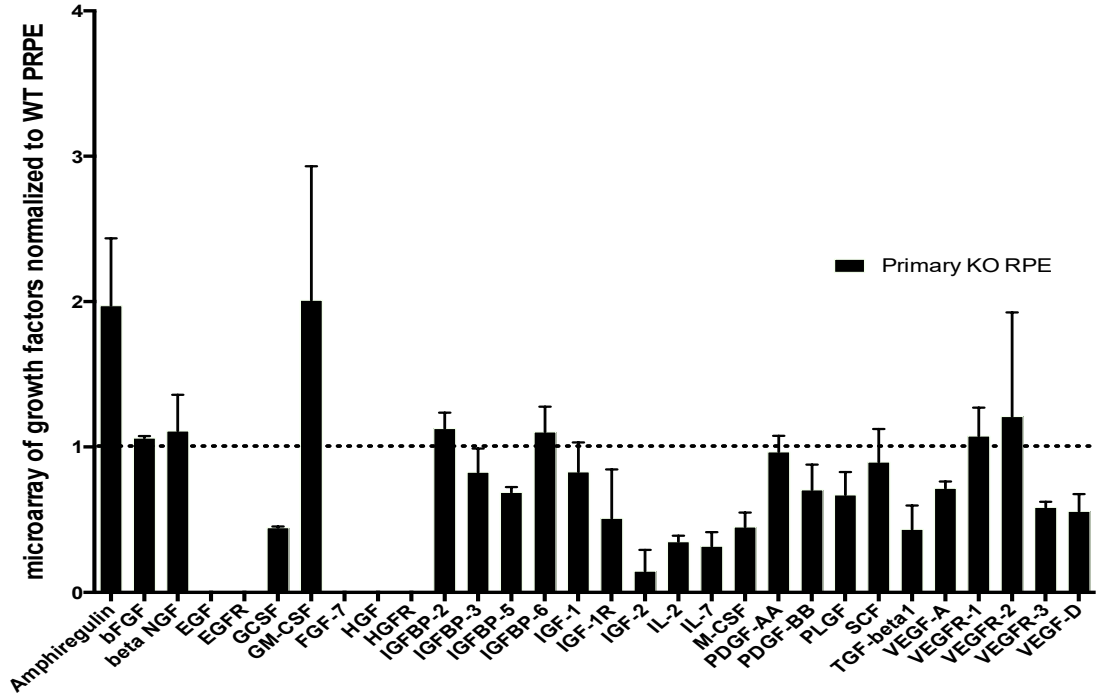
microarray of growth factors normalized to WT PRPE
Primary KO RPE
Amphiregulin
bFGF
beta NGF
EGF
EGFR
GCSF
GM-CSF
FGF-7
HGF
HGFR
IGFBP-2
IGFBP-3
IGFBP-5
IGFBP-6
IGF-1
IGF-1R
IGF-2
IL-2
IL-7
M-CSF
PDGF-AA
PDGF-BB
PLGF
SCF
TGF-beta1
VEGF-A
VEGFR-1
VEGFR-2
VEGFR-3
VEGF-D

Fig. 4.6 Fold changes of protein profiles.

Growth factors that are involved in cellular proliferation were detected by a commercial microarray kit, and values were presented as the fold changes of KO mice versus age-matched WT mice: (A) the fold changes of P9 mice; (B) the fold changes of P12 mice; (C) the fold changes of P30 mice; (D) the fold changes of primary RPE cells. Dash line represented 1. Data were presented as mean ± SEM. n≥4 per group. $^{\#}$: increased. bFGF: basic fibroblast growth factor; beta NGF: beta nerve growth factor; EGF: epidermal growth factor; EGFR: epidermal growth factor receptor; GCSF: granulocyte-colony stimulating factor; GM-CSF: granulocyte-macrophage colony-stimulating factor; FGF-7: fibroblast growth factor 7; HGF: hepatocyte growth factor; HGFR: hepatocyte growth factor receptor; IGFBP-2: insulin like growth factor binding protein 2; IGFBP-3: insulin like growth factor binding protein 3; IGFBP-5: insulin like growth factor binding protein 5; IGFBP-6: insulin like growth factor binding protein 6; IGF-1: insulin growth factor 1; IGF-1R: insulin growth factor 1 receptor; IGF-2: insulin growth factor 2; IL-2: interleukin-2; IL-7: interleukin-7; M-CSF: macrophage colony-stimulating factor; PDGF-AA: platelet-derived growth factor-AA; PDGF-BB: platelet-derived growth factor-BB; PLGF: placental growth factor; SCF: stem cell factor; TGF-beta1: transforming growth factor beta 1; VEGF-A: vascular endothelial growth factor A; VEGFR-1: vascular endothelial growth factor receptor 1; VEGFR-2: vascular endothelial growth factor receptor 2; VEGFR-3: vascular endothelial growth

factor receptor 3; VEGF-D: vascular endothelial growth factor D.

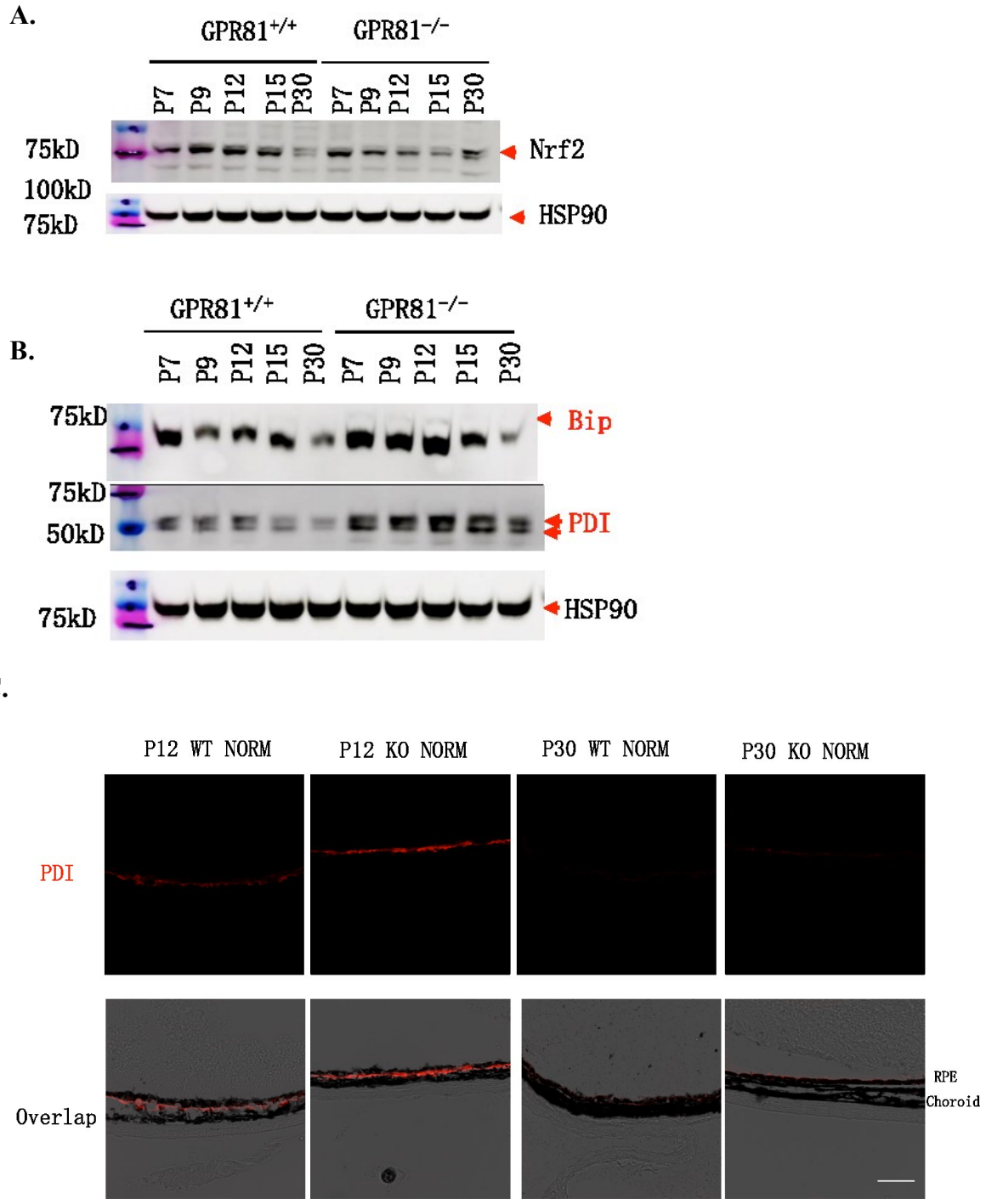
A.
GPR81+/+
GPR81-/-
P7
P9
P12
P15
P30
P7
P9
P12
P15
P30
75kD
Nrf2
100kD
75kD
HSP90
B.
GPR81+/+
GPR81-/-
P7
P9
P12
P15
P30
P7
P9
P12
P15
P30
75kD
Bip
75kD
50kD
PDI
75kD
HSP90
C.
P12 WT NORM
P12 KO NORM
P30 WT NORM
P30 KO NORM
PDI
Overlap
RPE
Choroid

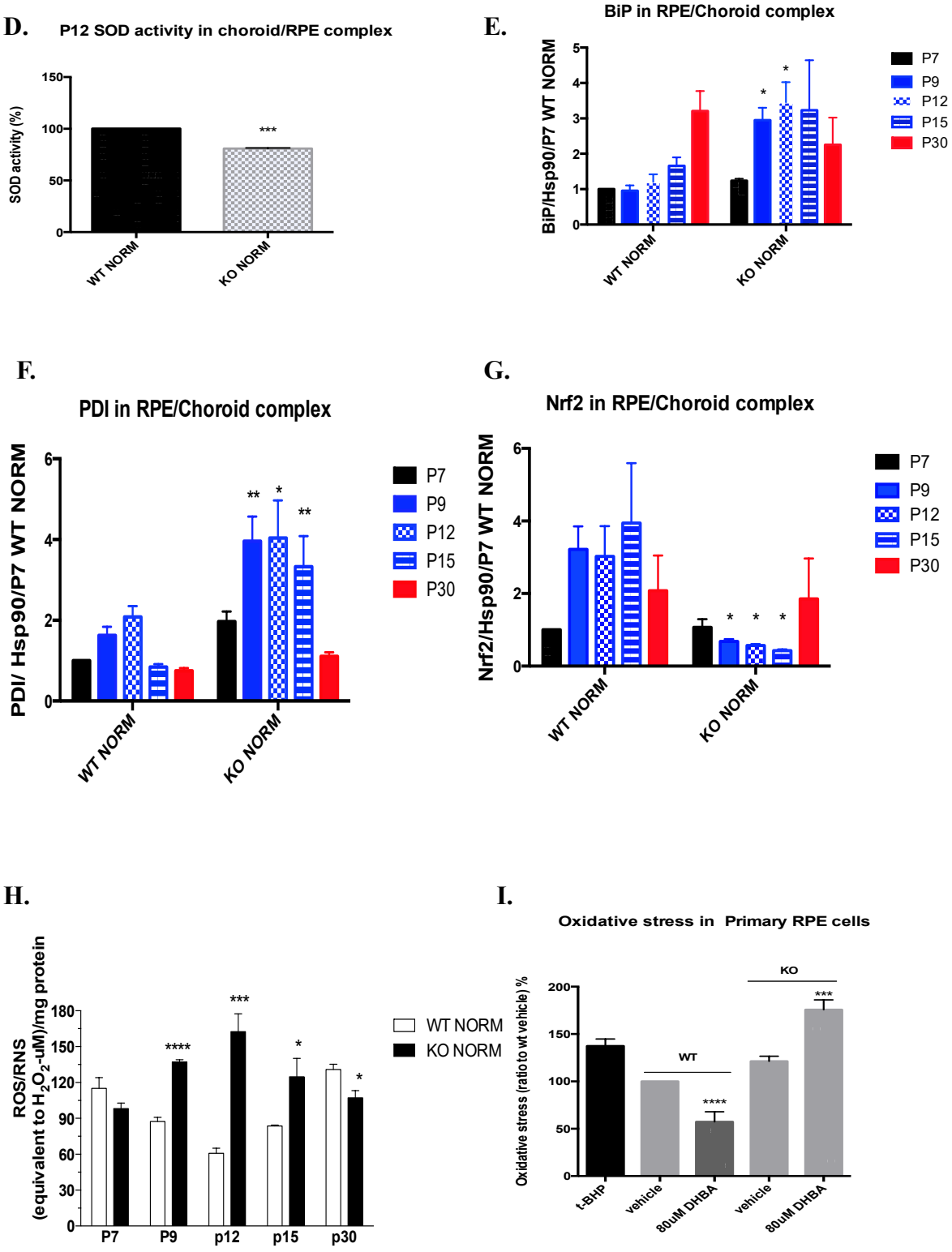
D.
P12 SOD activity in choroid/RPE complex
SOD activity (%)
150
100
50
0
***
WT NORM
KO NORM
E.
BiP in RPE/Choroid complex
BiP/Hsp90/P7 WT NORM
5
4
3
2
1
0
*
*
WT NORM
KO NORM
P7
P9
P12
P15
P30
F.
PDI in RPE/Choroid complex
PDI/ Hsp90/P7 WT NORM
6
4
2
0
**
*
**
WT NORM
KO NORM
P7
P9
P12
P15
P30
G.
Nrf2 in RPE/Choroid complex
Nrf2/Hsp90/P7 WT NORM
6
4
2
0
* * *
WT NORM
KO NORM
P7
P9
P12
P15
P30
H.
ROS/RNS
(equivalent to H2O2-uM)/mg protein
180
150
120
90
60
30
0
****
***
*
*
P7
P9
p12
p15
p30
WT NORM
KO NORM
I.
Oxidative stress in Primary RPE cells
Oxidative stress (ratio to wt vehicle) %
200
150
100
50
0
WT
KO
****
***
t-BHP
vehicle
80uM DHBA
vehicle
80uM DHBA

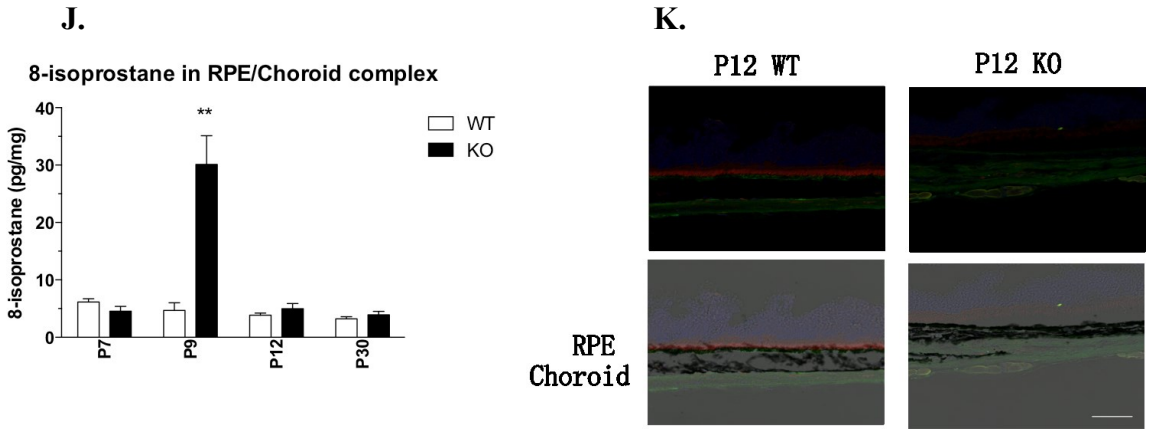

Fig. 4.7 Oxidative stress and ER stress are present in the outer retina of GPR81$^{-/-}$ mice. (A) Representative western blot images of anti-oxidant Nrf2 in mice at different ages. (B) Representative western blot images of ER stress markers (BiP and PDI) in mice at different ages. (C) Representative images of PDI staining in mice. (D) Histogram of SOD activity in mice at P12. (E-G) Quantifications of western blot images of BiP, PDI and Nrf2, respectively. (H-I) Levels of oxidative stress in fresh isolated RPE/Choroid complex (H) and primary RPE cells (I) with t-BHP as the positive control. (J) Quantification of 8-isoprostane in RPE/Choroid complex. (K) Representative images of Iba-1 staining (green) in mice, demonstrating no obvious inflammation exists in KO mice (RPE65, red; DAPI, blue). Values were presented as mean ± SEM. n≥4 per group. *p<0.05,**p<0.01, ***p<0.001, ****p<0.0001 (t-test). Scale bar: 50 μm.

BiP: endoplasmic reticulum binding protein; PDI: protein disulfide isomerase; Nrf2: the nuclear factor E2-related factor 2; SOD: superoxide dismutase; Iba-1, ionized calcium binding adaptor molecule 1.

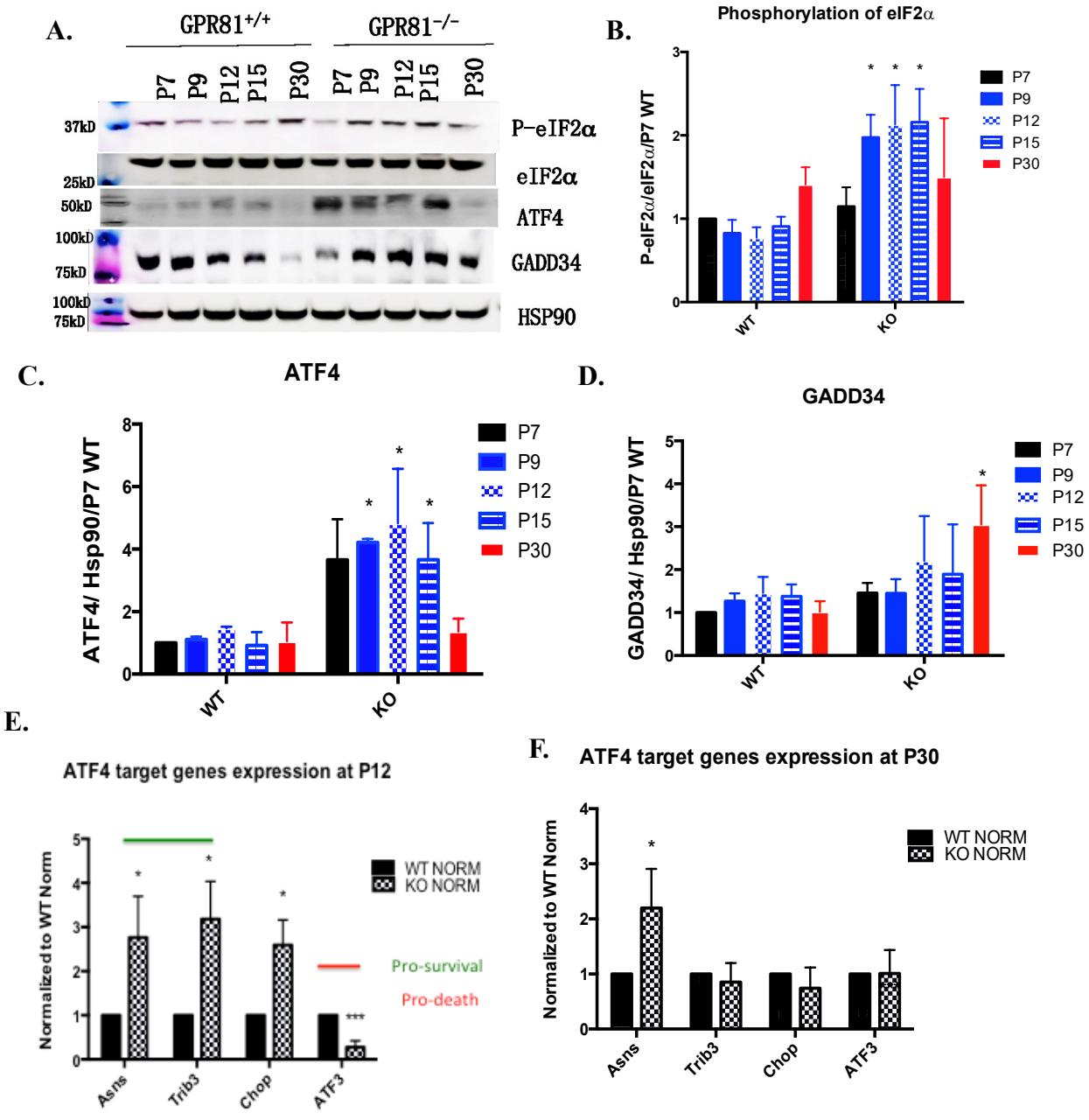
A.
GPR81+/+
GPR81-/-
P7
P9
P12
P15
P30
37kD
25kD
50kD
100kD
75kD
P-eIF2α
eIF2α
ATF4
GADD34
HSP90
B.
Phosphorylation of eIF2α
P-eIF2α/eIF2α/P7 WT
WT
KO
C.
ATF4
ATF4/ Hsp90/P7 WT
D.
GADD34
GADD34/ Hsp90/P7 WT
E.
ATF4 target genes expression at P12
Normalized to WT Norm
WT NORM
KO NORM
Pro-survival
Pro-death
Asns
Trib3
Chop
ATF3
F.
ATF4 target genes expression at P30

Fig. 4.8 Activation of integrated stress response (ISR) pathway.

(A) Representative western blot images of ISR elements including phosphorylation of eIF2α, ATF4 and GADD34. (B-D) Quantification of western blot images of phosphorylation of eIF2α, ATF4 and GADD34, respectively. (E) Levels of mRNA expression of ATF4 target genes at P12 and P30 (F).

Data were presented as mean ± SEM. n≥4 per group. *p<0.05,**p<0.01, ***p<0.001 (t-test).

eIF2α: alpha subunit of eukaryotic translation initiation factor 2; P- eIF2α, phosphorylation of alpha subunit of eukaryotic translation initiation factor 2; ATF4: the activating translation factor 4; GADD34: growth arrest and DNA-damage inducible protein 34; Asns, asparagine synthetase; Trib3, tribbles homolog 3; CHOP, C/EBP homologous protein or DNA damage-inducible transcript 3 or growth arrest and DNA-inducible protein 153 (GADD153); ATF3, the activating transcriptional factor 3;

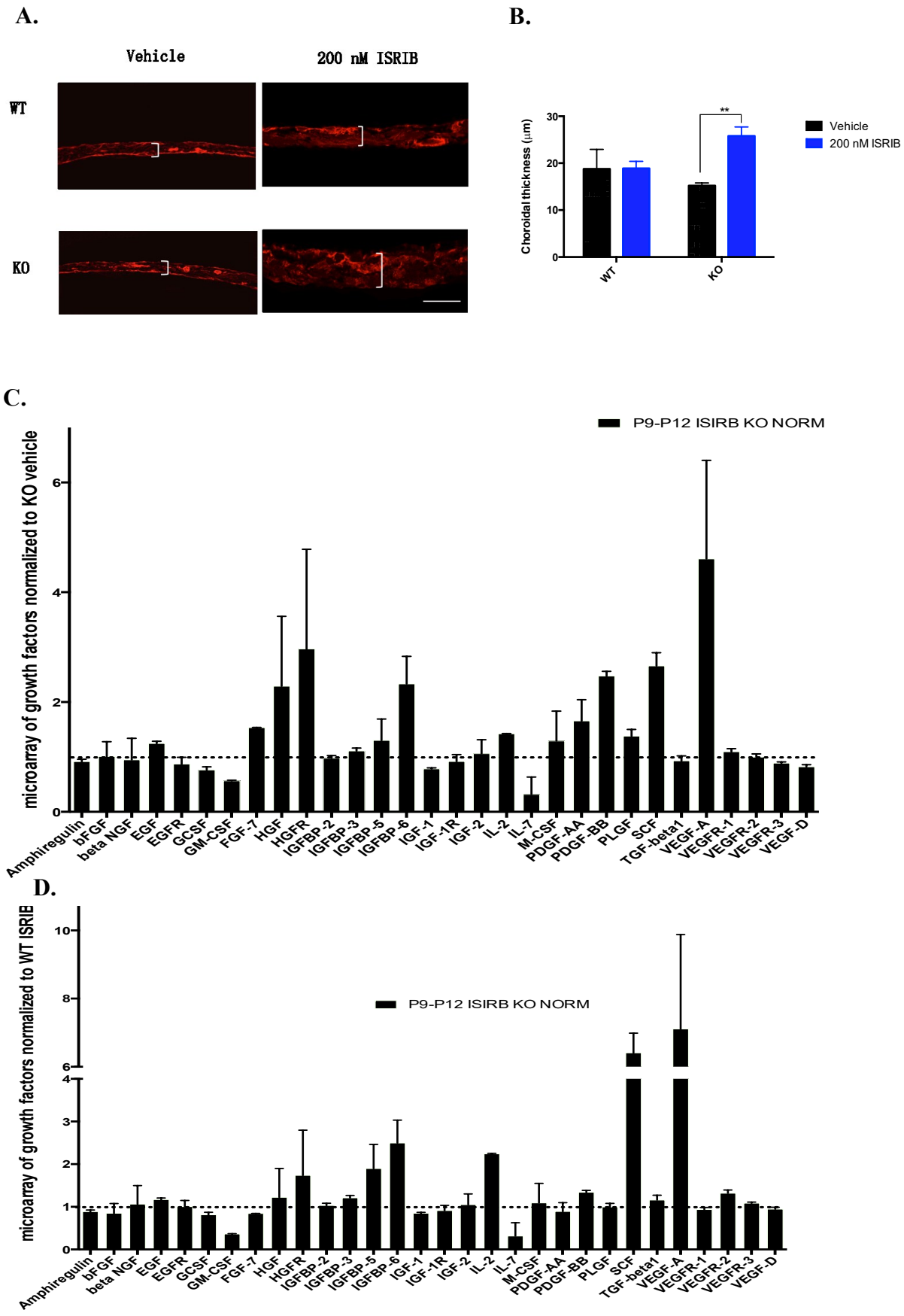
A.
Vehicle
200 nM ISRIB
WT
KO
B.
Choroidal thickness (μm)
30
20
10
0
**
WT
KO
Vehicle
200 nM ISRIB
C.
P9-P12 ISIRB KO NORM
microarray of growth factors normalized to KO vehicle
6
4
2
0
Amphiregulin
bFGF
beta NGF
EGF
EGFR
GCSF
GM-CSF
FGF-7
HGF
HGFR
IGFBP-2
IGFBP-3
IGFBP-5
IGFBP-6
IGF-1
IGF-1R
IGF-2
IL-2
IL-7
M-CSF
PDGF-AA
PDGF-BB
PLGF
SCF
TGF-beta1
VEGF-A
VEGFR-1
VEGFR-2
VEGFR-3
VEGF-D
D.
P9-P12 ISIRB KO NORM
microarray of growth factors normalized to WT ISRIB
10
8
6
4
3
2
1
0
Amphiregulin
bFGF
beta NGF
EGF
EGFR
GCSF
GM-CSF
FGF-7
HGF
HGFR
IGFBP-2
IGFBP-3
IGFBP-5
IGFBP-6
IGF-1
IGF-1R
IGF-2
IL-2
IL-7
M-CSF
PDGF-AA
PDGF-BB
PLGF
SCF
TGF-beta1
VEGF-A
VEGFR-1
VEGFR-2
VEGFR-3
VEGF-D

Fig. 4.9 Inhibition of ISR pathway.

(A) Representative images of choroidal vasculature stained by lectin (red); (B) Quantification of choroidal vasculature of mice intravitreally injected ISRIB or vehicle; (C) Fold changes of growth factors in KO mice intravitreally injected ISRIB normalized to vehicle controls at P12, demonstrating inhibition of ISR pathway partially reverses the attenuation of global translation in KO mice; (D) Fold changes of growth factors in KO mice intravitreally injected ISRIB normalized to ISRIB injected WT mice at P12, indicating VEGF A in particular mediates neovascularization in ISRIB treated KO mice. Data were presented as mean ± SEM. $n \geq 4$ per group. *$p<0.05$,**$p<0.01$ (t-test). Scale bar: 50 μm.

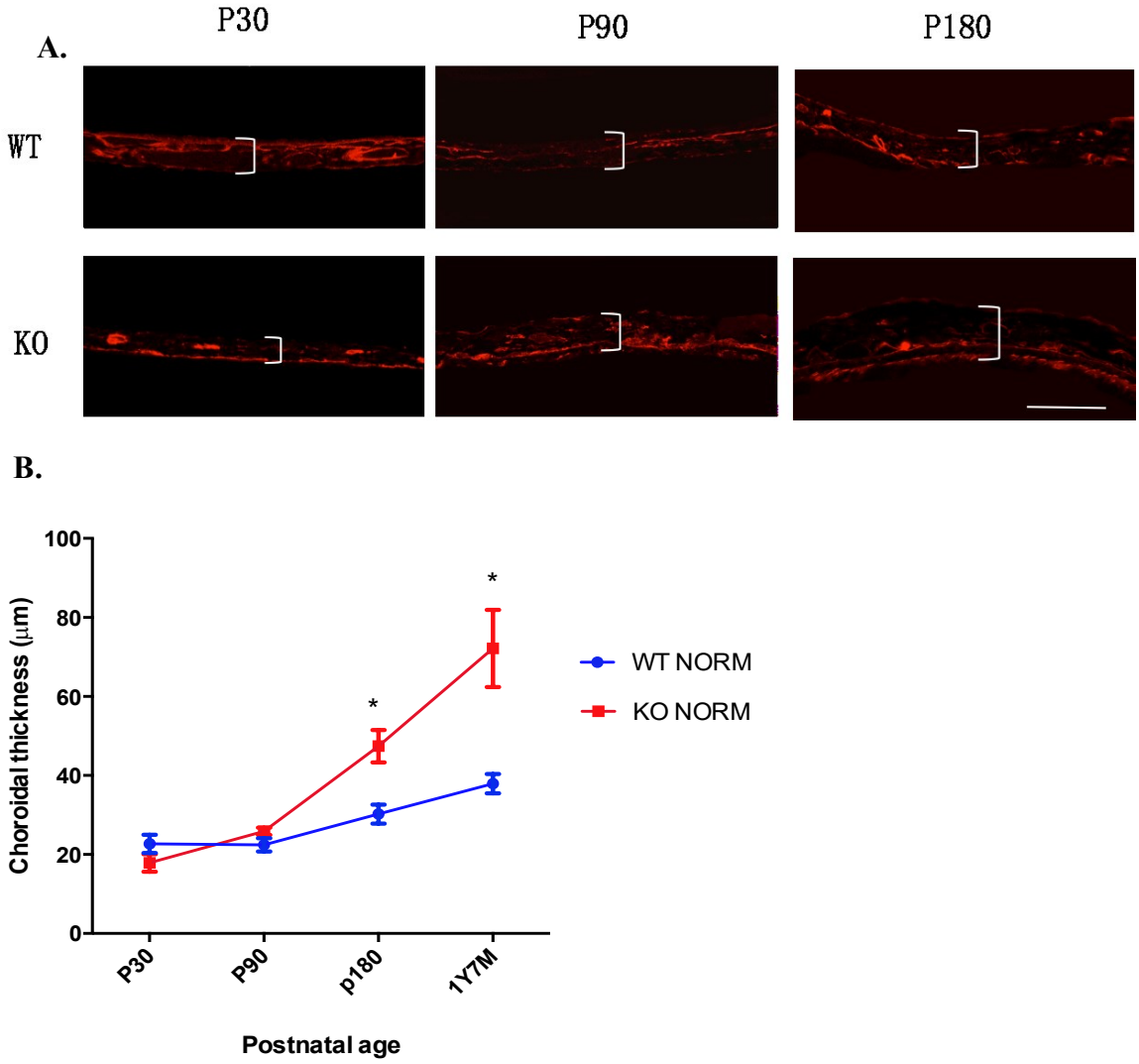

Fig. 4.10 Aged GPR81$^{-/-}$ mice display choroidal neovascularization (CNV).

(A) Representative images of choroidal vasculature stained by lectin (red) at different ages; (B) Quantification of choroidal vasculature of mice at different ages, suggesting that significant CNV began at P180 in KO mice. Data were presented as mean ± SEM. n≥4 per group. *p<0.05 (t-test). Scale bar: 50 μm.

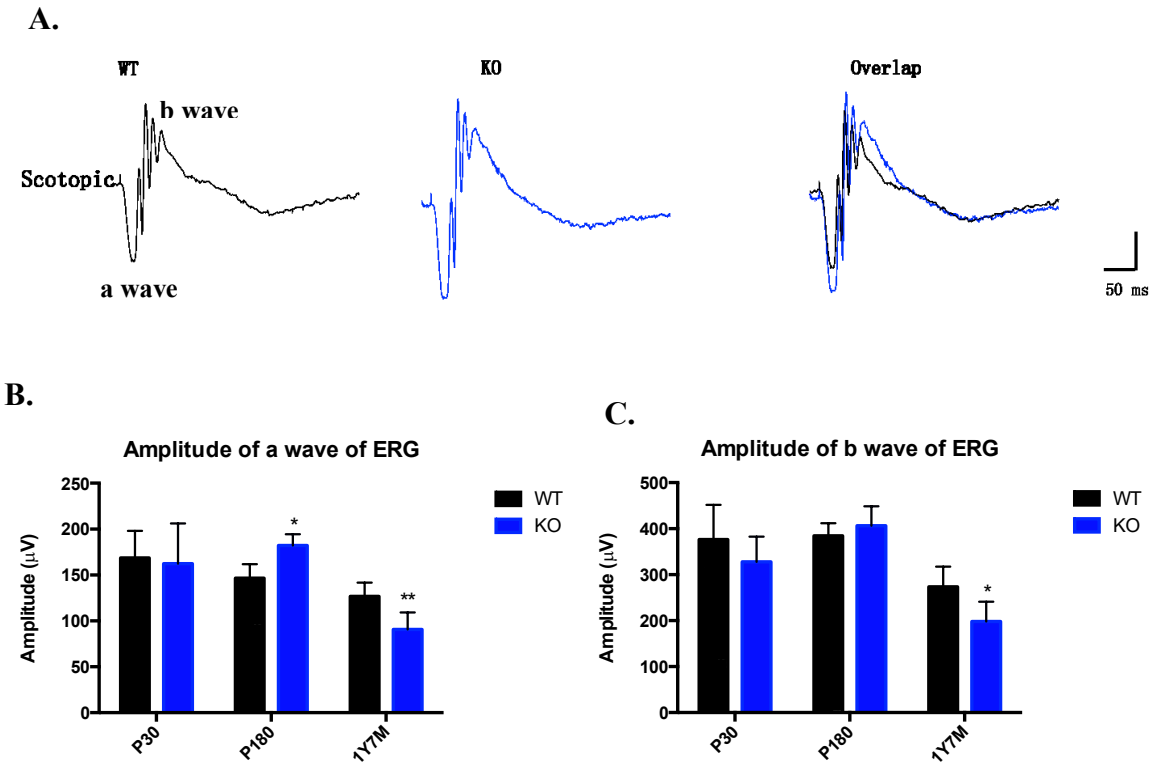

Fig. 4.11 Retinal function evaluated by ERG.

(A) Representative images of ERG recordings in WT and KO mice; (B) Quantification of photoreceptor-mediated response (a wave) in mice at different ages; (C) Quantification of photoreceptor-mediated response (b wave) in mice at different ages. Data were presented as mean ± SEM. n≥4 per group. *p<0.05, **p<0.01 (t-test). Scale bar of amplitude: 100 μV for scotpic ERG. Scale bar of timing: 50 ms.

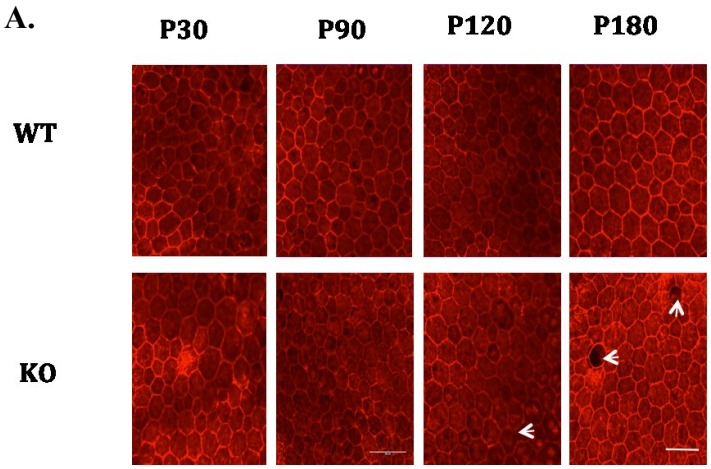
A.
P30
P90
P120
P180
WT
KO

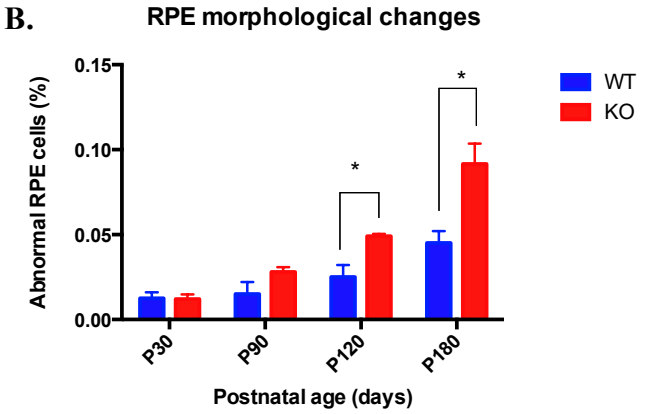
B.
RPE morphological changes
Abnormal RPE cells (%)
0.15
0.10
0.05
0.00
*
*
WT
KO
P30
P90
P120
P180
Postnatal age (days)

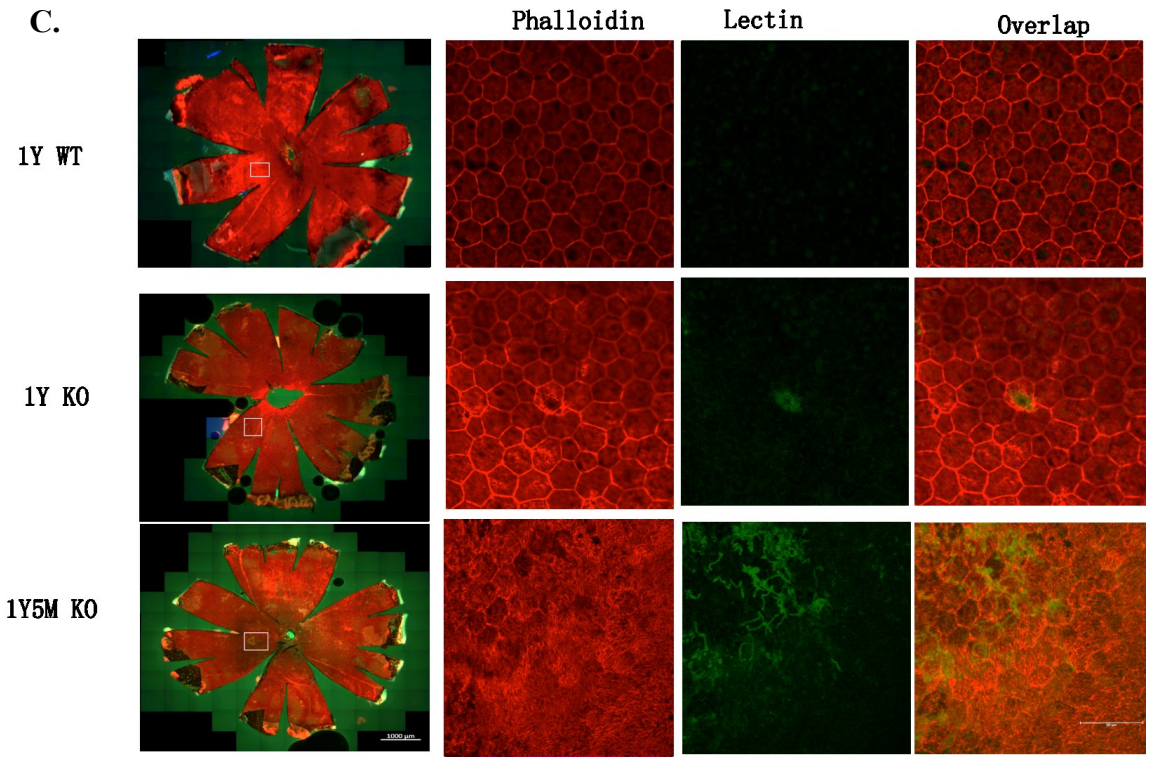

Fig. 4.12 The flat mount of RPE/choroid complex.

(A) Representative images of RPE morphology labeled by phalloidin (a marker of RPE cell membrane): white arrows indicate vanished conjunctions between RPE cells at P120 and ghost RPE cells at P180; (B) Quantification of abnormal RPE cells in flat mounts; (C) Representative images of flat mount double labeled with phalloindin and lectin (green) to examine the possibility of penetration of choroidal vessels into RPE layer. n≥4 per group. Scale bar: 50 μm. Data were presented as mean ± SEM. n≥4 per group. *$p<0.05$ (t-test).

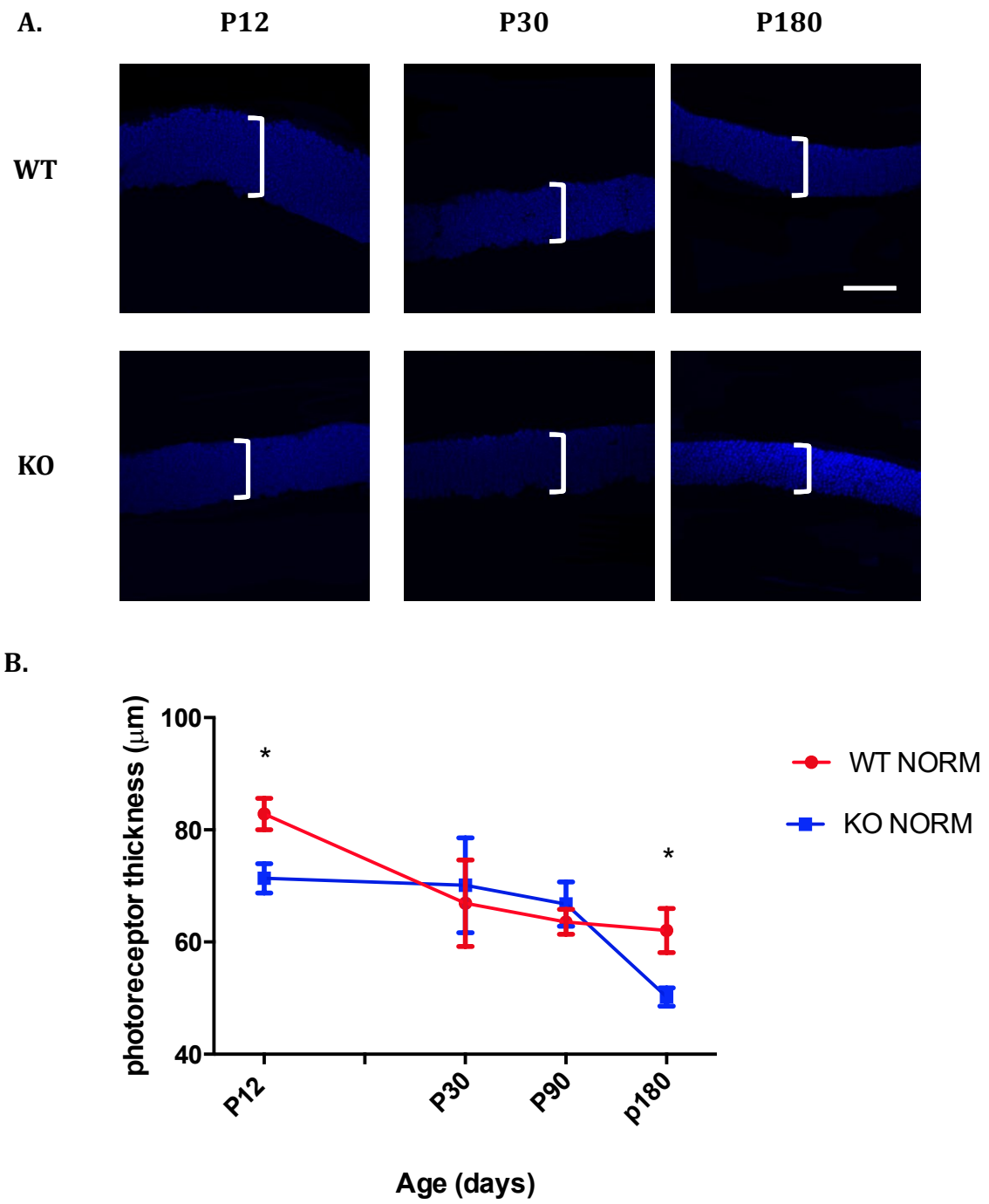

Fig. 4.13 The thickness of photoreceptors in mice. (A) Representative images of photoreceptors stained by DAPI; (B) Photoreceptor thickness was evaluated at different ages. Scale bar: 50 μm. Blue line represents WT NORM group while red line is the KO NORM group. Data were presented as mean ± SEM. n≥4 per group. *p<0.05 (t-test).

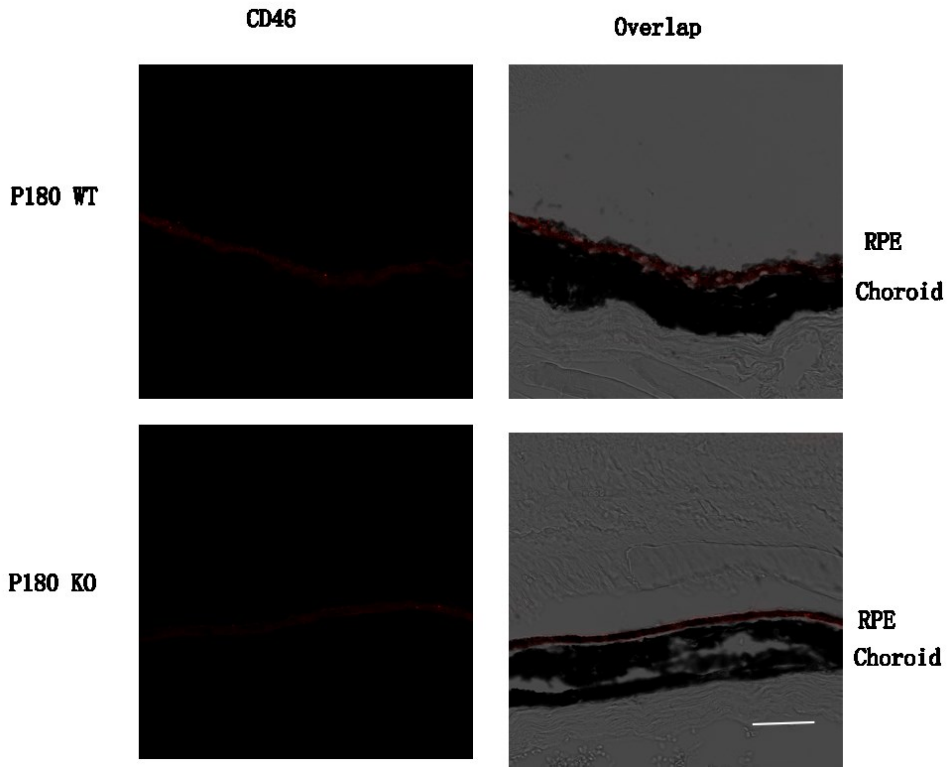

Fig. 4.14 Detection of drusen by labeling CD46 (a marker of drusen, red). No significant difference was found between WT and KO mice at P180, suggesting that drusen may be not involved in KO mice. Scale bar: 50 μm.

APPENDIX

Appendix 1: Graphic scheme for series of events where loss of GPR81 in mice lead to development of CNV in normal air (A) and that are exposed to hyperoxia (B).

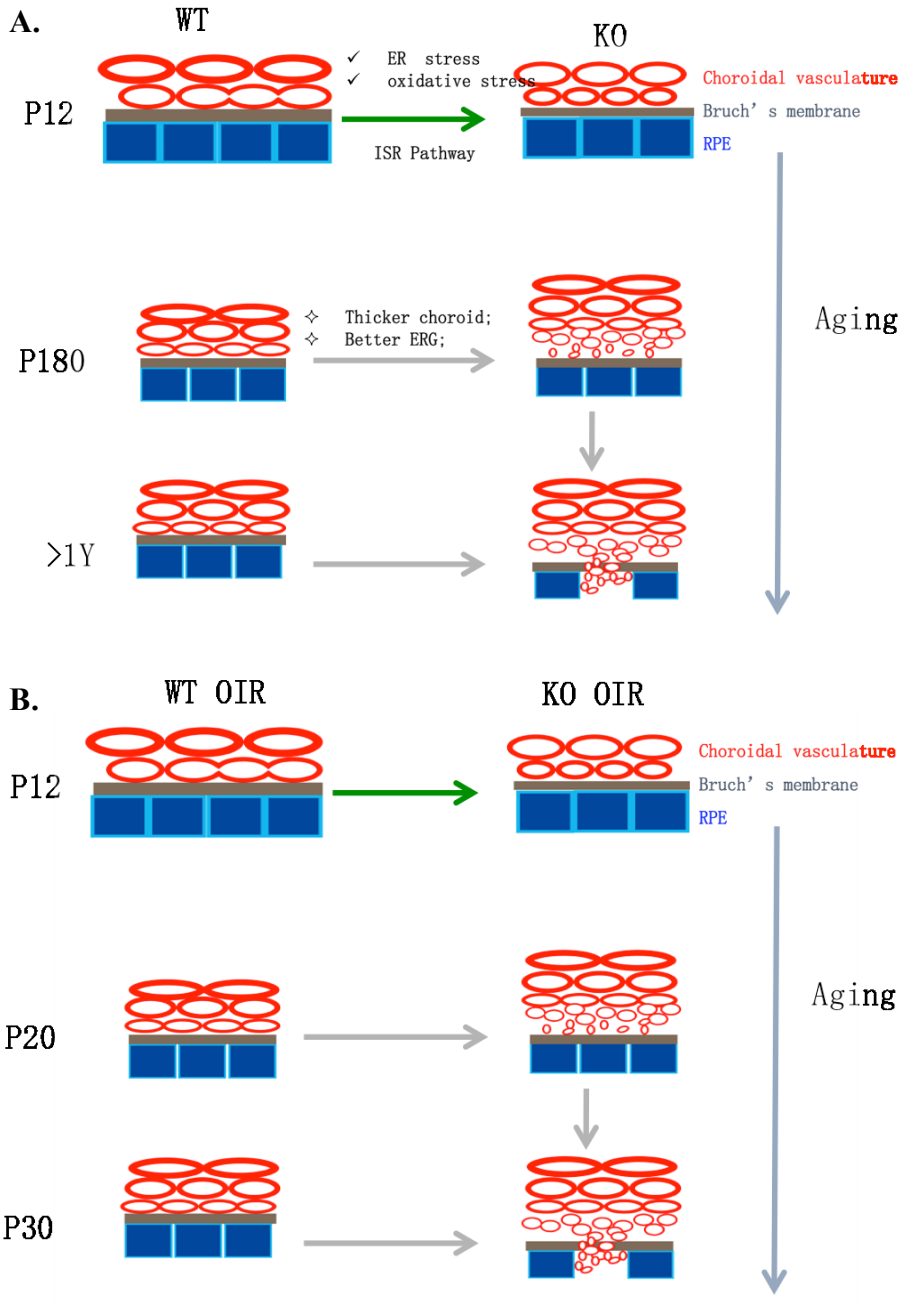

Appendix 2: Flat mounts and choroidal thickness in oxygen exposed mice.

(A) Representative flat mount images of RPE/choroid complex labeled by phalloidin (red) and lectin (green), suggesting that a pronounced CNV is developed in KO OIR mice at P30. White squares indicate the location that was zoomed in; white arrow represents the location of the macrophage (B). (C) Quantification of choroidal thickness at P15 and P30 (D). Values were presented as mean ± SEM. $n \geq 4$ per group. *$p < 0.05$ (one way ANOVA). Scale bar: 50 μm.

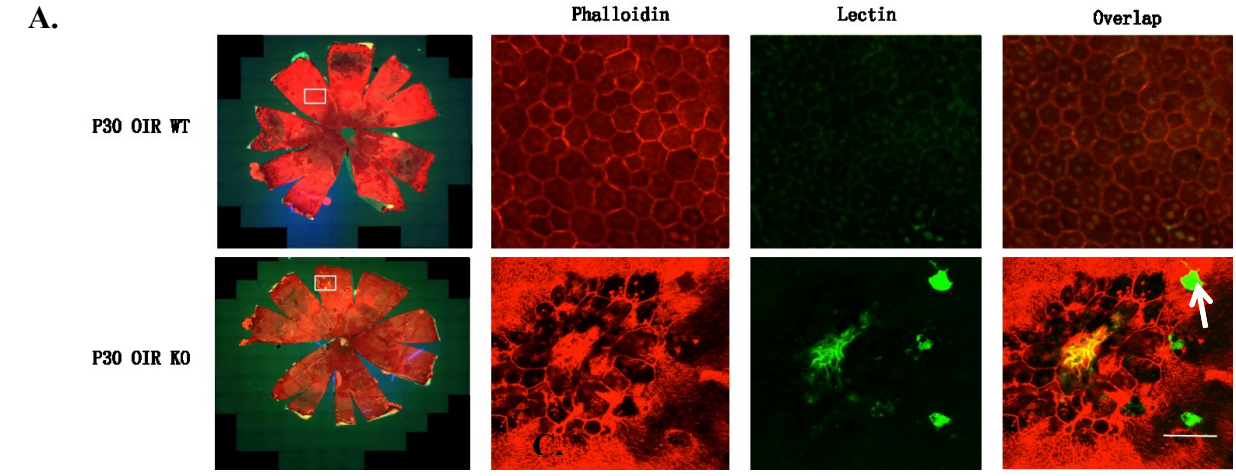
A.
Phalloidin
Lectin
Overlap
P30 OIR WT
P30 OIR KO
C.

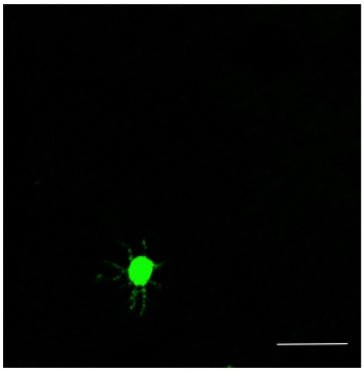
B.

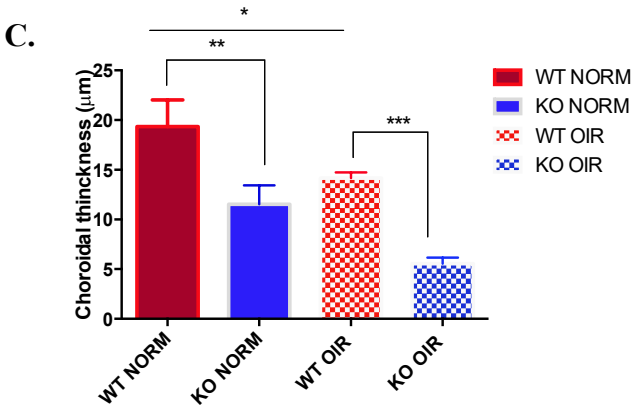
C.
*
**
***
Choroidal thinckness (μm)
25
20
15
10
5
0
WT NORM
KO NORM
WT OIR
KO OIR
WT NORM
KO NORM
WT OIR
KO OIR

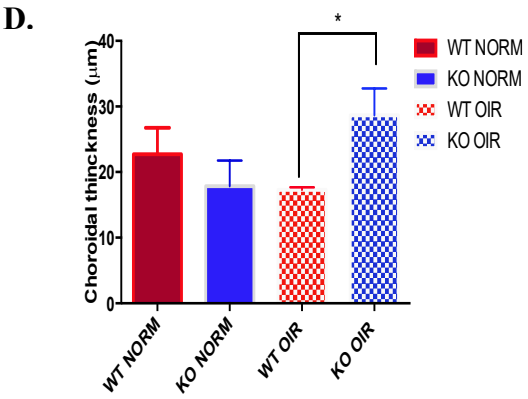
D.
*
Choroidal thinckness (μm)
40
30
20
10
0
WT NORM
KO NORM
WT OIR
KO OIR
WT NORM
KO NORM
WT OIR
KO OIR

Appendix 3:

Body weight of mice at P30 (A) and P180 (B). Data was presented as mean ± SEM, n≥4 per group. *p<0.05, **p<0.01 (t-test).

A.

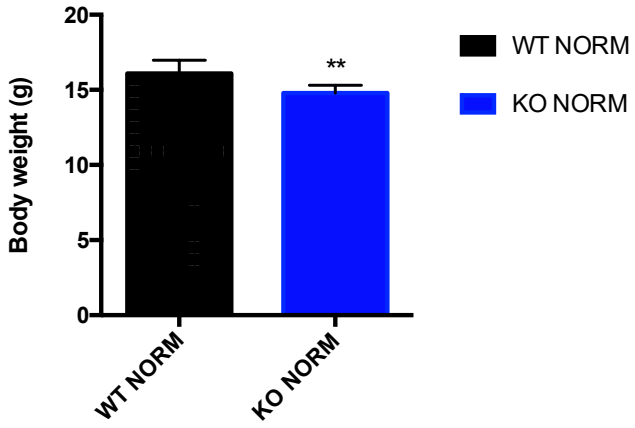

B.

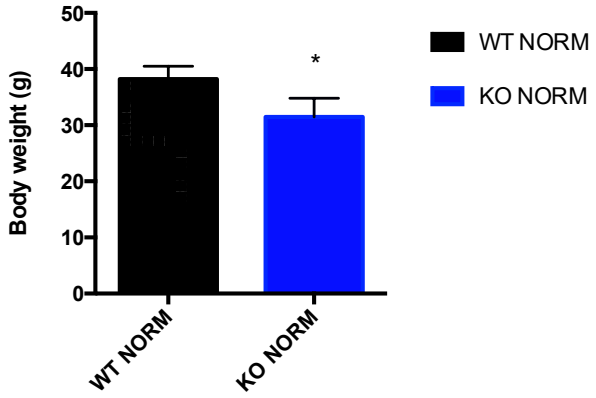

Appendix 4: The acetylation of Histone 3 (A and B) and activity of HDACs (C) at P9 and P12, indicating general elevation of gene expression in KO mice was associated with lower activity of HDACs. Data was presented as mean ± SEM, n≥4 per group. *p<0.05, **p<0.01 (t-test).

A.

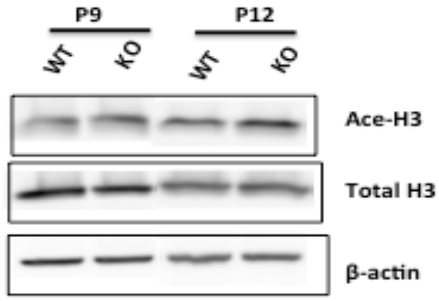

ace-H3 in choroid/RPE complex

B.

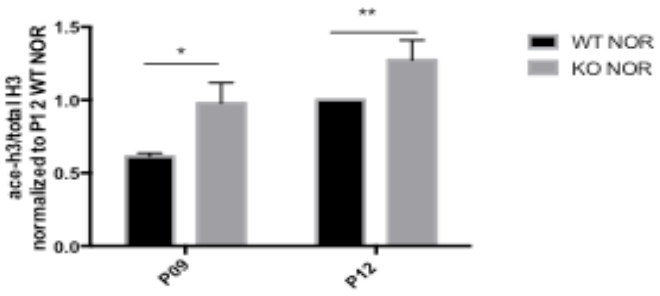

C.

HDAC activity in choroid/RPE complex on P12

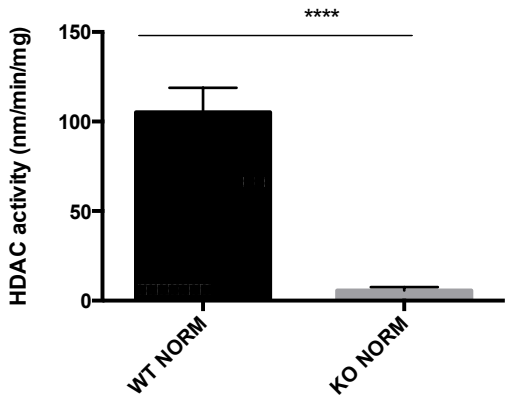

Appendix 5: The immunoactivity of GPR81. (A) Representative image of PCR detecting GPR81 expression in mice; (B) Representative image of western blot detecting GPR81 level in the outer retina; (C) Representative image of western blot detecting GPR81 level in Primary RPE cells (PRPE); (D) Representative image of RCR detecting GPR81 level in primary RPE cells (PRPE) rather than in the choroid; (E) Representative image of GPR81 staining (red) in the retina; (F) Representative images of GPR81 staining in brain sections. Scale bar: 50 μm.

A.

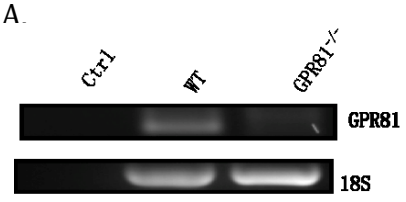
Ctrl
WT
GPR81-/-
GPR81
18S

B.

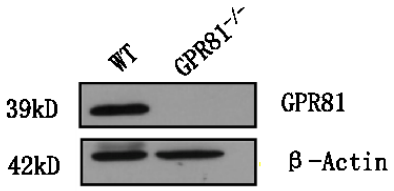
WT
GPR81-/-
39kD
GPR81
42kD
β-Actin

C.

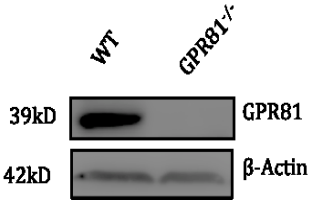
WT
GPR81-/-
39kD
GPR81
42kD
β-Actin

D.

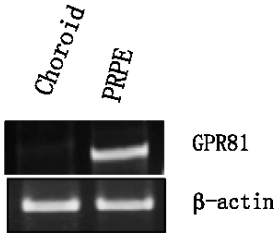
Choroid
PRPE
GPR81
β-actin

E.

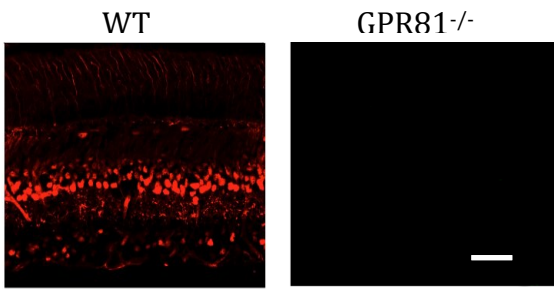
WT
GPR81-/-

F.

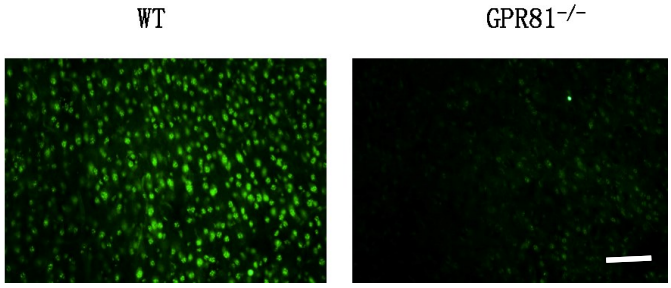
WT
GPR81-/-

Appendix 6: The scheme that summarizes the cellular and molecular effects of GPR81.